SPARK-PLASMA SINTERED SIC_w-AL_2O_3 COMPOSITES AND THE INFLUENCE OF 3YSZ ON THEIR MICROWAVE HEATING BEHAVIOR

A Dissertation
Presented to
The Academic Faculty

by

Miriam Rath

In Partial Fulfillment
of the Requirements for the Degree
Master of Science in the
School of Materials Science and Engineering

Georgia Institute of Technology
August 2022

SPARK-PLASMA SINTERED SIC_w-AL_2O_3 COMPOSITES AND THE INFLUENCE OF 3YSZ ON THEIR MICROWAVE HEATING BEHAVIOR

Approved by:

Dr. Rosario Gerhardt, Advisor
School of Materials Science and Engineering
Georgia Institute of Technology

Dr. Robert Speyer
School of Materials Science and Engineering
Georgia Institute of Technology

Dr. Chaitanya Deo
School of Nuclear and Radiological Engineering
Georgia Institute of Technology

Date Approved: [July 25, 2022]

ACKNOWLEDGEMENTS

I would like to express my gratitude to my advisor, Dr. Gerhardt, for her guidance and support in the completion of this work. Her knowledge, insights, and advice were invaluable throughout this research. Additionally, I would like to thank my committee members Dr. Deo and Dr. Speyer for their support and advice during the thesis process. I would also acknowledge the funding in part by Sandia National Laboratories during this period. I would like to thank Dr. Deo for allowing me use of his SPS machine, Yolande Berta at the IEN/IMAT for helping me gather SEM results, and David Tavakoli at the IEN/IMAT for helping to collect XRD data, although it was not used in this work specifically. Additionally, I would like to thank Roshaun Titus for his help in COMSOL.

I would also like to acknowledge my fellow lab-mates for their support and encouragement as well as my friends for making my graduate school experience a positive one. Lastly, I want to thank my parents for their constant love and support.

TABLE OF CONTENTS

LIST OF TABLES

LIST OF FIGURES

SUMMARY

Ceramic composites consisting of an alumina (Al_2O_3) matrix and silicon carbide whisker (SiC_w) reinforcing phase have found recent commercial use as microwave heating elements primarily due to the microwave absorption properties of SiC. Similarly, 3 mol% yttria stabilized zirconia (3YSZ) displays strong microwave absorption properties, experiencing a thermal runaway effect, causing the material to uncontrollably heat up to temperatures above 1000°C. However, a detailed understanding of the electrical and microwave heating behaviors of spark-plasma sintered (SPS) SiC_w-Al_2O_3 composites or how 3YSZ influences this behavior when added as an additional filler material to form 3YSZ- SiC_w-Al_2O_3 composites has not yet been established.

In Chapter 4, it is shown that the percolation threshold of SPS SiC_w-Al_2O_3 composites occurs at a whisker content of 7.68%, similar to that of previously made hot-pressed SiC_w-Al_2O_3 samples. At this composition, the semi-conducting behavior of the SiC begins to dominate the electrical response causing the bulk behavior of the composite to transition from insulating to conducting. Error analysis was also completed on the SPS SiC_w-Al_2O_3 composite samples, demonstrating that samples near or at the percolation threshold have the highest errors in both the repeatability and reproducibility of electrical measurements. This is due to whisker contact heterogeneity driving variations in electrical behaviors when interconnected conducting paths are just beginning to form. SEM imaging of samples below, at, and above the percolation threshold supported this theory. SPS 3YSZ-SiC_w-Al_2O_3 composites were fabricated in Chapter 5, using two different aluminas and varying annealing treatments. It was observed that the Advanced Composite Materials

alumina resulted in more homogenous samples, which was confirmed with both reproducibility error analysis and SEM images. However, it was found that in all SPS 3YSZ-SiC_w-Al_2O_3 composite samples, 3YSZ agglomerates formed due to insufficient dispersion from the mixing process.

Lastly, in Chapter 6, numerical simulations were done of microwave heating of both SiC_w-Al_2O_3 and 3YSZ-SiC_w-Al_2O_3 composites under a 2.45GHz frequency using the electrical conductivity data collected in Chapters 4 and 5, respectively. It was found that in the SiC_w-Al_2O_3 composites, the SiC volume content required to induce significant microwave heating behavior is 17.0%. This indicated that although electrical conductivity is tied to the microwave absorption properties in these composites, the compositions at which SiC begins to dominate the electrical response doesn't correspond to the same whisker content at which SiC begins to dominate the microwave heating response. For the 3YSZ-SiC_w-Al_2O_3 samples made, there was not enough 3YSZ volume content to induce thermal runaway in the composites. Additionally, it was found that the only 3YSZ-SiC_w-Al_2O_3 samples that demonstrated any significant heating under a microwave frequency were the more electrically conducting samples which again emphasized the relation between electrical conductivity and microwave absorption in these composites.

1 INTRODUCTION

Composites are materials made from two or more constituent materials that are microscopically heterogenous but can be combined to create a bulk material with specifically tailored mechanical, thermal, or electrical properties. Often these constituent materials are referred to as the filler and matrix. Altering volume content of the filler and matrix materials directly influences overall composite properties, and sometimes can drastically change the bulk behavior of the composite. As a result, studying how the volume content of the constituent materials affect overall composite properties is a critical field of study.

1.1 Percolation

Percolation occurs when the filler material forms an interconnected network within the matrix material. Depending on the similarity between the matrix and filler material, percolation often causes a large change in the overall mechanical, thermal, electrical, or chemical properties in the composite [1]. The amount of filler needed, often expressed as volume percent, such that percolation occurs in the composite is known as the percolation threshold. An example of percolation is shown in Figure 1.1.1, where the dotted green line marks the percolation threshold, distinguished by the filler volume content at which the electrical conductivity rises sharply when the filler conductivity is higher than that of the matrix [2]. Percolation has been studied extensively in the literature and can occur in

composites of various types such as polymer matrix composites (PMC's), ceramic matrix composites (CMC's), and metallic matrix composites (MMC's) [3]–[11].

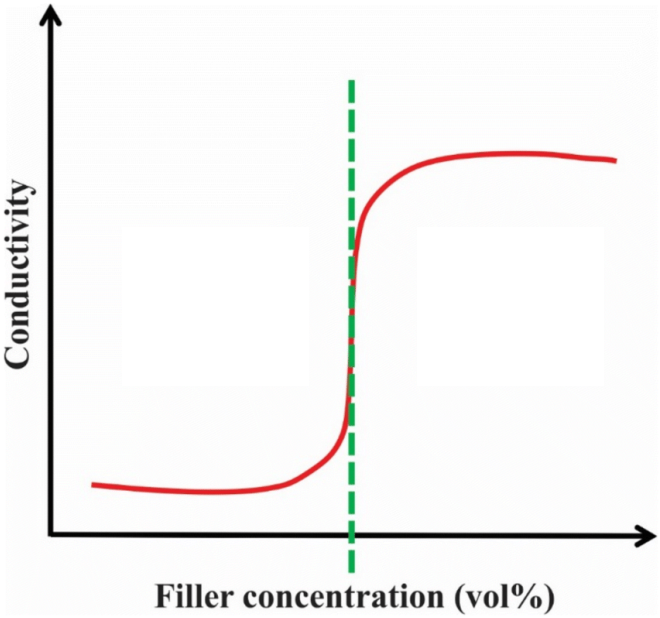

Figure 1.1.1 An example percolation curve with the percolation threshold shown by the dotted green line, characterized by the sharp increase in conductivity. Modified from [2].

1.2 Background on Microwave Heating

As opposed to conventional heating, microwave heating relies on the transfer of electromagnetic to thermal energy to generate volumetric heating of materials. This is done primarily by the electrical field interacting with molecules through ionic conduction or dipolar rotation. In dipolar rotation, molecular dipoles attempt to align themselves with the electric field and thus induce friction leading to heat generation. Similarly in ionic conduction, ionic particles or free ions oscillate back and forth in an attempt to align themselves with the electric field thereby generating heat through friction [12]. As a result,

it is possible to achieve rapid and uniform heating of thick materials as the heat transfer does not depend on diffusion through surfaces [12]–[14]. This is especially true for ceramics and polymers which have relatively low thermal conductivities.

In the context of microwave heating, materials are often classified by their interaction with the microwave field as being transparent, conducting, absorbing, or mixed absorbing [13]. Transparent materials usually have low dielectric loss with microwave frequencies passing through with little to no attenuation, conductors reflect microwave frequencies, and absorbers usually have high dielectric loss and readily absorb microwave energy. Mixed absorbers are materials that are often used to describe composite or multi-phase materials comprised of phases classified as the aforementioned groups. Microwave heating due to the absorption of a material, is based on the power absorbed per unit volume, P in units W/m^3, which is expressed in Equations (1.2.1 – 1.2.2) [12], [13].

$$P = \sigma E^2 = 2\pi f \varepsilon_0 \varepsilon_r' tan\delta E^2 \tag{1.2.1}$$

Here, σ is the electrical conductivity in S/m, E is the magnitude of the electric field in V/m, f is the microwave frequency in Hz, ε_0 is the permittivity of free space in F/m, ε_r' is the dielectric constant, which is unitless, and $tan\delta$ is the dissipation factor which is also unitless. Once the power is absorbed by the material it is then converted to heat where T is the temperature in K, t is time in s, ρ is the material density in kg/m^3, and C_p is the specific heat capacity in J/kgK . Note that the dielectric properties of the material dictate the microwave heating process in the material.

$$\Delta T \Delta t = 2\pi f \varepsilon_0 \varepsilon_r' tan\delta E^2 \rho C_p \tag{1.2.2}$$

1.3 SiC_w-Al_2O_3 Composites

SiC_w-Al_2O_3 composites are comprised of silicon carbide (SiC) whiskers, which serve as the filler of the composite, and an aluminum oxide or alumina (Al_2O_3) matrix. SiC has multiple polymorphs including α-SiC and β-SiC, which have hexagonal and cubic structures respectively, while Al_2O_3 has a corundum or hexagonal structure. Whiskers are characterized by their high aspect ratio (length divided by diameter), and by having very few defects and chemical impurities, with no grain boundaries and a uniform phase composition. SiC whiskers have high strength and modulus of elasticity, making it an ideal addition to improve the mechanical strength of Al_2O_3 [10]. As such, SiC_w-Al_2O_3 composites have found modern use as cutting tools and wear parts for their high hardness, chemical inertness, and high thermal shock resistance. Recently however, they have also found applications as commercial microwave heating elements due to their ability to rapidly heat up under microwave frequency [15].

1.3.1 Electrical Behavior

SiC_w-Al_2O_3 composites are considered electrical conductor-insulator composites, but their bulk electrical response can drastically vary depending on if percolation has occurred in the composite or not, as described in Chapter 1.1. The transition from electrically insulating to conducting in SiC_w-Al_2O_3 composites has been studied extensively both in simulation and experimental work [16]–[23]. Specifically, sample processing methods used, including extrusion and pressureless sintering, drypressing and pressureless sintering, and hot-pressing (HP) of SiC_w-Al_2O_3 composites has been studied in the literature [10], [16], [18], [19], [21]–[24]. Varying the processing method was found

to not only affect the percolation threshold, but also the magnitude of conductivity of SiC_w-Al_2O_3 samples made with comparable SiC whisker volume content as seen in Figure 1.3.1.

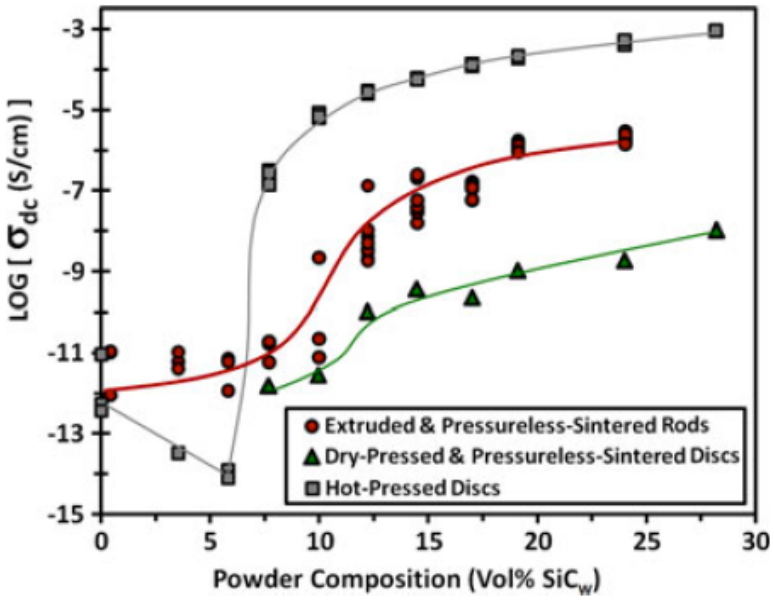

Figure 1.3.1 Percolation curves of SiC_w-Al_2O_3 composites made from various processing methods. Taken from [22].

1.3.2 Microwave Behavior

SiC is a well-known microwave absorbing material with resonance in the microwave frequency due to the establishment of polarized and dielectric loss caused by the external electric field [25]–[27]. However, SiC does not display magnetic loss and thus the electromagnetic wave absorption is usually improved by doping to induce stacking defects or by introducing SiC as a material in a composite [28]. Conversely, Al_2O_3 is a microwave transparent material with a relatively low dielectric loss [29], [30]. However, because both materials display excellent high-temperature stability and thermal shock resistance, they are ideal candidates to use in high temperature microwave applications.

As an overall composite however, SiC_w-Al_2O_3 is a mixed absorber. The microwave absorption and thus microwave heating properties of SiC_w-Al_2O_3 can be modified by changing the volume content of SiC_w with respect to Al_2O_3, with increased SiC_w content generally resulting in higher temperatures and higher heating rates reached when exposed to a microwave frequency [28].

1.4 3YSZ

3YSZ is comprised of zirconium oxide or zirconia (ZrO_2) with 3mol% yttrium oxide or yttria (Y_2O_3) added to partially stabilize the crystal structure of zirconia over a wider range of temperatures. This aids in the commercialization of zirconia products as it helps to form the tetragonal phase transformation and volume loss experienced by pure zirconia during the cooling period of the sintering process [31], [32]. At room temperature, 3YSZ has a tetragonal structure.

1.4.1 Electrical Behavior

The electrical conductivity of 3YSZ is highly dependent on temperature due to the phase transitions that zirconia undergoes over temperature ranges. However, generally 3YSZ has an electrical conductivity on the order of 10^{-4} S/m at room temperature, but as temperature increases, the electrical conductivity increases as well [32], [33]. 3YSZ also has high oxygen ion conductivity, resulting in the material being easily oxidized or reduced, which can drastically affect the electrical response of the material [34].

1.4.2 Microwave Behavior

3YSZ is a moderate microwave absorber and is able to convert microwave energy to thermal energy relatively efficiently. However, as the dielectric properties of 3YSZ are temperature dependent, at a certain temperature 3YSZ will display a thermal runaway effect where the temperature rapidly increases uncontrollably due to a small increase in the loss factor of the material [35]–[37]. This thermal runaway effect can be potentially prevented however, by reducing the power of the microwave frequency, although the heating rate will still be high [38].

1.5 Impedance and Dielectric Spectroscopy

Impedance and dielectric spectroscopy is a method of electrical characterization that measures AC voltage and current over a wide frequency range. It is able to measure interfacial effects at the electrode-material interface, bulk properties, and internal interfaces such as grain boundaries and interphase boundaries. These processes are a result of the different polarization mechanisms that occur in all materials, including electronic and ionic polarization, molecular or dipolar polarization, and space charge polarization [39], [40]. Therefore, impedance and dielectric spectroscopy is a useful characterization tool that can be used for non-destructive evaluation of any material in multiple forms such as solid or powder.

The complex impedance (Z^*), measured in Ohms (Ω) is a function of the voltage (V), current (I), and phase angle (θ) over a wide frequency range (f), which is shown in Equations (1.5.1-1.5.4) [41].

$$Z^* = \frac{V(\omega)}{I(\omega)} \tag{1.5.1}$$

Where,

$$V(\omega) = V_m \sin(\omega t) \tag{1.5.2}$$

$$I(\omega) = I_m \sin(\omega t + \theta) \tag{1.5.3}$$

$$\omega = 2\pi f \tag{1.5.4}$$

Here θ is the phase difference between the voltage and the current, ω is the angular frequency, and V_m and I_m are the applied AC voltage and current, respectively. Additionally, the complex impedance is comprised of a real part of the impedance (Z') and an imaginary part of the impedance (Z''), which are functions of the impedance magnitude $|Z|$ and phase angle, shown in Equations (1.5.5-1.5.10). The real and imaginary impedance represents energy that passes though the material and energy that is stored and lost in the material, respectively.

$$Z^* = Z' + jZ'' \tag{1.5.5}$$

$$Z' = |Z| \cos(\theta) \tag{1.5.6}$$

$$Z'' = |Z| \sin(\theta) \tag{1.5.7}$$

$$|Z| = [(Z')^2 + (Z'')^2]^{\frac{1}{2}} \tag{1.5.8}$$

$$\theta = \tan^{-1} \frac{Z''}{Z'} \tag{1.5.9}$$

Where,

$$j = \sqrt{-1} \tag{1.5.10}$$

1.5.1 Conversion to the Other Dielectric Functions

Although impedance is directly measured from impedance and dielectric spectroscopy, it is often converted to the other dielectric functions to fully capture the electrical response of the material. The equations to calculate the admittance (Y^*) measured in Siemens (S), permittivity (ε^*), modulus (M^*), and dissipation factor ($tan\delta$) are presented below in Equations (1.5.11-1.5.15) [42].

$$Z^* = \frac{1}{j\omega C_0 \varepsilon^*} \tag{1.5.11}$$

$$\varepsilon^* = \varepsilon' + j\varepsilon'' \tag{1.5.12}$$

$$M^* = \frac{1}{\varepsilon^*} = M' + jM'' \tag{1.5.13}$$

$$Y^* = \frac{1}{Z^*} = Y' + jY'' \tag{1.5.14}$$

$$tan\delta = \frac{\varepsilon''}{\varepsilon'} \tag{1.5.15}$$

In the above equations C_0 is the geometric capacitance, which in the context of this thesis can be calculated as a function of the permittivity of free space or vacuum permittivity (ε_0) and sample geometry because the samples are measured in a parallel plate configuration. The equation used to calculate the geometric capacitance is presented in Equations (1.5.16-1.5.17) where A is the surface area in contact with the electrode, and t is the thickness through the sample between the two electrode plates.

$$C_0 = \frac{A}{t}\varepsilon_0 \tag{1.5.16}$$

Where the permittivity of free space is constant expressed as,

$$\varepsilon_0 = 8.8542 * 10^{-12}\ F/m \tag{1.5.17}$$

Additionally, the impedance and admittance are often normalized to sample geometry to calculate resistivity (ρ^*) and conductivity (σ^*), respectively. This normalization accounts for slight differences between sample geometry to allow for better comparison of electrical behavior. These equations are presented in Equations (1.5.18-1.5.19).

$$\rho^* = \frac{A}{t}Z^* = \rho' + j\rho'' \tag{1.5.18}$$

$$\sigma^* = \frac{t}{A}Y^* = \sigma' + j\sigma'' \tag{1.5.19}$$

1.5.2 Nyquist and Bode Plots

The dielectric functions are often plotted on Nyquist plots (frequency implicit) and Bode plots (frequency explicit) plots. In Nyquist plots, the real and imaginary parts are plotted on the x and y axis, respectively, with the y-axis inverted [43]. In Bode plots, the frequency is plotted on a log scale on the x-axis and the real part, imaginary part, function magnitude, or phase angle is plotted on the y-axis. For the magnitude and real part of the dielectric function, the y-axis is often plotted on a log scale and for the phase angle and the imaginary part of the dielectric function, the y-axis is often plotted on an inverted axis.

1.6 Measurement Error Analysis

A novel error analysis was developed in this work that condenses standard deviation errors measured across a wide frequency range to a single value. This allows for ease of comparison between composite samples made of the same compositions, and composite samples of varying compositions. The error analysis can be used to measure repeatability, which refers to error regarding consecutive measurements done of the same single sample, and reproducibility, which refers to the error regarding measurements done of different samples but of the same composition. The procedure developed is robust enough to use for any part (real, imaginary, magnitude, and phase angle) of the dielectric functions [44].

To calculate the repeatability error between the consecutive electrical measurements done for each respective sample, Equations (1.5.20-1.5.21) were used. Using Equation (1.5.20), a standard deviation percent error (std % $err_{meas,f}$) was calculated for each frequency point by dividing the standard deviation between the respective

measurements done at the frequency point of interest ($std_{meas,f}$) by the mean of the respective measurements at the same frequency point ($mean_{meas,f}$). To then condense these standard deviation errors between measurements done of the same sample down to a single value to represent the repeatability error of the sample, the standard deviation percent errors were then averaged over the total number of frequency points measured (N_f).

$$std\ \%\ err_{meas,f} = \frac{std_{meas,f}}{mean_{meas,f}} * 100\% \tag{1.5.20}$$

$$repeatability\ error = \frac{\Sigma\left(std\ \%\ err_{meas,f}\right)}{N_f} \tag{1.5.21}$$

To calculate the reproducibility error between different samples made of the same composition, Equation (1.5.22-1.5.23) were used. Similar to the repeatability error procedure, the standard deviation percent error (std % $err_{comp,f}$) was calculated for each frequency point. However, the standard deviation ($std_{comp,f}$) and mean ($mean_{comp,f}$) at the given frequency point for the reproducibility error is calculated using the mean responses of each respective sample of the same composition from their respective consecutive measurements. To then condense the standard deviation percent errors between samples of the same composition, the values were averaged over the total number of frequency points to represent the reproducibility error of the samples.

$$std\ \%\ err_{comp,f} = \frac{std_{comp,f}}{mean_{comp,f}} * 100\% \tag{1.5.22}$$

$$reproducibility\ error = \frac{\Sigma\left(std\ \%\ err_{comp,f}\right)}{N_f} \tag{1.5.23}$$

1.7 Research Objective

A goal of this work was to build upon the previous research done by Brian Bertram, who determined the percolation thresholds for SiC_w-Al_2O_3 composites fabricated using various densification methods such as hot-pressing, dry-pressing and pressureless-sintering, and extrusion and pressureless-sintering [10], [16], [21]–[23]. Additionally, although Justin Brandt previously studied spark-plasma sintered (SPS) SiC_w-Al_2O_3 composites [45], his focus was on the effect sintering aids play in the densification process rather than percolation. A primary goal in completing this research was to establish the percolation threshold of SPS SiC_w-Al_2O_3 composites, which had not been established yet in the literature, to compare to other densification methods. Hot-pressing in particular is of interest to compare to SPS as they are similar in their methods with both techniques using high temperature and pressure to sinter.

Furthermore, there has been extensive work done regarding the microwave sintering of SiC, Al_2O_3, and SiC-Al_2O_3 composites [46]–[50], but these studies do not focus on the microwave heating behaviors of the samples once sintered. Similarly, 3YSZ has been studied in the context of microwave sintering [51], [52] and its thermal runaway effect has also been reported in literature during the sintering process [53], [54]. The microwave heating behavior of already densified SiC-Al_2O_3 composites with varying compositions have not been extensively studied, although some research has been done in the area [28].

Another objective in this work was to characterize the microwave heating behaviors of SiC-Al_2O_3 densified composites, looking more closely at the effect the composition plays in bulk behavior. Additionally, although there has been work in simulating the

thermal runaway of pure ZrO_2 [37], there has not been an investigation of the thermal runaway of 3YSZ in its sintered form specifically, nor has there been studies looking into the impact 3YSZ has when introduced as an additional material in SiC-Al_2O_3 composites. Thus, this was another area of interest in this research.

2 EXPERIMENTAL METHODS

This chapter describes the equipment and techniques used to fabricate and characterize the samples. All samples were densified by spark plasma sintering (SPS) in vacuum, under the same temperature and pressure of 1500℃ and 50MPa for a hold time of 5 minutes, respectively. The primary characterization technique used was impedance and dielectric spectroscopy but other techniques such as SEM and EDS were used for further characterization.

2.1 Materials

In this study, the main composite matrix and filler materials used were Al_2O_3 and whisker β-SiC_w, respectively. However, 3 mol% yttria stabilized zirconia (3YSZ) was added as an additional matrix material to influence the microwave heating rate of the composite. The alumina from the Advanced Composites Materials manufacturer was from a previous study [10] and thus the particle size was unknown. All the materials used in this research study are presented below in Table 2.1.1.

Table 2.1.1 Materials used and presented in this work.

	Material	Particle Size	Manufacturer
Matrix	Al_2O_3	-	Advanced Composite Materials
	Al_2O_3	3 μm	AdValue
	3YSZ	40-80 nm	MSE Supplies
Filler	β-SiC whisker	d: 0.2-1.0 μm, l: 5-50 μm	Advanced Composite Materials

2.2 Spark-Plasma Sintering

SPS is a densification technique common for ceramic materials and involves the use of high temperatures and pressures to densify powders. SPS also includes a DC current that runs through the die, which allows for significantly higher heating rates and faster densification times as compared to other densification techniques such as hot-pressing for example. For this reason, graphite was used as the tooling and graphite foil was placed between tooling contact points due to graphite being conductive. A schematic of the SPS technique is shown in Figure 2.2.1[55].

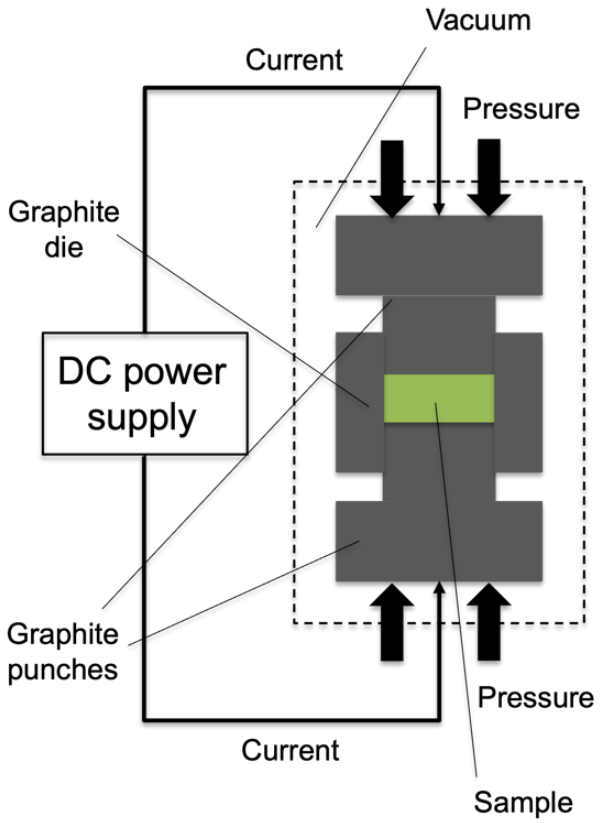

Figure 2.2.1 Schematic of the spark-plasma sintering technique. Modified from [55].

To densify the samples, a Fuji Electronic Industrial Co., LTD Dr. Sinter model SPS-211Lx was used, shown in Figure 2.2.2. Each sample was made using a uniaxial pressure of 50 MPa and a maximum hold temperature of 1500℃ in vacuum. The graphite die used had a diameter of 10 mm and was wrapped in carbon felt fastened with carbon twine to help insulate the die. A CHINO IR-AH series digital pyrometer was used to monitor the temperature pointed directly on the graphite die through a small viewing window cut out from the carbon felt as shown in Figure 2.2.2(b). The pyrometer used was unable to measure temperature below 573℃, and thus the first ramp in the temperature profile used in the densification process which was to ramp to 600℃ in 4 minutes is mostly uncaptured in temperature data and the heating rate is undetermined. However, the next ramp using a heating rate of 100℃/min up to 1500℃ with a hold of 5 minutes was able to be captured by the pyrometer.

(a) **(b)**

Figure 2.2.2 (a) Dr. Sinter model SPS-211Lx with a CHINO IR-AH pyrometer setup during an SPS run and (b) the graphite tooling used.

The hold temperature, time, and pressing pressure used was based on earlier work done by Justin Brandt who worked with 15% SiC_w-Al_2O_3 samples densified using the Model 10-4 Thermal Technology LLC spark-plasma-sintering machine at the Arizona Materials Laboratory led by Dr. Erica Corral [45].

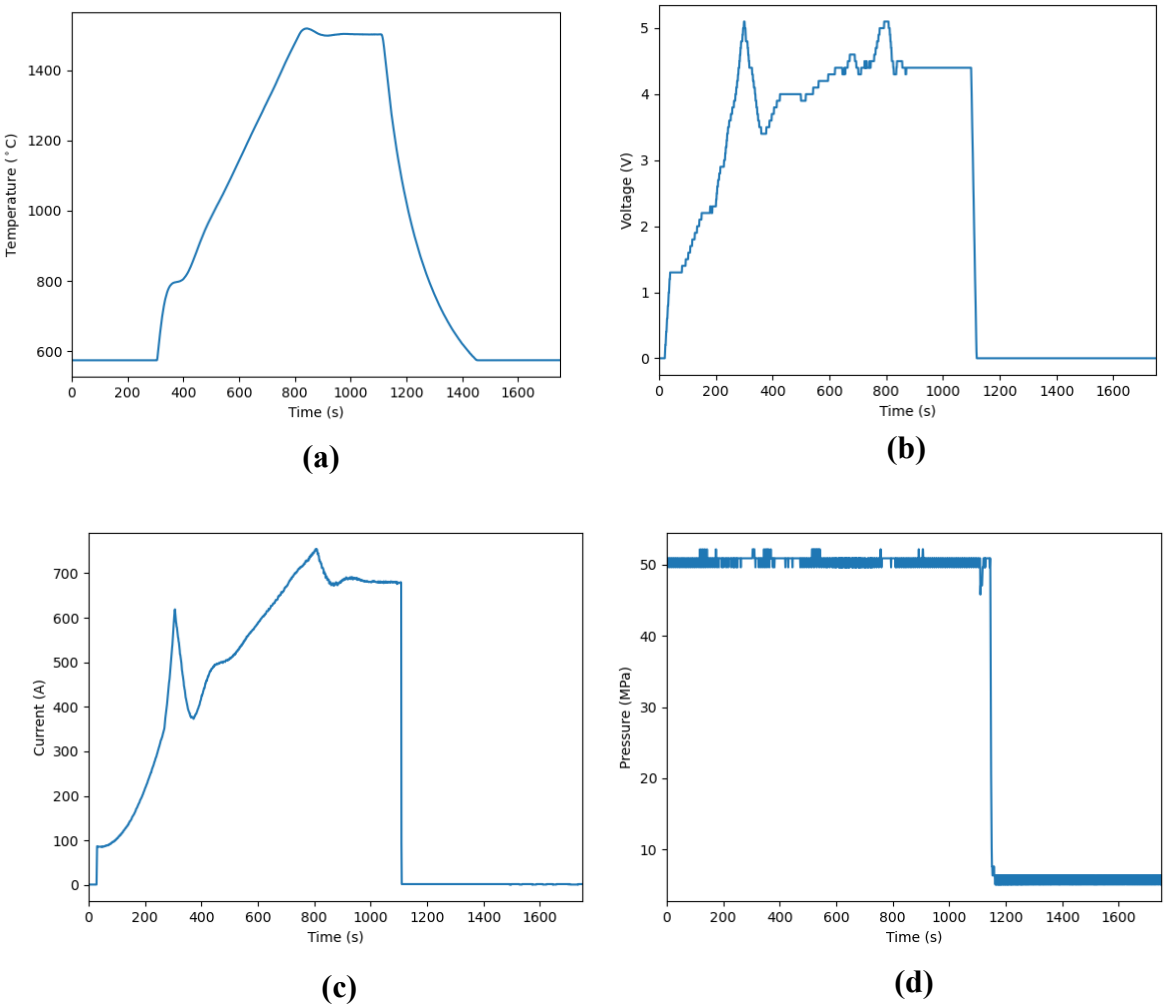

Figure 2.2.3 SPS (a) temperature, (b) voltage, (c) current, and (d) pressure during a run.

During densification, the equipment was connected to the Keyence WAVE LOGGER software to collect the temperature, pressure, tooling displacement, current, and voltage readings during a SPS run, as shown in Figure 2.2.3.

2.2.1 Expected Microstructure of SPS Samples

Similar to hot-pressing (HP), in SPS the SiC whisker orientation is influenced by the uniaxial pressing direction (PD) of the tooling, densifying the powder along the z-axis. Due to this and the SiC whiskers having a high aspect ratio, with a longer length than diameter, the SiC whiskers become aligned perpendicular to the pressing direction, but randomly oriented along the pressing direction as shown in Figure 2.2.4 [56].

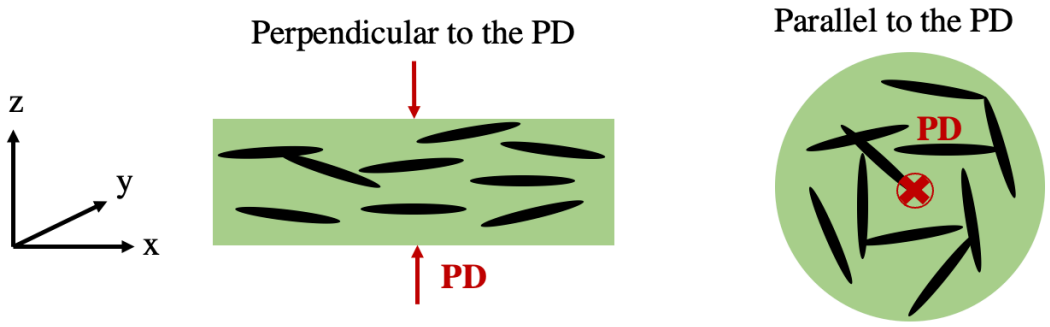

Figure 2.2.4 Expected microstructure and alignment of SiC whiskers (black) in the Al_2O_3 matrix (green) relative to the SPS pressing direction.

2.3 Polishing

Once the samples were sintered, they were then polished by hand using PSA backed diamond grinding discs from Buehler attached to glass platens on the Buehler Ecomet 250 Grinder Polisher shown in Figure 2.3.1. A 250 μm polishing disc was first used to grind

off the graphite foil on the sides and faces of the samples. Then 125, 70, 45, 15, and 6 μm diamond discs were used, respectively, to continue polishing down the surface of the samples with each disc being used for a total of 5 minutes grinding on each sample surface. The samples were rotated during the polishing process by 90° every minute or so to achieve uniform polishing across the surface. Additionally, a dressing stick was used after each sample face was polished to help remove contaminants on the polishing disc surface and maintain disc quality. If the samples were to be imaged, the polishing process was continued using Buehler MetaDi 3, 1, and 0.25 μm diamond polishing pastes on Buehler MicroCloth polishing pads. Additionally, Buehler MetaDi diamond suspensions of matching diamond paste grit were used rather than tap water to minimize contaminants scratching the surfaces of the samples during the diamond polishing paste step.

Figure 2.3.1 Buehler Ecomet 250 Grinder Polisher.

2.4 Electrode Deposition

If the samples were only measured and not imaged however, the diamond polishing paste step was not done, and the samples remained at a polishing step of 6 μm. Silver electrodes were then deposited onto the sample faces at this step to promote good electrode contact during electrical measurement in a parallel plate setup using the Denton Vacuum Desk II Turbo Sputter Coater shown in Figure 2.4.1. The pressure in the chamber was set at 50 millitorr, and the equipment was ran at 30% total power for 15 minutes under argon gas to adequately deposit silver on each face of the sample. Tape was wrapped along the edges of the samples to protect it from silver deposition to prevent electrical shorting when taking measurements. If silver was deposited on the sides of the sample, the sides were polished to remove the silver.

Figure 2.4.1 Denton Vacuum Desk II Turbo Sputter Coater.

2.5 Annealing Treatment

Some samples required an annealing treatment in order to oxidize samples that were reduced during the sintering process. The samples were placed in an alumina boat and placed into a tube furnace, shown in Figure 2.5.1, which was run at 900°C for a total of 4 hours with a temperature ramp of 300°C/hour. The furnace was run with oxygen gas flow and no gas flow (in air), depending on the annealing treatment used.

Figure 2.5.1 Tube furnace connected to oxygen gas tank used for annealing treatment.

2.6 Characterization Techniques

All techniques used to characterize the samples presented in this study are discussed in this section.

2.6.1 Impedance and Dielectric Spectroscopy

Electrical characterization of the samples was performed by using AC impedance and dielectric spectroscopy. All samples were measured using a parallel plate configuration through the thickness of the sample with the Solartron 12962 sample holder as shown in Figure 2.6.1. Impedance measurements were taken using the Solartron 1260 connected in parallel to the Solartron 1296 using an AC voltage of 500 mV over a frequency range of 10 MHz to 100 mHz, gathering 15 datapoints per decade. Prior to the samples being sputtered with silver electrodes, each sample's diameter and thickness was measured using the Mitutoyo Corp model 500-196 digital calipers to measure sample geometry.

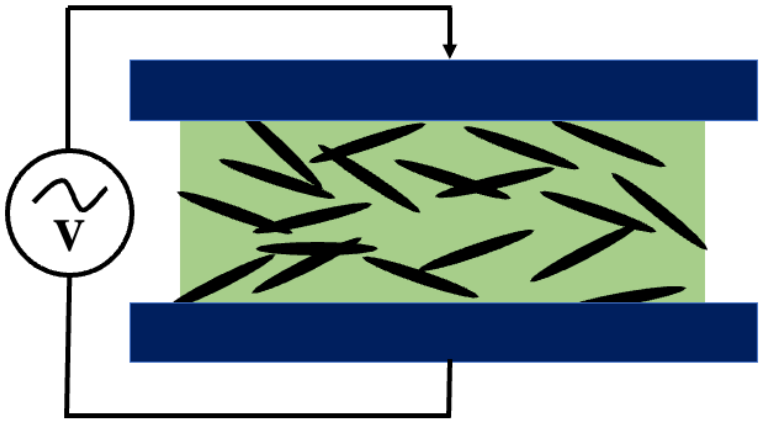

Figure 2.6.1 Measurement of a sample in a parallel plate configuration through the sample thickness.

The sample holder was placed inside an ETS humidity chamber to isolate the sample from the surrounding environment and control the humidity and temperature of the

measurement. All electrical measurements were taken at 16% room humidity and 22°C, controlled by the ETS Dual Control Model 5200, to minimize the effects of humidity on the electrical behavior of the sample. The experimental set-up for electrical measurements is shown in Figure 2.6.2.

(a) **(b)**

Figure 2.6.2 (a) The Solartron 1260, the Solartron 1296, and ETS humidity chamber with the ETS Dual Controller Model 5200 on top, from left to right and (b) the Solartron 12962 Sample Holder inside the ETS humidity chamber.

2.6.2 Optical Microscopy

The densified samples were imaged using a Celestron Infiniview LCD Digital Microscope, shown in Figure 2.6.3, to visually inspect the surface porosity and homogeneity of the samples.

Figure 2.6.3 Celestron Infiniview LCD Digital Microscope.

2.6.3 Scanning Electron Microscopy

Scanning electron microscopy (SEM) was used to gain insight into the microstructure of the SiC_w-Al_2O_3 and 3YSZ-SiC_w-Al_2O_3 composite samples. A Zeiss Ultra 60 SEM was used with aid from Yolande Berta at the IEN/IMAT Materials Characterization Facility at Georgia Tech to capture images of the samples [57]. The images were taken using the InLens detector at an accelerating voltage of 5kV with all samples mounted onto metal SEM stubs using conductive carbon tape. No sputtering was necessary to image the samples. An energy dispersive X-ray spectroscopy (EDS) attachment was also used with the SEM to perform element mapping on regions of interest on samples. 5kV was used as the accelerating voltage with the EDS attachment to prevent charging in the samples.

Figure 2.6.4 Zeiss Ultra 60 SEM at the IEN/IMAT at Georgia Tech.

2.6.4 COMSOL Simulations

COMSOL Multiphysics was used as a finite element analysis, solver, and multiphysics simulation software. Specifically, the built-in physics for heat transfer, electromagnetic heating, and microwave heating was used to simulate otherwise experimentally difficult studies regarding the heating of composite materials under a microwave frequency. The simulated temperature, electric field, and resistive losses of these composite materials were used as the primary metrics to measure how the materials heat up with time.

2.7 Summary

This chapter presented the materials used, the methods used to fabricate the composite samples, and outlines the procedure used to prepare the samples for measurement. The primary characterization method used was impedance spectroscopy but additional techniques such as optical microscopy, SEM, and COMSOL simulations were used. The next chapter will describe the composites made.

3 SAMPLES FABRICATED

This chapter describes the composite samples made and presented for this thesis, as well as the conditions and methods used to fabricate them. All compositions are expressed in terms of volume percent not weight percent. For each composition, a minimum of three samples were made and measured to ensure that the electrical behavior was reflective of the composition. The samples are composites and thus will vary slightly between sample to sample made from the same composition. Additionally, each sample was measured out to an initial mass of 0.6g but the resulting sample geometry presented in this chapter varies slightly due to the polishing process.

3.1 SiC_w-Al_2O_3 Composites with Varying SiC_w Content

The SiC_w-Al_2O_3 sample compositions used were made in bulk in a previous percolation study for HP densified SiC_w-Al_2O_3 samples and contained SiC whisker content ranging from 0% to 30% with a total of 1% MgO and 1% Y_2O_3 [22]. The actual whisker content was determined using a LECO carbon analyzer which tracked the oxidized carbon products of SiC decomposition are presented in Table 3.1.1. Using these same mixes, new SiC_w-Al_2O_3 samples were densified with the SPS technique using a constant temperature and pressure of 1500°C and 50 MPa, respectively.

Table 3.1.1 Target and measured volume percents of SiC_w used in the SPS SiC_w-Al_2O_3 composites study.

Target vol% SiC_w [22]	0	2.5	5	7.5	10	12.5	15	17.5	20	25	30
Actual vol% SiC_w [22]	1.09	3.52	5.81	7.68	9.96	12.2	14.5	17.0	19.1	24.0	28.2
SPS Temp (°C)	1500	1500	1500	1500	1500	1500	1500	1500	1500	1500	1500
SPS Pressure (MPa)	50	50	50	50	50	50	50	50	50	50	50

To complete the percolation study, three samples of each composition were made, and each respective sample's geometry are reported below in Table 3.1.2. The sample geometries presented are averaged values from three separate measurements made of the respective diameter and thickness of the samples.

Table 3.1.2 SiC_w-Al_2O_3 SPS composites made and their measured geometry.

SiC_w Content	**Sample**	**Average Diameter (mm)**	**Average Thickness (mm)**	**Area/Thickness Ratio (cm)**
1.09%	S1	10.040	1.397	5.668
	S2	10.017	1.383	5.697
	S3	9.953	1.417	5.492
3.52%	S1	10.003	1.410	5.572
	S2	9.997	1.441	5.446
	S3	9.754	1.509	4.951
5.81%	S1	9.960	1.517	5.137
	S2	9.897	1.457	5.281
	S3	9.923	1.477	5.237

7.68%	S1	9.993	1.517	5.172
	S2	10.000	1.513	5.190
	S3	9.963	1.557	5.008
9.96%	S1	10.140	1.557	5.188
	S2	10.063	1.533	5.187
	S3	10.020	1.567	5.033
12.2%	S1	10.027	1.527	5.172
	S2	10.020	1.583	4.980
	S3	10.033	1.540	5.134
14.5%	S1	10.153	1.570	5.157
	S2	10.117	1.543	5.208
	S3	10.117	1.550	5.186
17.0%	S1	10.077	1.580	5.047
	S2	10.040	1.653	4.788
	S3	10.093	1.590	5.032
19.1%	S1	10.167	1.537	5.283
	S2	10.077	1.557	5.123
	S3	10.077	1.583	5.037
24.0%	S1	10.073	1.627	4.899
	S2	10.147	1.640	4.931
	S3	10.083	1.613	4.950
28.2%	S1	10.147	1.647	4.911
	S2	10.090	1.563	5.115
	S3	10.070	1.623	4.906

3.2 3YSZ-SiC_w-Al_2O_3 Composites

Before adding any 3YSZ to the mixes, 6 total samples were made with no 3YSZ volume content to compare the electrical response of the composites before and after 3YSZ was added as an additional material. Two mixes were made with different aluminas; one alumina powder from AdValue referred to as the 15% SiC_w-Al_2O_3 mix, and one alumina from Advanced Composite Materials referred to as the 15% Type E SiC_w-Al_2O_3 mix. The Advanced Composite Materials 15% Type E SiC_w-Al_2O_3 mix was already made from a previous study [45] and contained no sintering additives, but the AdValue 15% SiC_w-Al_2O_3 samples were made by measuring 15% SiC_w and 85% Al_2O_3 by volume. The mix was then

speed-mixed at 1000 RPM for a total of 5 minutes, manually shaking the composition between each 1 minute run, and then mortar and pestled for ~35 minutes total. The samples with no 3YSZ are summarized below in Table 3.2.1.

Table 3.2.1 15% SiC_w-Al_2O_3 and 15% Type E SiC_w-Al_2O_3 SPS composites made and their measured geometry.

Mix	Alumina Manufacturer	Sample	Average diameter (mm)	Average thickness (mm)	Area/thickness ratio (cm)
15% SiC_w-Al_2O_3	AdValue	S1	9.787	1.463	5.141
		S2	9.800	1.547	4.877
		S3	9.720	1.567	4.736
15% Type E SiC_w-Al_2O_3	Advanced Material Composites	S1	10.183	1.653	4.927
		S2	10.15	1.61	5.026
		S3	10.043	1.613	4.910

Table 3.2.2 Masses and related data of Al_2O_3, SiC_w, and 3YSZ used to create a total of 5g of 2% 3YSZ – 15% SiC_w – 83% Al_2O_3 composites.

Material	Density (g/cm)	Volume Percent (%)	Mass (g)
Al_2O_3	3.95	83	4.2238
SiC_w	3.21	15	0.6203
3YSZ	6.05	2	0.1559

3YSZ-SiC_w-Al_2O_3 composite samples were fabricated with 3 mol% YSZ (3YSZ) using the same SPS densification procedure outlined in Chapter 2. A volume composition of 15% SiC_w, 2% 3YSZ, and 83% Al_2O_3 was made by measuring out the masses of the

respective constituent materials to yield a total of 5g, as listed in Table 3.2.2. No sintering aids were added in the 3YSZ-SiC_w-Al_2O_3 composite sample compositions.

Table 3.2.3 3YSZ-SiC_w-Al_2O_3 composites made with AdValue Al_2O_3, their measured geometry, and annealing conditions.

Sample	Average diameter (mm)	Average thickness (mm)	Area/thickness ratio (cm)	Notes
S1	9.823	1.533	4.943	Not annealed
S2	9.680	1.453	5.064	Not annealed
S3	9.687	1.463	5.036	Not annealed
S4	9.960	1.497	5.206	Annealed in air, 900°C 4 hrs
S5	9.880	1.510	5.077	Annealed in air, 900°C 4 hrs
S6	9.927	1.527	5.069	Annealed in air, 900°C 4 hrs
S7	9.963	1.517	5.141	Annealed in O_2, 900°C 4 hrs
S8	9.960	1.477	5.276	Annealed in O_2, 900°C 4 hrs
S9	9.810	1.500	5.039	Annealed in O_2, 900°C 4 hrs

The mixed ratios shown in Table 3.2.2 were speed-mixed at 1000 RPM for a total of 5 minutes, manually shaking the composition between each 1 minute run. The powder composition was then mixed by hand using a mortar and pestle. For samples S1-S3 listed in Table 3.2.3, the powder composition was only mortar and pestled for ~10 minutes, but for samples S4-S9, the powder composition was mixed for an additional ~25 minutes resulting in a total mortar and pestle time of ~35 minutes. In the SPS procedure, the samples were densified under vacuum which resulted in the 3YSZ being reduced. An annealing treatment was done in an effort to oxidize the 3YSZ in the samples to capture the true electrical response of the composite samples. Samples S4-S6 were annealed in air for 4

hours at 900°C, and samples S7-S9 were annealed in oxygen for 4 hours at 900°C. The sample geometries are also presented in Table 3.2.3.

Additionally, 3YSZ-Type E SiC_w-Al_2O_3 samples were fabricated by adding 2% 3YSZ volume content to the already made 15% Type E SiC_w-Al_2O_3 mix. Similar to the other samples, the mix was speed-mixed at 1000 RPM for a total of 5 minutes, manually shaking the composition between each 1 minute run and was then mortar and pestled for ~35 minutes. A total of 6 samples were made, S1-S3 which were not annealed and S4-S6 which were annealed in O_2 at 900°C for 4 hours. The list of all 3YSZ-Type E SiC_w-Al_2O_3 composites fabricated and their relevant information is shown in Table 3.2.4.

Table 3.2.4 3YSZ-Type E SiC_w-Al_2O_3 composites made with Advanced Composite Materials Al_2O_3, their measured geometry, and annealing conditions.

Sample	Average diameter (mm)	Average thickness (mm)	Area/thickness ratio (cm)	Notes
S1	9.990	1.520	5.157	Not annealed
S2	10.050	1.457	5.446	Not annealed
S3	9.963	1.503	5.186	Not annealed
S4	9.973	1.523	5.128	Annealed in O_2, 900°C 4 hrs
S5	10.013	1.557	5.059	Annealed in O_2, 900°C 4 hrs
S6	10.063	1.503	5.291	Annealed in O_2, 900°C 4 hrs

3.3 Summary

To understand the percolation threshold of SPS fabricated SiC_w-Al_2O_3 composite samples, 3 samples were made for the 11 different compositions made ranging from 1.09% to 28.2% SiC whisker content, totaling 33 SiC_w-Al_2O_3 composite samples. Additionally,

15% SiC_w-Al_2O_3 composite samples were made from two different manufacturers of alumina to compare the differences of the samples prior to any 3YSZ being added. Lastly, 2% 3YSZ- SiC_w-Al_2O_3 composite samples were made with the different aluminas and underwent varying annealing treatments to ultimately influence the microwave heating behavior of the samples. All samples presented in this chapter were fabricated using SPS. This chapter listed the samples made, their composition, their geometry, and their annealing treatment if applicable. In the next chapter, the experimental percolation study results are presented, which were completed using the SiC_w-Al_2O_3 composite samples.

4 PERCOLATION STUDY OF SPARK PLASMA SINTERED SiC_w-AL_2O_3 COMPOSITES

Previous work has been done to establish the percolation threshold of SiC_w-Al_2O_3 composites made with various densification techniques such as hot-pressing (HP), extrusion and pressureless sintering, and dry-pressing and pressureless sintering [22]. However, the percolation threshold for SPS densified SiC_w-Al_2O_3 composites has not yet been established in the literature and is presented in this chapter.

4.1 Electrical Characterization

As described previously in Chapter 3, 3 SiC_w-Al_2O_3 composite samples were made for each composition and were measured using impedance spectroscopy. Figure 4.1.1 shows the average resistivity magnitude response across the frequency range. Each resistivity magnitude response plotted of a given SiC_w composition is of a single sample for the sake of conciseness. Note that the standard deviation of the three consecutive impedance measurements is plotted as the error bars since the standard deviation percent error would be too small to see on the plot. With increasing SiC_w content, the resistivity magnitude decreases slightly, and is followed by a large drop in resistivity at 7.68% SiC_w volume percent indicating that the percolation threshold lies at 7.68% SiC_w volume percent. As SiC_w continues to increase past this point, the resistivity drastically decreases again from 7.68% to 9.96% SiC_w content before gradually decreasing in magnitude again.

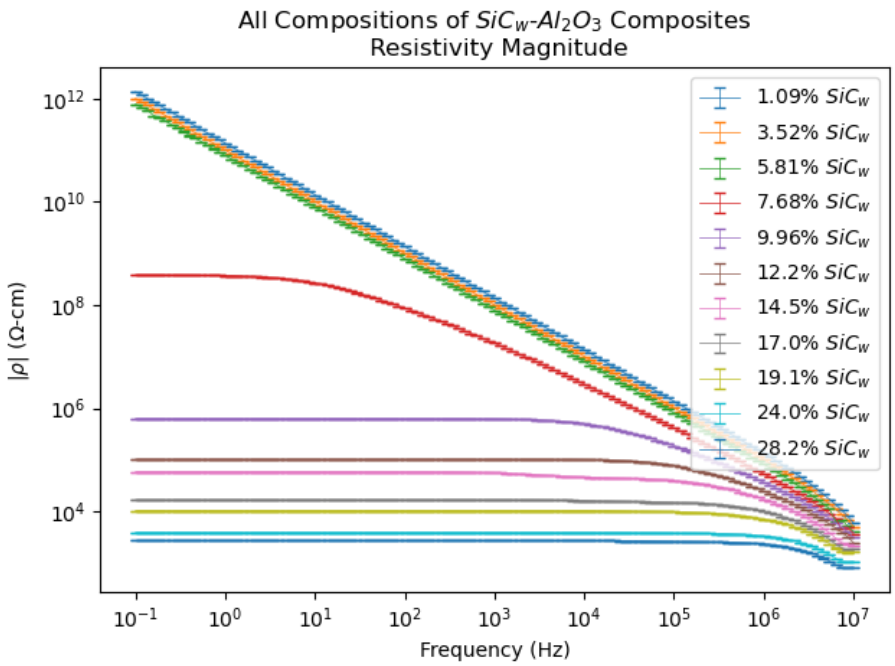

Figure 4.1.1 Average resistivity magnitude of SiC_w-Al_2O_3 composites with varying SiC_w volume content.

In the regions above and below the percolation threshold, where the resistivity magnitude decreases only slightly with increasing SiC_w content, the composite demonstrates stable and consistent conducting or insulating behavior, respectively. At the highest SiC_w content, the response is almost completely dominated by DC behavior from the conducting whiskers as indicated by the "flat" region, where there is little to no change in the resistivity magnitude with decreasing frequency. Conversely, the compositions containing lower SiC_w content are more dominated by the insulating matrix as indicated by decreasing resistivity magnitude with increasing frequency with little to no "flat" region observed. Additionally, the standard deviation errors for all respective compositions across the entirety of the frequency range is relatively small, indicating that the three measurements made of the respective samples show a relatively high level of repeatability.

The same trend can be seen in the complex resistivity of the varying SiC_w-Al_2O_3 compositions in Figure 4.1.2. As with Figure 4.1.1. the responses plotted are of a single sample of each respective composition, with the standard deviation of the three consecutive electrical measurements plotted across the frequency range.

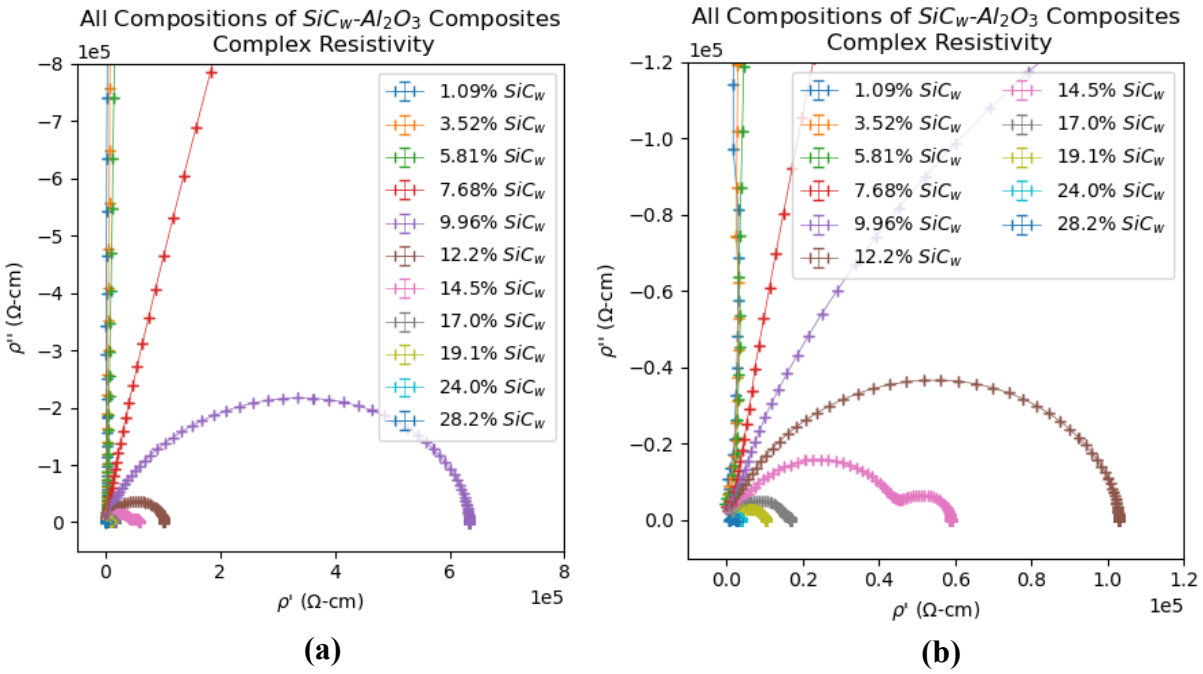

Figure 4.1.2 Complex resistivity of SiC_w-Al_2O_3 composites with varying SiC_w volume content and (b) a zoomed-in view.

At low SiC_w volume contents below the percolation threshold, the observed semi-circle is too large to be displayed on the same plot and appears almost like a vertical line, indicating a large overall resistance of the samples made with compositions of 1.09% and 3.52% SiC_w content. At 7.68% SiC_w, there is a noticeable decrease in the diameter of the semi-circle indicating that the resistance of the samples has decreased. As the whisker content is increased past this composition, a full semi-circle is formed with some

compositions forming two semi-circles in the complex resistivity. The width of the semi-circle increases with increasing whisker content, indicating increasing conductivity with increasing SiC_w content. The composition where the complex resistivity response changes most drastically however is at the 7.68% SiC_w further supporting the conclusion that the percolation threshold occurs at this composition.

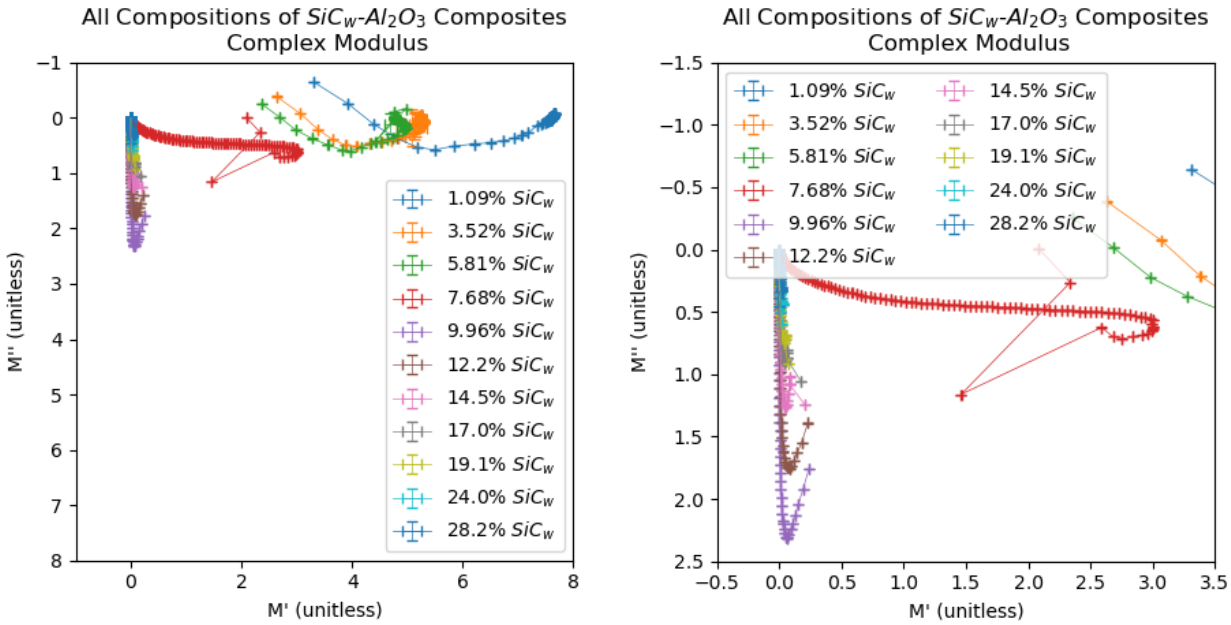

Figure 4.1.3 Complex modulus of SiC_w-Al_2O_3 composites with varying SiC_w volume content and (b) a zoomed-in view.

A similar response is seen in the complex modulus response of the compositions in Figure 4.1.3, where the behavior of the compositions can be grouped into insulating behavior, conducting behavior, with the 7.68% SiC_w composition response displaying the transition between the two groups.

The samples with low whisker content are characterized by not starting at the origin and having a low imaginary modulus response but large real modulus response. Conversely, the samples with higher whisker content all start at the origin of the plot and have a larger imaginary modulus response than real imaginary response, which decreases with increasing whisker content. The 7.68% SiC_w composition displays transitionary behavior between the two previously described groups. At 7.68% SiC_w content, the complex modulus response begins at the origin and has a large real modulus response compared to the imaginary modulus response. This again demonstrates that the 7.68% SiC_w composition is the whisker content percentage at which a transition occurs in the overall electrical behavior of the composite samples.

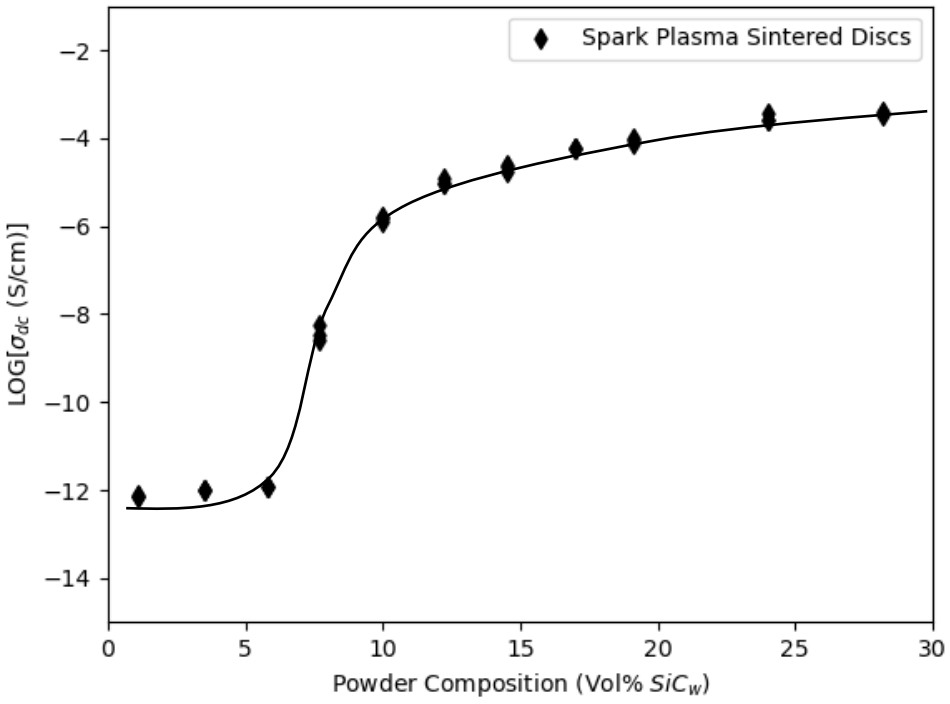

Figure 4.1.4 Percolation curve of SPS SiC_w-Al_2O_3 of varying SiC whisker content. Modified from [44].

The transition from insulating to conducting behavior is more evident in the DC conductivity percolation curve presented in Figure 4.1.4 where each sample is plotted as a single data point yielding three points per composition. The DC conductivity was calculated using the conductivity magnitude value of each respective sample at the lowest frequency (10^{-1} Hz) as the imaginary magnitude is negligible at this frequency. Inversely related to the resistivity, the DC conductivity rises with increases SiC_w content and sharply increases from 5.81% to 9.96% SiC_w content, indicated that the composite has undergone a transition from insulating, characterized by a low conductivity, to conducting, indicated by a high DC conductivity. The DC conductivity continues to gradually increase with increasing SiC_w content, with the highest DC conductivity seen in the 28.2% SiC_w samples. There is, however, a single sample of the 24.0% SiC_w composition that yields the highest DC conductivity overall. Compared to the other two samples of the 24.0% SiC_w composition, this sample appears to be an outlier.

4.1.1 Error Analysis

As shown in Figure 4.1.4, the spread of DC conductivity values is widest at the percolation threshold of 7.68% SiC_w content, where the slight difference in whisker contact within the composite can result in drastic differences in the electrical response. Additionally, the 14.5% SiC_w samples also show a relatively wide spread in the DC conductivity, as compared to the compositions both below and above the percolation threshold which show little variance in the DC conductivity between samples. In the 14.5% SiC_w composition, a single sample shows a lower DC conductivity that the other two samples of the same composition. At a SiC_w content of 14.5%, the samples are well above

the percolation threshold and therefore are expected to show high reproducibility with only slight difference in the DC conductivity or resistivity. This could be due to the heterogeneous nature of the composites. At higher concentrations, deviations are much smaller as previously described.

Table 4.1.1 Total reproducibility errors across the measured frequency range in all resistivity measurements of SiC_w-Al_2O_3 composite compositions.

SiC_w Volume Percent (%)	**1.09**	**3.52**	**5.81**	**7.68**	**9.96**	**12.2**	**14.5**	**17.0**	**19.1**	**24.0**	**28.2**
Reproducibility Error – Real Resistivity (%)	4.78	3.98	6.84	8.54	3.67	3.01	5.92	2.12	2.90	3.01	2.15
Reproducibility Error – Imaginary Resistivity (%)	3.24	4.20	5.33	3.49	2.09	3.70	2.88	3.91	2.04	1.09	2.46
Reproducibility Error – Resistivity Magnitude (%)	3.87	6.90	6.19	4.89	4.05	3.64	3.12	3.05	2.89	3.05	1.08
Reproducibility Error – Resistivity Phase Angle (%)	2.58	4.91	4.90	4.45	2.84	2.88	3.95	3.59	2.08	1.93	2.09

Performing the error analysis outlined in Chapter 1, the total standard deviation percent errors of overall composite compositions (reproducibility errors) of the samples shown in Figure 4.1.4 are presented in Table 4.1.1. Generally, the reproducibility errors for all resistivity measurements done for each composition is calculated to be <5% across the frequency range measured. This is especially true for compositions far below or far above the percolation threshold, where the transition in electrical behavior has not yet occurred or has already occurred, respectively, meaning that the samples are highly reproducible.

However, the 5.81% and 7.68% SiC_w compositions show the highest errors overall, particularly in the real resistivity where the whisker contact begins to dominate the response. This supports the assumption that the resistivity magnitude taken where the imaginary resistivity is negligible can be taken as the inverse of the DC conductivity of the sample, as the high real resistivity errors near the percolation threshold arises from the sensitivity and formation of SiC_w interconnected DC paths.

However, the imaginary resistivity, resistivity phase angle, and resistivity magnitude show higher errors at these compositions as well. Near the percolation threshold, slight differences in whisker contact homogeneity of the sample can result in a large difference in the resulting complex resistivity components.

The higher reproducibility errors in the real resistivity of the 14.5% and 24.0% SiC_w samples is in agreement with the variance of the DC conductivity data at these compositions due to the outlier samples as seen in Figure 4.1.4. Although the differences in the DC conductivities of the respective samples containing 14.5% and 24.0% SiC_w volume content are small, they are able to be captured in the total real resistivity reproducibility errors. The imaginary resistivity as well as the resistivity magnitude and phase angle at these compositions do not show significantly higher errors at these compositions, however.

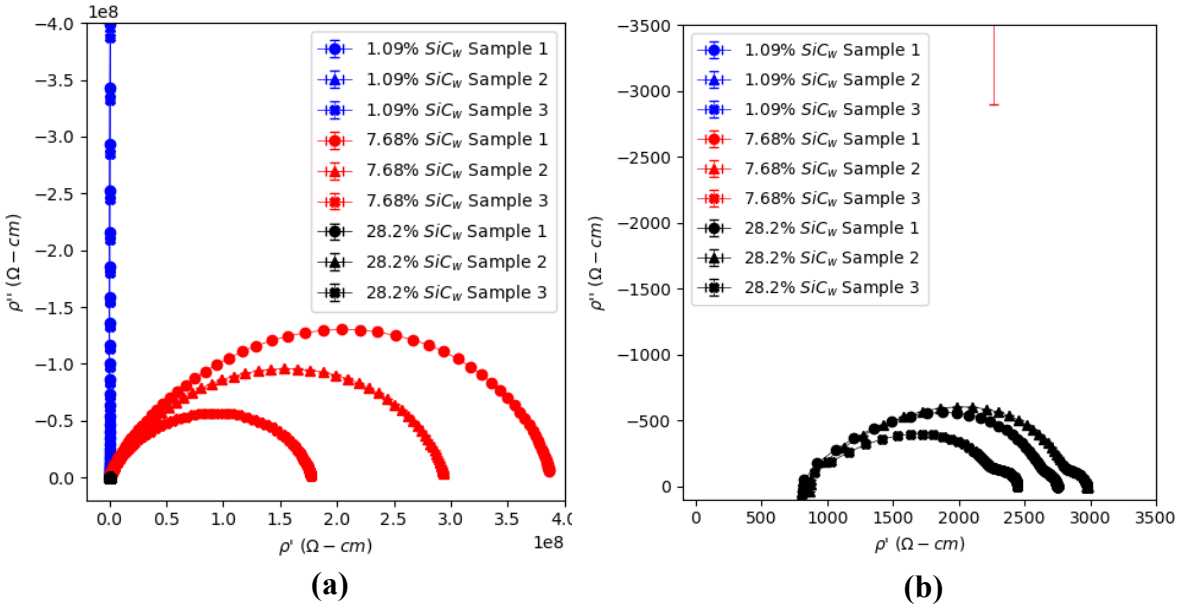

Figure 4.1.5 (a) Complex resistivity of SiC_w -Al_2O_3 composites below, near, and above the percolation threshold and (b) a zoomed in view of the 28.2% SiC_w samples.

To demonstrate the reproducibility more clearly in the samples made from the same composition Figure 4.1.5 plots the average complex resistivity of the individual respective samples made for compositions below, near, and above the percolation threshold. This corresponds to 1.09%, 7.68%, and 28.2% SiC_w volume content compositions, respectively. The standard deviation of the three individual measurements taken of each sample is plotted for the real and imaginary resistivity values. However, since these errors are calculated from consecutive measurements done of the same sample, the resulting standard deviation error is too small to see across the frequency range on the plot and are rather presented in Table 4.1.2. The repeatability errors for all 33 SiC_w-Al_2O_3 samples are presented in the Appendix Chapter A.1.

Figure 4.1.5 again demonstrates the clear transition in electrical behavior from insulating to conducting as indicated by the width of the semi-circle in the complex plot decreasing with increasing SiC_w content. All samples of 1.09% SiC_w composition have a semi-circle that is too large to capture from the frequency range measured, but the samples show slight variance in the imaginary resistivity values. The data for the 28.2% SiC_w content samples also demonstrate high reproducibility, with Sample 3 having a slightly smaller semi-circle than Samples 1 and 2, which closely overlap in the complex resistivity plot.

The largest spread in the complex resistivity responses between samples of the same composition is seen in the 7.68% SiC_w composite samples. Sample 1 of the 7.68% SiC_w composition has a complex resistive response more than double the size of the semi-circle belonging to Sample 3 of the same composition, with Sample 2 falling between the two respective semi-circles. Between these three samples, both the real resistivity and the imaginary resistivity varies by more than double. This variance in the in the complex resistivity responses of the samples at the 7.68% SiC_w composition is due to the sensitivity of the composite closer to the percolation threshold. Similar variations in values around the percolation threshold has also been observed in other insulator-conductor composite samples [58], [59]. At this point, slight differences in whisker contact in the microstructure of the sample can determine whether the sample forms a fully interconnected SiC whisker network within the insulating alumina matrix. The formation of this network would provide a clear path for DC current to travel through within the microstructure. This would thereby decrease the overall resistance of the composite given by the width of the semi-circle in

the complex resistivity response. This is reflected in the differences in the complex resistivity spectra of the 7.68% SiC_w samples shown in Figure 4.1.5.

Table 4.1.2 Total repeatability errors across the measured frequency range in all resistivity measurements of SiC_w-Al_2O_3 composite samples shown in Figure 4.1.5.

SiC_w Volume Percent		Repeatability Error – Real Resistivity (%)	Repeatability Error – Imaginary Resistivity (%)	Repeatability Error – Resistivity Magnitude (%)	Repeatability Error – Resistivity Phase Angle (%)
1.09%	**Sample 1**	0.088	0.018	0.017	0.026
	Sample 2	0.059	0.014	0.024	0.023
	Sample 3	0.032	0.014	0.044	0.067
7.68%	**Sample 1**	0.045	0.103	0.034	0.010
	Sample 2	0.066	0.170	0.058	0.015
	Sample 3	0.374	0.480	0.178	0.410
28.2%	**Sample 1**	0.039	0.045	0.039	0.067
	Sample 2	0.011	0.043	0.011	0.053
	Sample 3	0.038	0.089	0.038	0.013

In all the resistivity measurements, the total repeatability error calculated is <0.1% generally, with slightly higher errors calculated for Samples 2 and 3 of the 7.68% SiC_w compositions. The total errors for the 1.09% and 28.2% SiCw composites are particularly low, with the majority of repeatability errors being less than <0.05%. similar error values were calculated for all samples across the composition range. Low errors in consecutive electrical measurements carried out on the same sample given identical measurement

conditions are expected to be low regardless of percolation behavior. However, at the percolation threshold of 7.68% SiC_w content, the repeatability errors are consistently higher than those for the 1.09% and 28.2% compositions, which lie far below and above the percolation threshold, respectively. That is, the samples at the percolation threshold have lower overall repeatability.

This higher error is attributed to the SiC_w network potentially only having a few number of paths or even a single path for the DC current to travel through as compared to when the sample is fully percolated at 28.2% SiC_w, where multiple interconnected whisker paths are formed and multiple DC paths are available. The samples at the percolation threshold therefore demonstrate higher errors in the electrical measurements of the same sample likely due to the DC current having limited complete paths to travel through, with a higher number of almost fully interconnected path formed, resulting in more varied electrical responses and lower repeatability.

4.1.2 Comparison to Hot Pressing

As mentioned previously, the SiC_w-Al_2O_3 compositions used in the SPS percolation study were used in a similar HP percolation study. SPS and HP are similar densification techniques because they both use high temperatures and uniaxial pressure to densify the material, but SPS includes a current that runs through the tooling that allows for higher heating rates and faster sintering times. Due to the similarity of the techniques, SiC_w-Al_2O_3 samples made from HP and SPS should be similar in microstructure and electrical behavior.

Plotting the respective SiC_w-Al_2O_3 samples densified using SPS and HP in Figure 4.1.6, however, there are distinct differences between the samples made from the two respective densification techniques. For the HP samples, as the SiC whisker content is increased from 1.09% to 5.81%, there is a decrease in conductivity whereas for the sample compositions made from SPS, there is an increase in conductivity with increasing whisker content. For the 1.09% SiC_w HP samples, there is a large variance with one sample having a significantly higher conductivity as compared to the other samples made at the same composition. Additionally, there is also a relatively high variance in conductivities for the 5.81% SiC_w HP samples. For the SPS samples below the percolation threshold, the variance in conductivities between the samples are low.

At a composition of 7.68% SiC whisker content however, there is a sharp increase in the conductivity for the HP and SPS samples indicating that for both densification methods, the percolation threshold lies at 7.68% SiC whisker composition. At the percolation threshold, the HP samples are ~ 2 orders of magnitude more conductive than the SPS samples, but the spread of conductivities at the percolation threshold are comparable for both densification methods. Past the percolation threshold, the HP samples have consistently higher conductivities than the SPS samples by less than an order of magnitude as shown in Table 4.1.3. From 9.96% to 28.2% SiCw content, the samples made from HP and SPS both steadily increase as the SiC whisker semi-conducting behavior begins to dominate the bulk response of the composites.

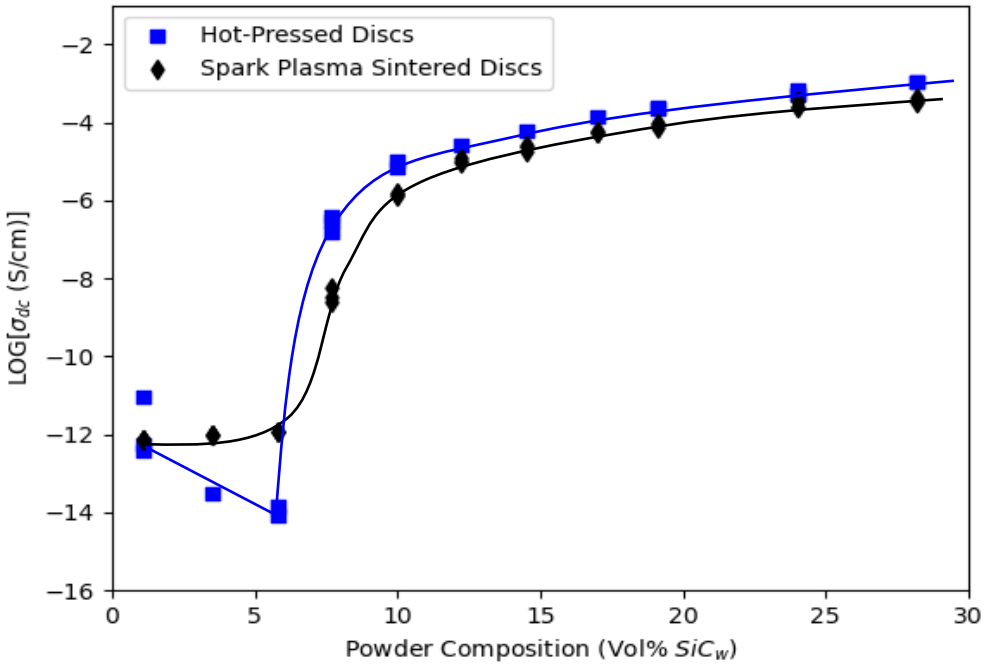

Figure 4.1.6 Percolation curves of SPS and HP SiC_w-Al_2O_3 composites of varying SiC whisker contents. Modified from [55].

The difference in behavior is likely due to the differences in relative densities of the samples made from the two different sintering methods. The HP samples have higher densities than the SPS samples, although it is worth noting that the HP sample densities were calculated using the Archimedes method while the SPS sample densities were calculated using geometric density. With the exception of the 24.0% and 28.2% SiC whisker compositions, the HP samples are fully dense, whereas for the SPS samples, only the 1.09% and 3.52% SiC whisker compositions reach full density. The HP densification method is unable to achieve as high heating rates as SPS, and thus the overall sintering

time for HP is longer than that of SPS. This could potentially be a factor in the density differences between the respective samples.

Table 4.1.3 Average log of the conductivities of the SiC_w-Al_2O_3 compositions fabricated using HP and SPS and their average densities.

SiC_w Volume Percent (%)	Average HP $\log(\sigma_{DC})$ (S/cm)	Average SPS $\log(\sigma_{DC})$ (S/cm)	Average HP Density (% Theoretical)	Average SPS Density (% Theoretical)
1.09	-11.908	-12.132	100	100
3.52	-13.498	-12.003	100	100
5.81	-13.967	-11.927	100	99.9
7.68	-6.602	-8.433	100	99.5
9.96	-5.082	-5.839	100	99.5
12.2	-4.569	-4.989	100	99.1
14.5	-4.207	-4.670	100	98.7
17.0	-3.868	-4.243	100	98.6
19.1	-3.624	-4.069	100	97.9
24.0	-3.251	-3.548	99.8	97.1
28.2	-2.950	-3.434	99.1	96.3

4.2 Microstructure Characterization (Optical and SEM)

All compositions of the SPS SiC_w-Al_2O_3 composites were imaged using the Celestron Infiniview optical microscope and are shown in Figure 4.2.1. Starting from Figure 4.2.1(a) to Figure 4.2.1(k), as the SiC whisker content is increased, the surface of the samples become more heterogenous. Darker regions are introduced as the SiC whiskers are dispersed throughout the microstructure of the composite samples. Additionally, the surfaces of the samples do not appear to be porous, supporting the density measurements in Table 4.1.3, nor do they appear to have significant agglomerates.

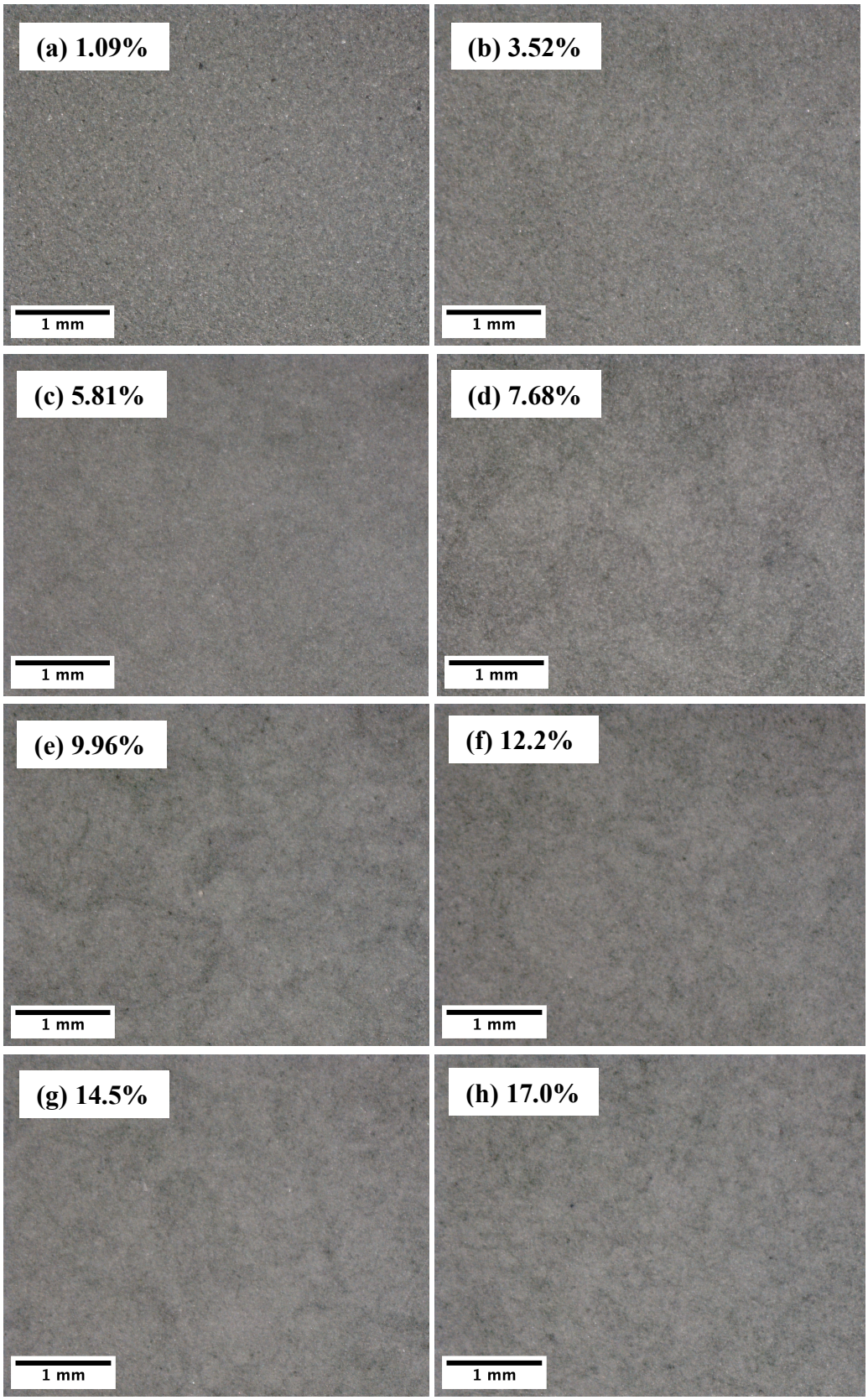
(a) 1.09%
1 mm
(b) 3.52%
1 mm
(c) 5.81%
1 mm
(d) 7.68%
1 mm
(e) 9.96%
1 mm
(f) 12.2%
1 mm
(g) 14.5%
1 mm
(h) 17.0%
1 mm

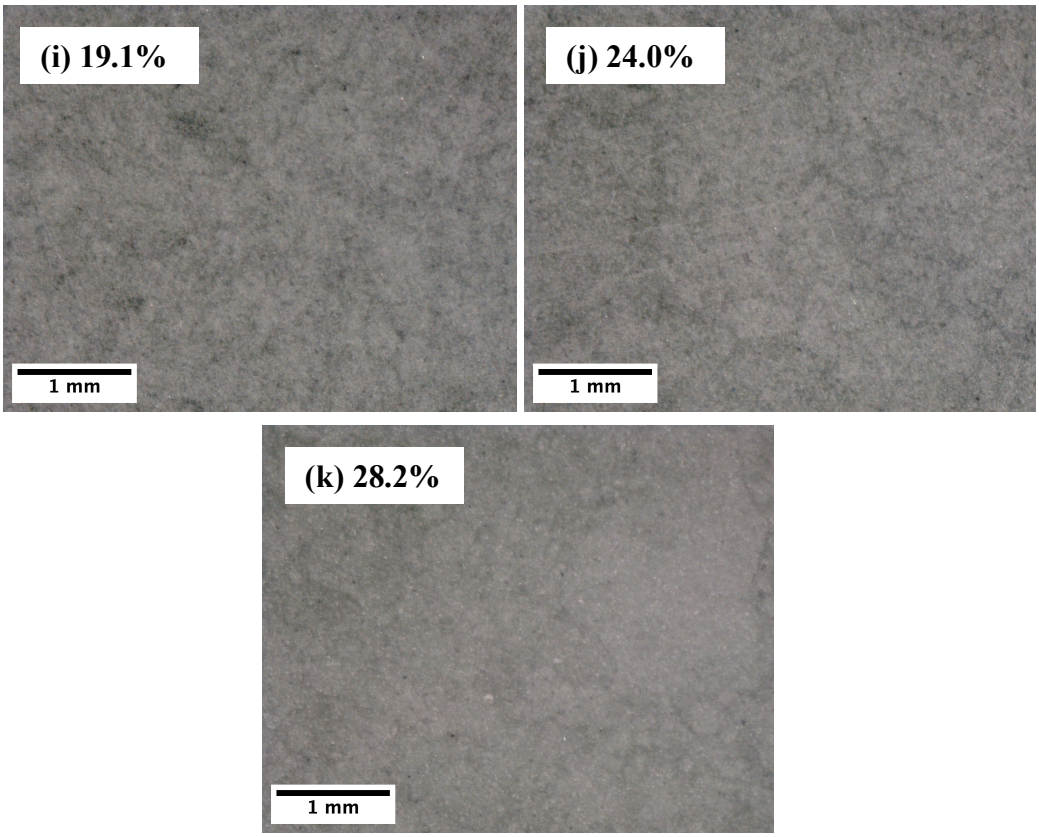

Figure 4.2.1 Optical images of SPS SiC_w-Al_2O_3 composites with (a) 1.09%, (b) 3.52%, (c) 5.81%, (d) 7.68%, (e) 9.96%, (f) 12.2%, (g) 14.5%, (h) 17.0%, (i) 19.1%, (j) 24.0%, (k) 28.2% SiC whisker content.

SEM images were also taken at 5kV in the Zeiss Ultra 60 on samples far below, at, and far above the percolation threshold corresponding to SiC whisker contents of 1.09%, 7.76%, and 28.2%, respectively, and are presented in Figure 4.2.2. In the 1.09% SiC_w content sample, the alumina matrix is clearly shown with distinct grains and grain boundaries visible. Despite there being a whisker content of 1.09%, the whiskers were unable to be captured using SEM, likely because they were embedded further within the composite sample. Note that in this sample, charging was present as seen in Figure 4.2.2(a).

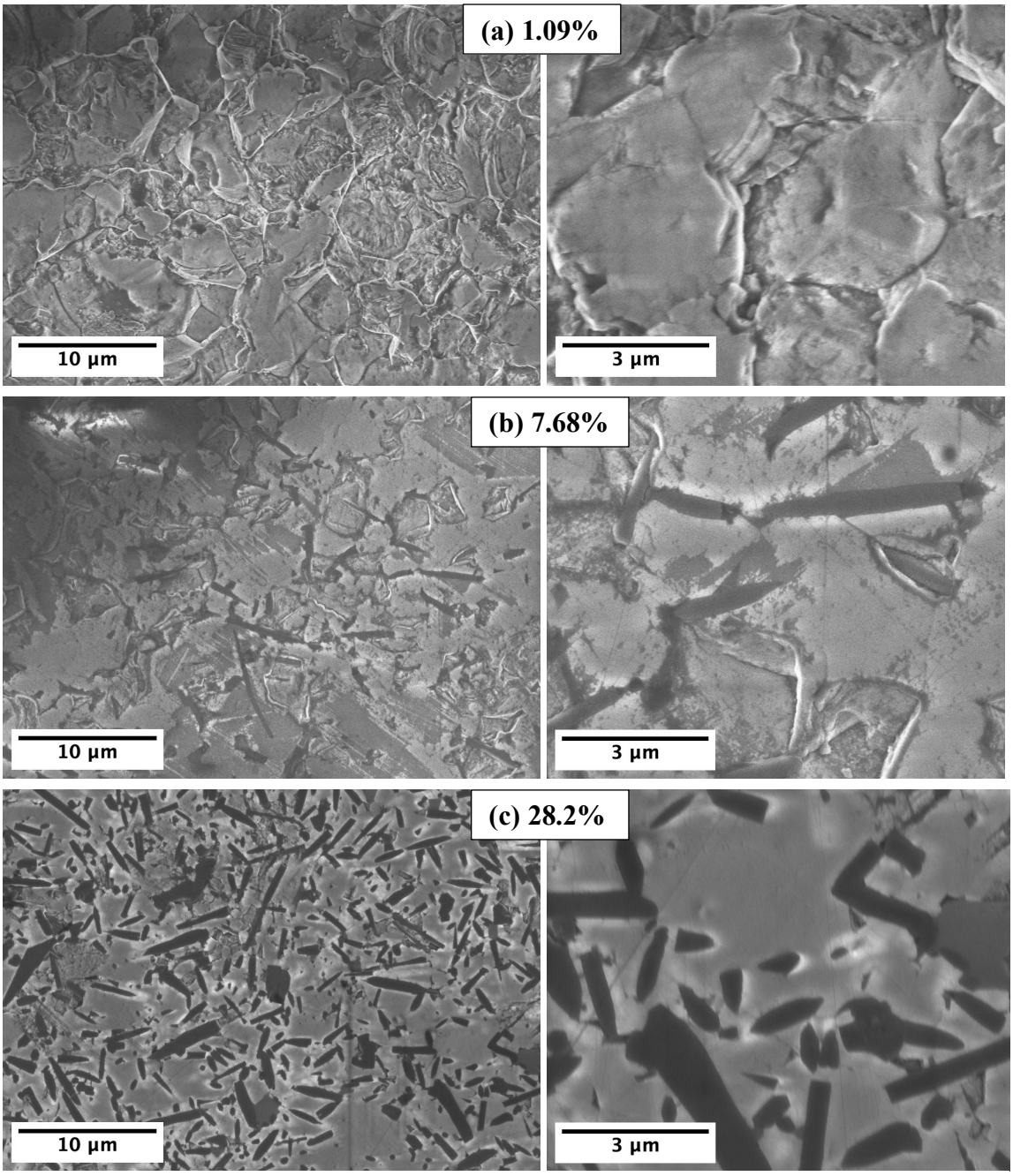

Figure 4.2.2 SEM images of SPS samples with SiC_w content (a) 1.09% far below the percolation threshold, (b) 7.68% at the percolation threshold, and (c) 28.2% far above the percolation threshold.

As the whisker content is increased in the 7.68% SiC_w content sample, Figure 4.2.2(b) shows the percolation path just forming as the whiskers (shown in black) begin to touch and form a conducting path within the insulating Al_2O_3 matrix. At this composition, the whiskers are just touching or about to touch, and with a low whisker density such that only some whiskers are forming the conducting percolating path. This supports the theory that 7.68% SiC_w is the percolation threshold, and that whisker heterogeneity drives the higher errors, both in reproducibility and repeatability, presented in Tables 4.1.1 and 4.1.2, respectively. Charging was especially apparent in this sample as well. The 28.2% SiC_w sample, shows a high number of SiC whiskers which is to be expected, with most whiskers touching or overlapping. This again supports the claim that because the percolating path is well established, the overall errors for samples are lower as seen in Tables 4.1.1 and 4.1.2.

Overall, the orientation of the whiskers is in agreement with the expected microstructure, with the whiskers aligned perpendicular to the pressing direction as shown in Figure 2.2.4. It would be helpful however, to slice the samples and image the microstructure through the thickness as this is the direction in which the electrical measurements were taken. This would further support the theory that whisker contact homogeneity drives electrical measurement repeatability and reproducibility.

4.3 Summary

A percolation study was completed on SiC_w-Al_2O_3 composites made with compositions ranging from 1.09% to 28.2% SiC_w. The percolation threshold was experimentally found to be at a composition of 7.68% SiC_w, characterized by a transition

from insulating to conducting in the bulk behavior of the composite. This percolation threshold composition was found to be similar to that of the previously made hot-pressed SiC_w-Al_2O_3 composites [22]. Overall, the hot-pressed samples were slightly more conductive than the SPS samples due to the hot-pressed samples having a higher density, likely due to the longer hold time required in the hot-pressing technique. Additionally, the SPS samples did have the expected microstructure, where the whiskers were aligned perpendicular to the pressing direction similar to the hot-pressed samples [10], [45], as seen in the SEM images.

Moreover, the repeatability and reproducibility errors of the SPS SiC_w-Al_2O_3 composite samples were highest at and near the percolation threshold of 7.68% SiC whisker content. This is because at the percolation threshold, the electrical response is more varied due to the DC current having a limited number of fully percolated paths to travel through. At this point, the whisker contact heterogeneity is highest which was supported by the SEM images taken which confirmed that the whiskers had just begun to touch at the 7.68% SiC_w composition.

5 3YSZ-SICw-AL$_2$O$_3$ COMPOSITES

After the percolation curve of SPS SiC_w-Al_2O_3 composites had been established, a fixed volume percentage of 15% SiC_w was chosen as it was far above the percolation threshold, and therefore reproducible and conductive. 2% 3YSZ by volume was added as an additional phase to influence the microwave heating behavior of the composite. The remaining volume percent was added as Al_2O_3 to form 3YSZ-SiC_w-Al_2O_3 composites. In this chapter, the electrical and microstructural characterization of the 3YSZ- SiC_w-Al_2O_3 composites are presented. One set of samples was made from AdValue alumina powder and are referred to as 3YSZ-SiC_w-Al_2O_3 samples, while the other set of samples was made from Advanced Composite Materials alumina and are referred to as 3YSZ-Type E SiC_w-Al_2O_3.

5.1 Electrical Characterization

Prior to adding the 3YSZ to the 15% SiC_w-Al_2O_3 mixes, samples were made of each respective 15% SiC_w-Al_2O_3 mix to provide a baseline electrical response as a reference. The 15% SiC_w-Al_2O_3 samples that were fabricated using the AdValue Al_2O_3, are referred to as simply 15% SiC_w-Al_2O_3 samples, and the 15% SiC_w-Al_2O_3 samples that were fabricated using the Advanced Composite Materials Al_2O_3, are referred to as 15% Type E SiC_w-Al_2O_3 samples. The real resistivity of the respective samples with no 3YSZ are plotted below in Figure 5.1.1

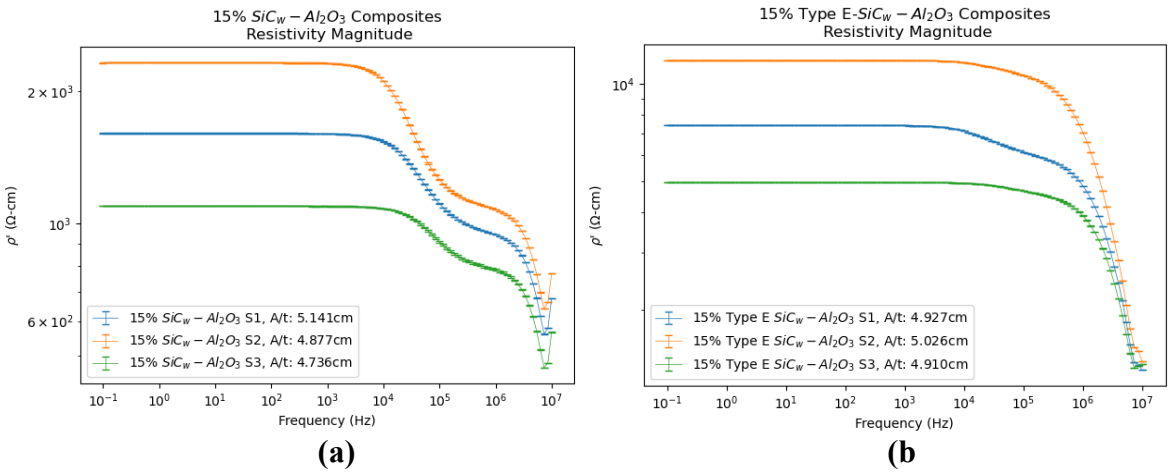

Figure 5.1.1 Real resistivity response of (a) 15% SiC_w-Al_2O_3 S1-S3 and (b) 15% Type E SiC_w-Al_2O_3 S1-S3.

The 15% SiC_w-Al_2O_3 samples made with the AdValue alumina have a real resistivity response on the order of 10^3 Ω-cm while the Advanced Composite Materials alumina 15% Type E SiC_w-Al_2O_3 samples have a real resistivity response on the order of 10^4 Ω-cm at the lowest frequency of 10^{-1} Hz. The samples are roughly of the same area to thickness ratio, made from the same SiC whiskers, and of the same volume compositions, but have noticeable different electrical responses due to the alumina used. The AdValue alumina 15% SiC_w-Al_2O_3 samples have two sharp rises in the real resistivity response from 10^7 to 10^6 Hz and from 10^5 to 10^4 Hz, respectively, before plateauing at 10^4 Hz. The Advanced Composite Materials 15% Type E SiC_w-Al_2O_3 samples only has a single sharp increase from 10^7 to 10^4 Hz before leveling off. Overall, the 15% Type E SiC_w-Al_2O_3 samples have a higher resistivity than the samples made from the 15% SiC_w-Al_2O_3 mix, but the samples made from each respective mix are comparable to each other.

For the 3YSZ-SiC_w-Al_2O_3 composite samples, nine total samples were made; three of which had no annealing treatment, three of which were annealed in air at 900°C for 4 hours, and three of which were annealed in O_2 at 900°C for 4 hours. Due to the heterogenous nature of composites, samples of the same annealing treatment varied slightly in electrical behavior as shown in the real resistivity in Figure 5.1.2. As a result, one sample of each annealing treatment was chosen to be representative for the sake of conciseness.

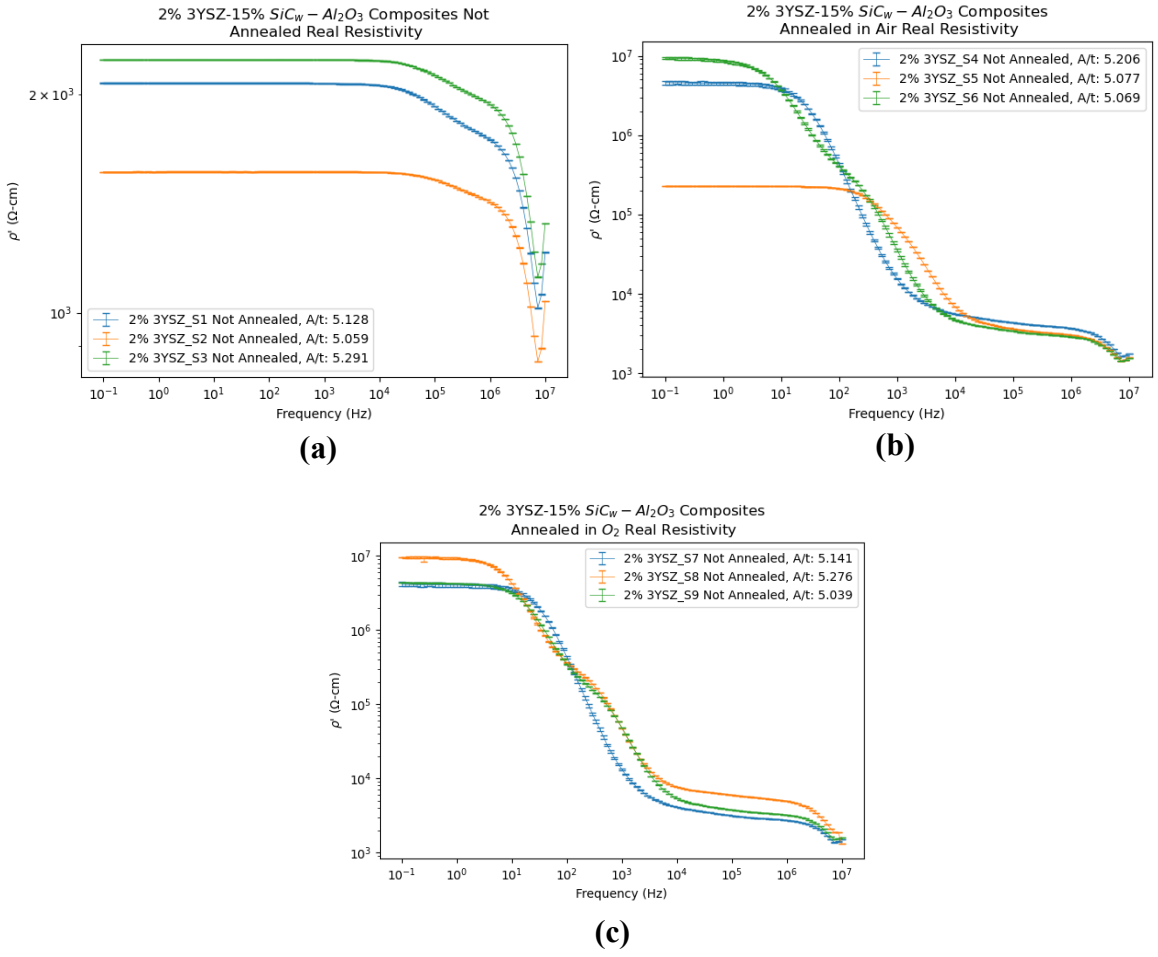

Figure 5.1.2 Real resistivity response of (a) 3YSZ-SiC_w-Al_2O_3 S1-S3 not annealed, (b) 3YSZ-SiC_w-Al_2O_3 S4-S6 annealed in air, and (c) 3YSZ-SiC_w-Al_2O_3 S7-S9 annealed in O_2.

The samples from each respective annealing treatment, however, behave similarly. Samples 3YSZ-SiC_w-Al_2O_3 S1-S3 all behave similarly to each other within the same order of magnitude, for example in Figure 5.1.2. Samples 3YSZ-SiC_w-Al_2O_3 S4-S6 have more of a spread in behavior likely because some samples reach different levels of oxidation during the annealing treatment since they are annealed in air. This is supported by samples 3YSZ-SiC_w-Al_2O_3 S7-S9 behaving more homogenously with the samples having a real resistivity response falling within the same order of magnitude across the frequency range measured.

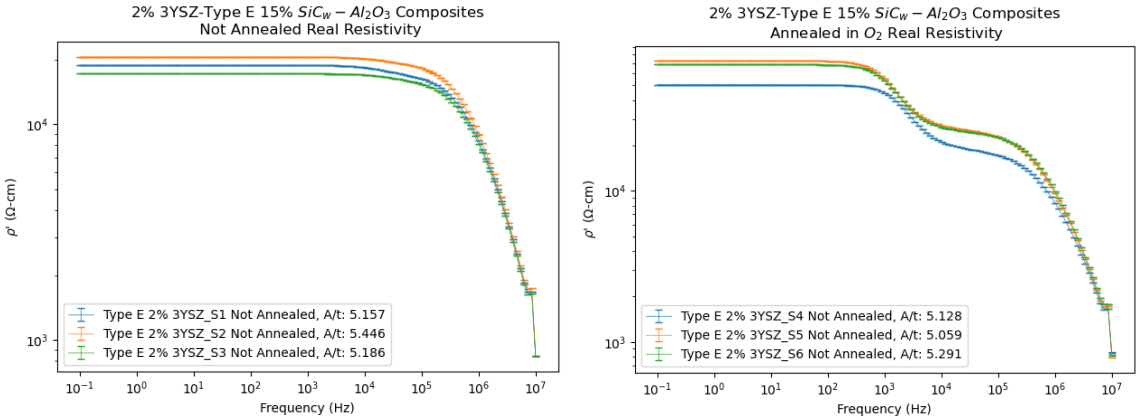

(a) **(b)**

Figure 5.1.3 Real resistivity response of (a) 3YSZ-Type E SiC_w-Al_2O_3 S1-S3 not annealed, (b) 3YSZ-Type E SiC_w-Al_2O_3 S4-S6 annealed in O_2.

A similar spread of responses is seen in the 3YSZ-Type E SiC_w-Al_2O_3 composite samples but to a lesser degree, where samples 3YSZ-Type E SiC_w-Al_2O_3 S1-S3 are not annealed and samples 3YSZ-Type E SiC_w-Al_2O_3 S4-S6 are annealed in O_2 as shown in Figure 5.1.3. Samples 3YSZ-Type E SiC_w-Al_2O_3 S1-S3 all follow similar behavior in the real resistivity response across the frequency range with a sharp increase from 10^7 to 10^5

Hz, and then a plateau from 10^5 to 10^{-1} Hz. Samples 3YSZ-Type E SiC_w-Al_2O_3 S4-S6, have more variance between the responses but are still within an order of magnitude of each other, where sample 3YSZ-Type E SiC_w-Al_2O_3 S4 has a lower real resistivity response.

To more easily compare the samples made from different alumina mixes and annealing treatments, one sample from each alumina mix and group was chosen to represent the overall behavior. This was done primarily to account for the spread in behaviors between 3YSZ-SiC_w-Al_2O_3 samples annealed in air and O_2 as seen in Figure 5.1.2. If those samples had been averaged, features in the electrical response would have been lost.

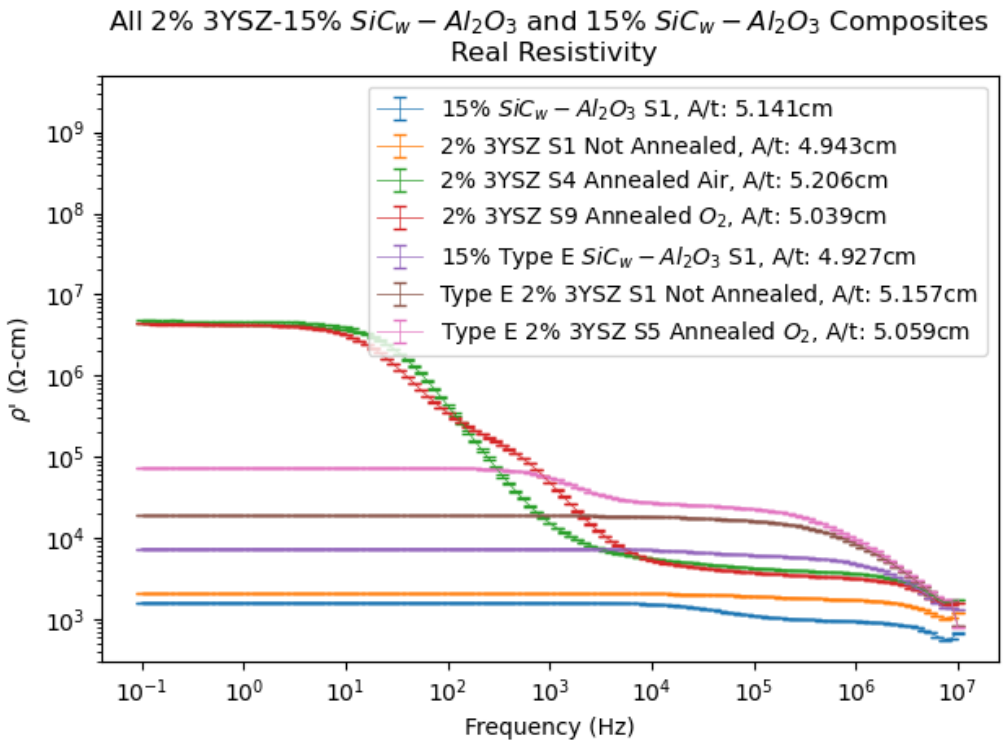

Figure 5.1.4 Real resistivity response of a representative sample of all 2% 3YSZ- SiC_w-Al_2O_3 and 15% SiC_w-Al_2O_3 composites.

Figure 5.1.4. plots the real resistivity of a single representative sample of all the 3YSZ-SiC_w-Al_2O_3 mixes and annealed types and 15% SiC_w-Al_2O_3 sample types. For the AdValue alumina mix, the 15% SiC_w-Al_2O_3 sample with no 3YSZ showed the lowest real resistivity response at the lowest frequency, and with the addition of 2% 3YSZ with no annealing treatment, the real resistivity increased slightly. Once the samples were annealed however, the real resistivity increased dramatically by ~4 orders of magnitude at the lowest frequency. The 3YSZ-SiC_w-Al_2O_3 sample annealed in air and in O_2 have a sharp increase in the real resistivity beginning at 10^4 Hz before leveling off at 10^2 Hz. The 3YSZ- SiC_w-Al_2O_3 sample annealed in O_2 shows a slight leveling off in the real resistivity before increasing again at 10^3 Hz.

The Advanced Composite Materials alumina 3YSZ- Type E SiC_w-Al_2O_3 samples display a similar trend as well where the 15% Type E SiC_w-Al_2O_3 sample had the lowest real resistivity response. With the additional of 2% 3YSZ, the 3YSZ- Type E SiC_w-Al_2O_3 sample that was not annealed increased in real resistivity by less than an order of magnitude. The 3YSZ- Type E SiC_w-Al_2O_3 sample annealed in O_2 however, did not drastically increase in real resistivity as seen with the 3YSZ- SiC_w-Al_2O_3 samples. This is again likely due to the different aluminas used in making the composite samples, with the AdValue alumina resulting in higher real resistivity responses than the Advanced Composites Materials alumina.

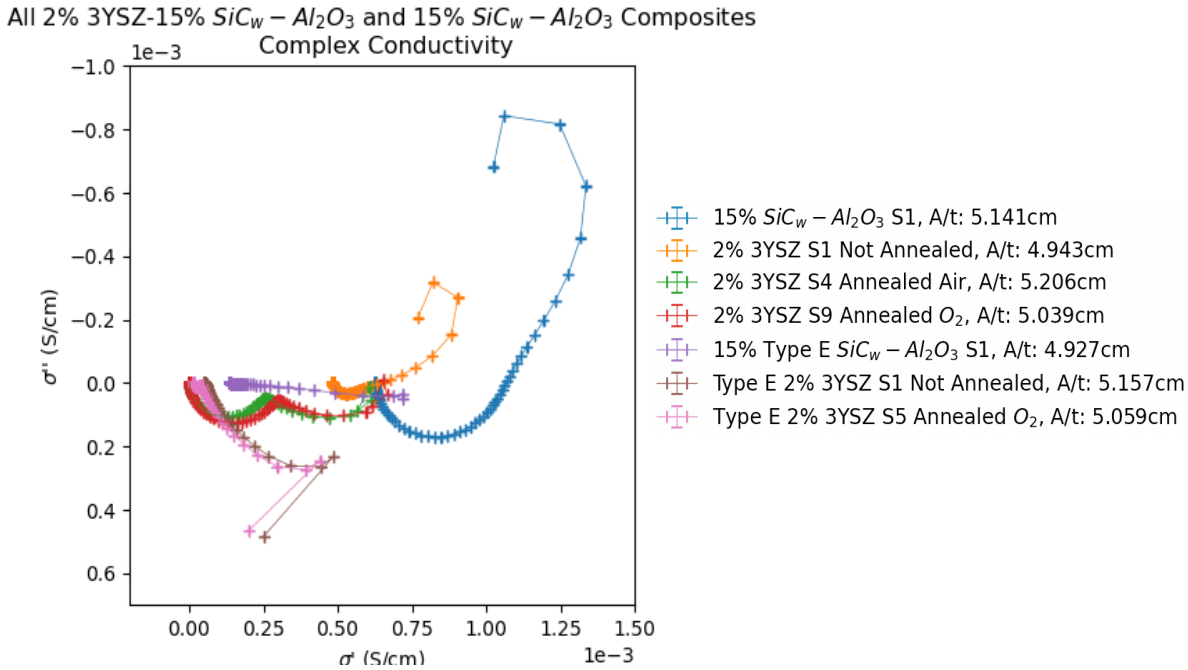

Figure 5.1.5 Complex conductivity response of a representative sample of all 2% 3YSZ-SiC_w-Al_2O_3 and 15% SiC_w-Al_2O_3 composites.

The influence of the 3YSZ and annealing treatments is also clear in the complex conductivity response of the samples shown in Figure 5.1.5. For the AdValue alumina 15% SiC_w-Al_2O_3 sample, the overall conductivity of the samples is the highest and displays overall electrical behavior similar to that of a resistor and capacitor connected in parallel, as indicated by the semi-circle in the fourth quadrant of the cartesian plane and highest real conductivity response. However, there is strong inducting behavior as indicated by the "tail" in the negative conductivity. With the addition of the 3YSZ without annealing in the 3YSZ- SiC_w-Al_2O_3 not annealed sample, the overall trend is the same but with less conducting and inducting behavior as shown by the smaller semi-circle and tail. The 3YSZ-SiC_w-Al_2O_3 samples annealed in air and O_2 are almost identical in the complex conductivity

response, with two semi-circles in the fourth quadrant and no inducting behavior. The two semi-circles can be expressed as two parallel resistors and capacitors connected in series, with each semi-circle representing a separate mechanism; a bulk response and an interfacial response, likely between the different phases in the composite. However, it is worth noting that during the annealing treatment, the alumina was also likely oxidized and thus the electrical response of the annealed samples cannot be completely attributed to the addition of the 3YSZ.

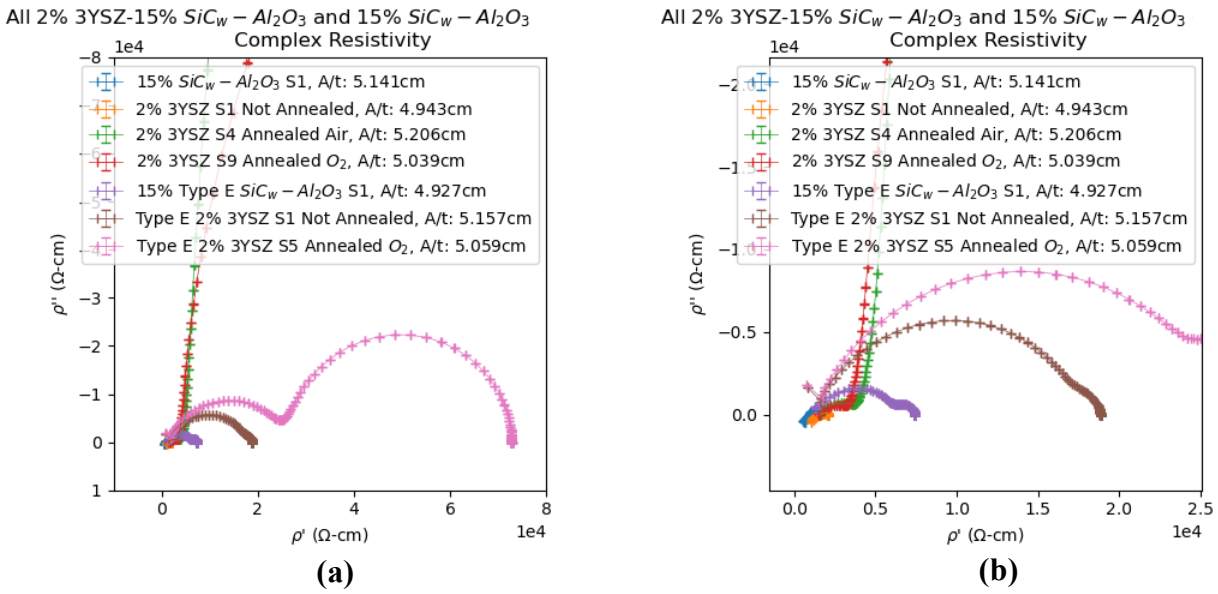

Figure 5.1.6 Complex resistivity response of (a) a representative sample of all 2% 3YSZ- SiC_w-Al_2O_3 and 15% SiC_w-Al_2O_3 composites, emphasizing the response of the Advanced Composite Material alumina samples, and (b) a zoomed in view.

The Advanced Composite Materials alumina samples decrease in conductivity with the addition of 3YSZ as seen by the decrease in the real conductivity part of the response between the 15% Type E SiC_w-Al_2O_3 and the 3YSZ-Type E SiC_w-Al_2O_3 not annealed

samples. This is more clearly seen in the complex resistivity response shown in Figure 5.1.6. Inversely related to conductivity, there is an increase in the resistivity between the 15% Type E SiC_w-Al_2O_3 and the 3YSZ-Type E SiC_w-Al_2O_3 not annealed samples as seen by the increase in the width of the semi-circle in the complex resistivity response. The 3YSZ-Type E SiC_w-Al_2O_3 sample annealed in O_2 sample again shows an increase in resistance indicated by the increase in the size of the semi-circle again, due to the increase in insulating behavior from the oxidation of the 3YSZ and possibly Al_2O_3.

It is worth noting however, that the 15% Type E SiC_w-Al_2O_3 sample has a dual semi-circle response even without the addition of the 3YSZ or annealing treatment, with the first semi-circle being larger than the second semi-circle. This dual semi-circle response is seen again in the 15% Type E SiC_w-Al_2O_3 sample not annealed, illustrating that the Advanced Composite Material alumina is likely driving the dual mechanism response as shown by the two semi-circles. For the 15% Type E SiC_w-Al_2O_3 sample annealed in O_2, the most drastic difference is seen in the large increase in the size of the second semi-circle. Prior to any annealing treatment, the second semi-circle is the smaller of the two semi-circles showing that the oxidation of the sample when annealed in O_2 is clearly captured in the electrical response of the complex resistivity of the sample.

5.2 Microstructure Characterization (Optical and SEM)

As mentioned in Chapter 3.2, the 3YSZ-SiC_w-Al_2O_3 S1-S3 not annealed samples were only mortar and pestled for ~10 minutes while the 3YSZ-SiC_w-Al_2O_3 S4-S6 samples annealed in air and S7-S9 samples annealed in O_2 were mortar and pestled for an additional

~25 minutes for a total of ~35 minutes. This was done because after optically inspecting the surfaces of 3YSZ-SiC_w-Al_2O_3 samples S1-S3 after sintering with the Celestron Infiniview optical microscope, it was determined that only ~10 minutes of mortar and pestling the mix was not sufficient for a homogenous composition as seen in Figure 5.2.1. This is apparent by the white agglomerates, likely 3YSZ based on the color, on the surface of the sample.

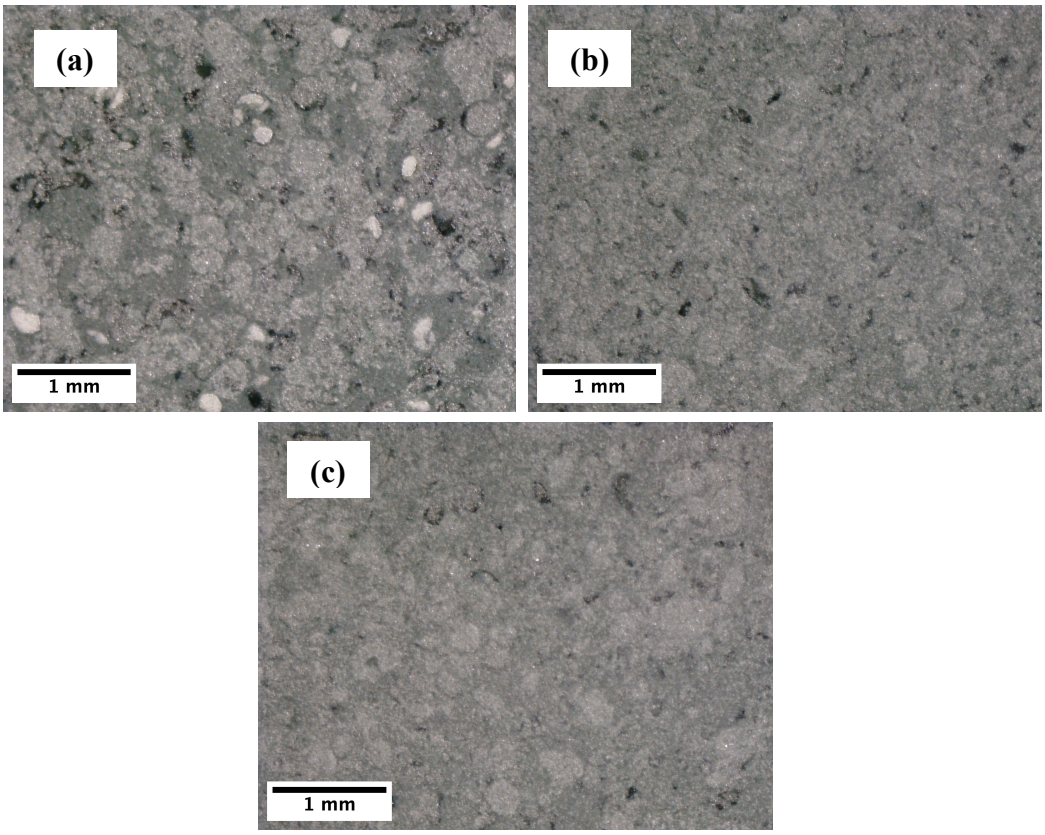

Figure 5.2.1 Optical images of sintered samples (a) 3YSZ-SiC_w-Al_2O_3 S2 not annealed, (b) 3YSZ-SiC_w-Al_2O_3 S5 annealed in air, and 3YSZ-SiC_w-Al_2O_3 S8 annealed in O_2.

After the 3YSZ-SiC_w-Al_2O_3 composite mix was mortar and pestled for the additional time of ~25 minutes and sintered, it is clear in Figure 5.2.1(b)-(c) that this resulted in a far more homogenous mix for samples 3YSZ-SiC_w-Al_2O_3 S5 and S9. In these samples, there are no longer any white agglomerates or areas of dark discoloration on the surface.

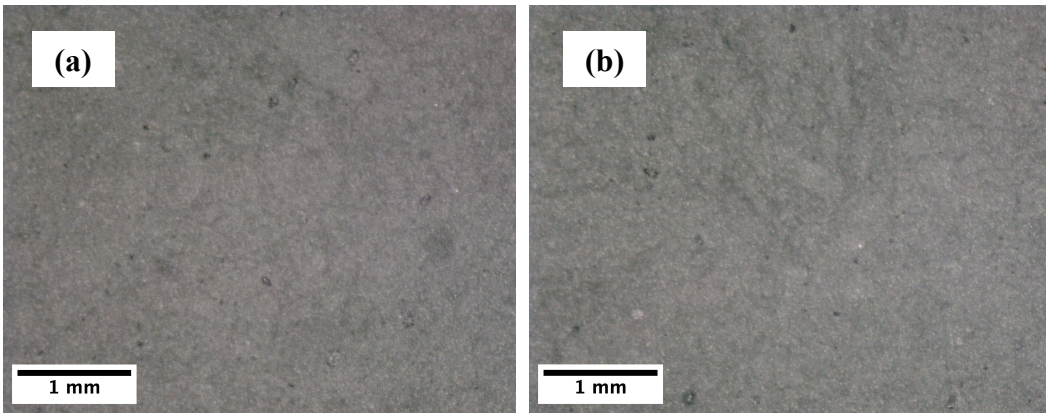

Figure 5.2.2 Optical images of sintered samples (a) 3YSZ-Type E SiC_w-Al_2O_3 S2 not annealed and (b) 3YSZ-Type E SiC_w-Al_2O_3 S5 annealed in O_2.

Optically comparing the surfaces of 3YSZ-SiC_w-Al_2O_3 composites Figure 5.2.1 to the 3YSZ-Type E SiC_w-Al_2O_3 composites, shown in Figure 5.2.2, the differences in aluminas become clearer. The 3YSZ-SiC_w-Al_2O_3 composites visually appear more porous than the 3YSZ-Type E SiC_w-Al_2O_3 composite samples as they have a high number of dark regions, likely pores, that are relatively large. In comparison, the 3YSZ-Type E SiC_w-Al_2O_3 composites only have a small number of relatively small pores. To confirm that the 3YSZ was not playing a role in the porosity of the surfaces, the optical images are also shown of the 15% SiC_w-Al_2O_3 and 15% Type E SiC_w-Al_2O_3 samples, which contain no 3YSZ in Figure 5.2.3.

As with the 3YSZ samples, the 15% Type E SiC_w-Al_2O_3 sample made with the Advanced Composites alumina appears to be less porous than the 15% SiC_w-Al_2O_3 sample made with the AdValue alumina. This again is made apparent by smaller dark porous regions that are less abundant than the 15% SiC_w-Al_2O_3 sample.

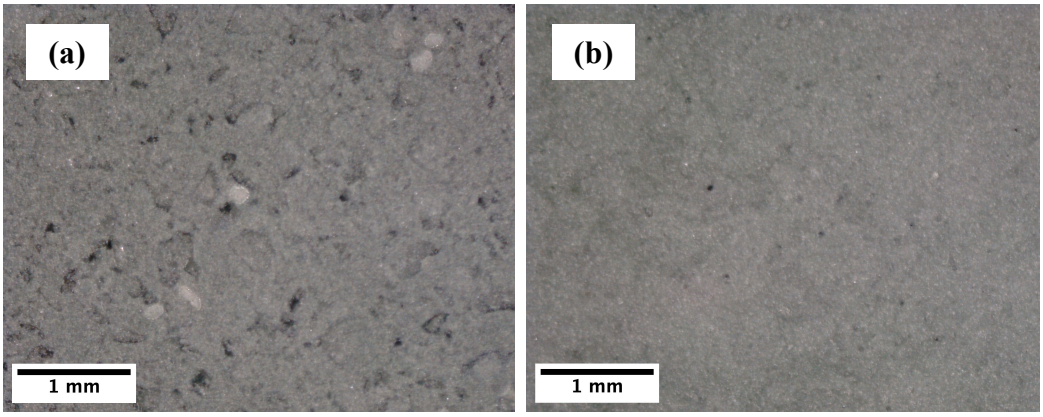

Figure 5.2.3 Optical images of sintered samples (a) 15% SiC_w-Al_2O_3 S2 and (b) 15% Type E SiC_w-Al_2O_3 S2.

The samples were also imaged at 5kV in the Zeiss Ultra 60 SEM to better understand the composite microstructure and homogeneity. Overall, the SEM images confirmed that the samples made from the Advanced Composite Materials alumina were denser as well as more homogenous than the samples made from the AdValue alumina. The 15% Type E SiC_w-Al_2O_3 mix was previously made by ball milling [10] and thus likely yielded a more homogenous mix than the speed mixer and mortar and pestle which was used to make all the AdValue alumina composites.

As shown in the SEM images in Figure 5.2.4, the 15% Type E SiC_w-Al_2O_3 sample is visually similar to the SEM images of SiC_w-Al_2O_3 samples in Chapter 4, which is to be

expected as they are made from the same base mix. Although the sample appears dense, there are still some small pores on the surface as seen in Figure 5.2.4(a). As the 3YSZ in introduced into the composition, it appears that it agglomerates despite only being present as 2% volume as shown by the dark spots in Figure 5.2.4(b)-(c). Additionally, there are larger pores visible in on the surface in both the 3YSZ-Type E SiC_w-Al_2O_3 not annealed and annealed in O_2 samples. Between the 3YSZ-Type E SiC_w-Al_2O_3 not annealed and annealed in O_2 samples, however, there is no discernible differences between them in the SEM images.

An EDS attachment was used to verify that the black agglomerates observed in Figure 5.2.4(b)-(c) was 3YSZ, as shown in Figure 5.2.5 which presents EDS elemental mapping of sample 3YSZ-Type E SiC_w-Al_2O_3 annealed in O_2 S5. As seen in the plots, the dark region in the SEM image in Figure 5.2.5(a), has an abundance of zirconium (Zr) and a clear lack of aluminum (Al). Additionally, there appears to be a higher concentration of yttrium (Y) in the region but significantly less than the zirconium which is to be expected as 3YSZ has only 3%mol percent yttrium. However, it is difficult to tell that there is an abundance of yttrium in the region of interest due to the underlying noise of the mapping. Furthermore, the region is not devoid of oxygen (O) confirming that the dark areas observed in Figure 5.2.4(b)-(c) are likely 3YSZ agglomerates due to the presence of zirconium, oxygen, and small amounts of yttrium. The region also does not contain any silicon (Si), carbon (C), or aluminum (Al), again confirming that it is likely an agglomerate of 3YSZ.

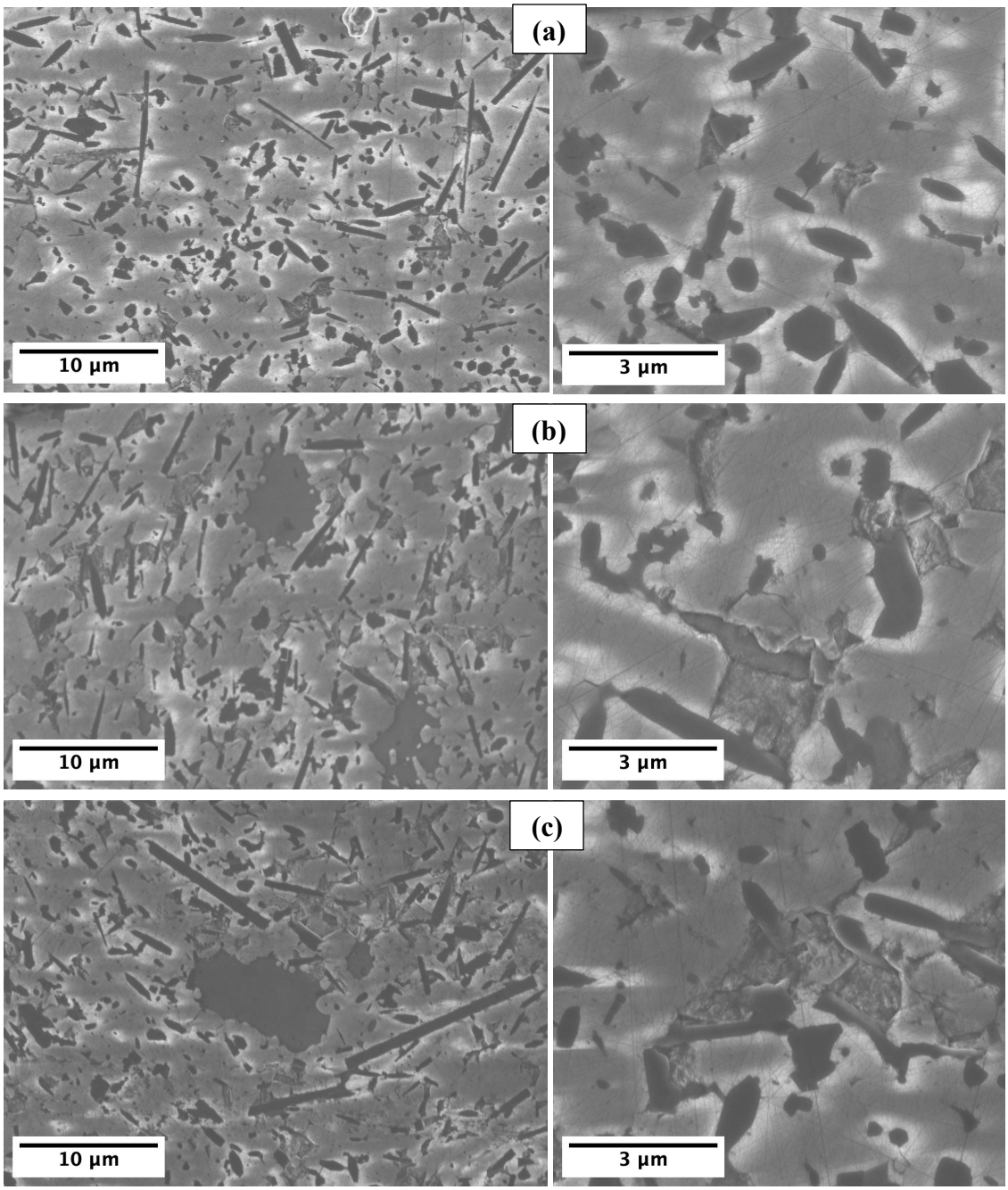

Figure 5.2.4 SEM images of samples (a) 15% Type E SiC_w-Al_2O_3 S2, (b) 3YSZ-Type E SiC_w-Al_2O_3 not annealed S2, and 3YSZ-Type E SiC_w-Al_2O_3 annealed in O_2 S5.

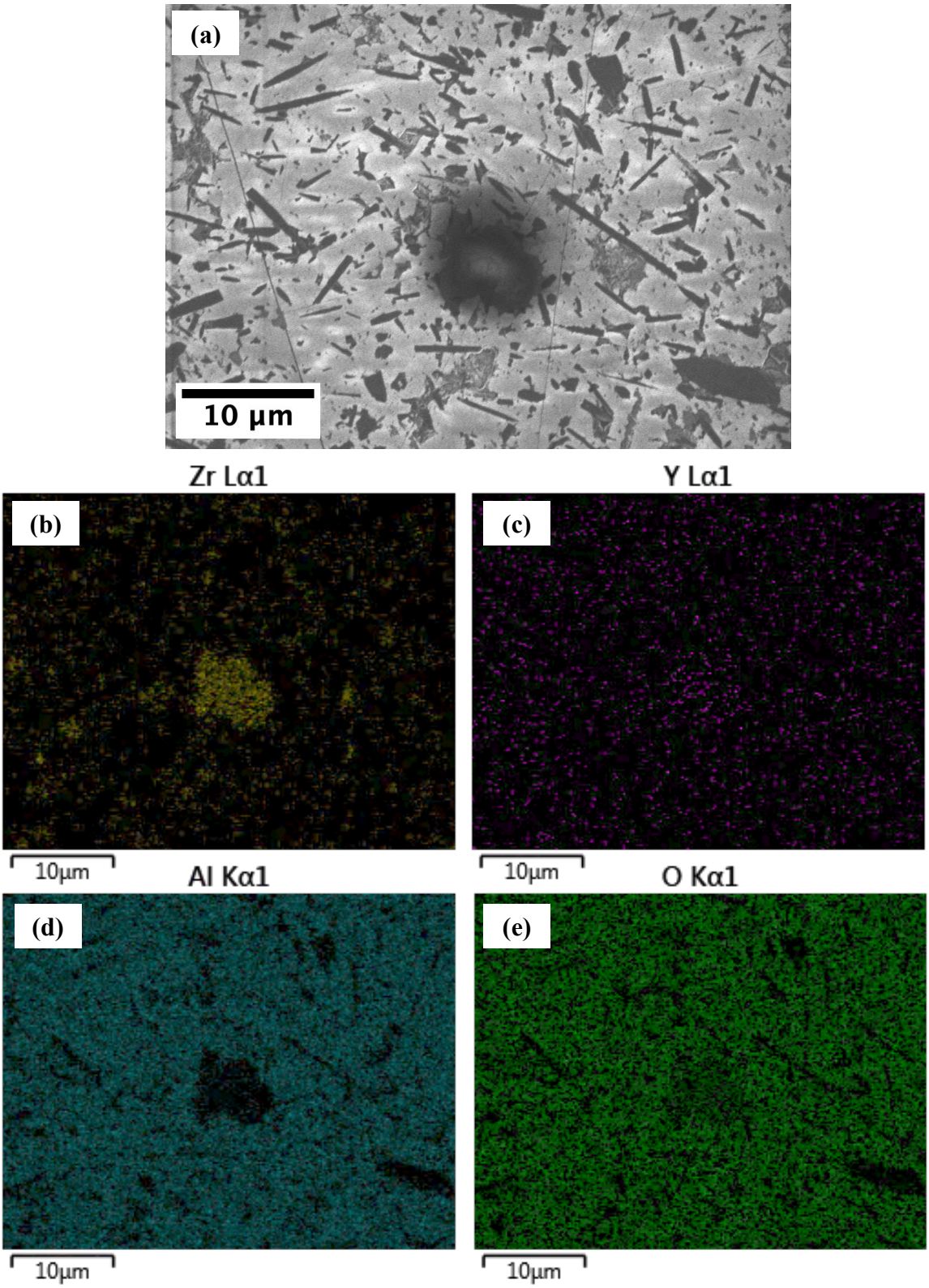
(a)
10 µm
Zr Lα1
(b)
10µm
Y Lα1
(c)
10µm
Al Kα1
(d)
10µm
O Kα1
(e)
10µm

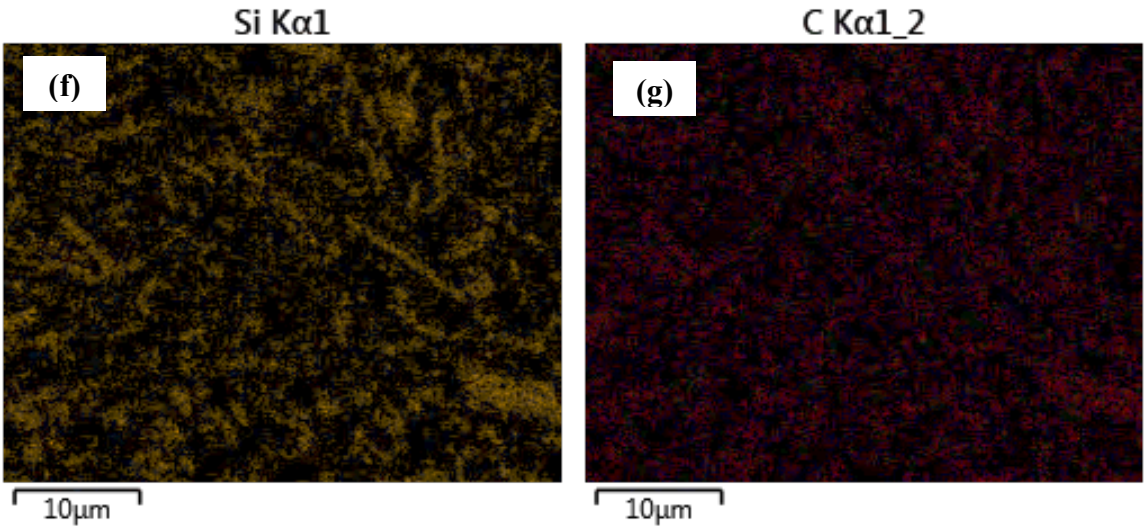

Figure 5.2.5 (a) SEM image of 3YSZ-Type E SiC_w-Al_2O_3 annealed in O_2 S5 and EDS elemental mapping of (b) yttrium, (c) zirconium, (d) aluminum, (e) oxygen, (e) silicon, and (f) carbon in the region.

As indicated by the optical images in Figure 5.2.2 and Figure 5.2.3, the samples made with the AdValue alumina are extremely porous and inhomogeneous, with the most porous and heterogenous sample being the 3YSZ- SiC_w-Al_2O_3 not annealed samples which were only mortar and pestled for ~10 min. The 3YSZ- SiC_w-Al_2O_3 not annealed sample S2 is shown specifically in Figure 5.2.6 to highlight the heterogeneity and porosity of the composite sample.

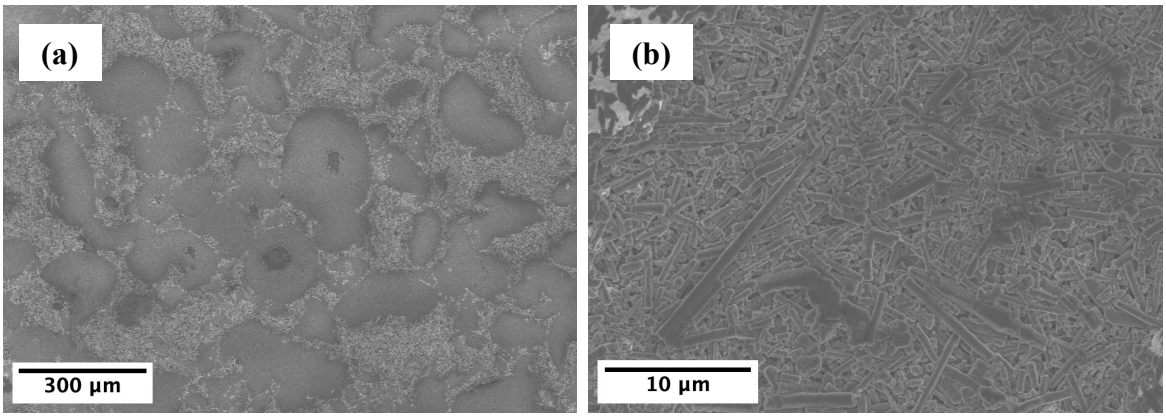

Figure 5.2.6 SEM images of 3YSZ-SiC_w-Al_2O_3 not annealed S2 (a) highlighting the different regions and (b) a SiC_w agglomerate.

As shown in Figure 5.2.6(a), there are distinct regions on the surface of the sample including, dark regions which are 3YSZ agglomerates, gray regions which are agglomerates of the Al_2O_3 matrix, and the speckled region which are regions in which the SiC whiskers are dispersed evenly in the Al_2O_3 matrix. Although the AdValue alumina particle size was 3μm, the alumina was sprayed dried during the manufacturing process resulting in large ~200 μm agglomerates. However, there are also agglomerates of SiC whiskers in the composite as seen in Figure 5.2.6(b). This is the only sample in which SiC whisker agglomerates were observed and again is likely due to the poor mixing procedure done on these samples. The remaining AdValue composite samples are shown in Figure 5.2.7.

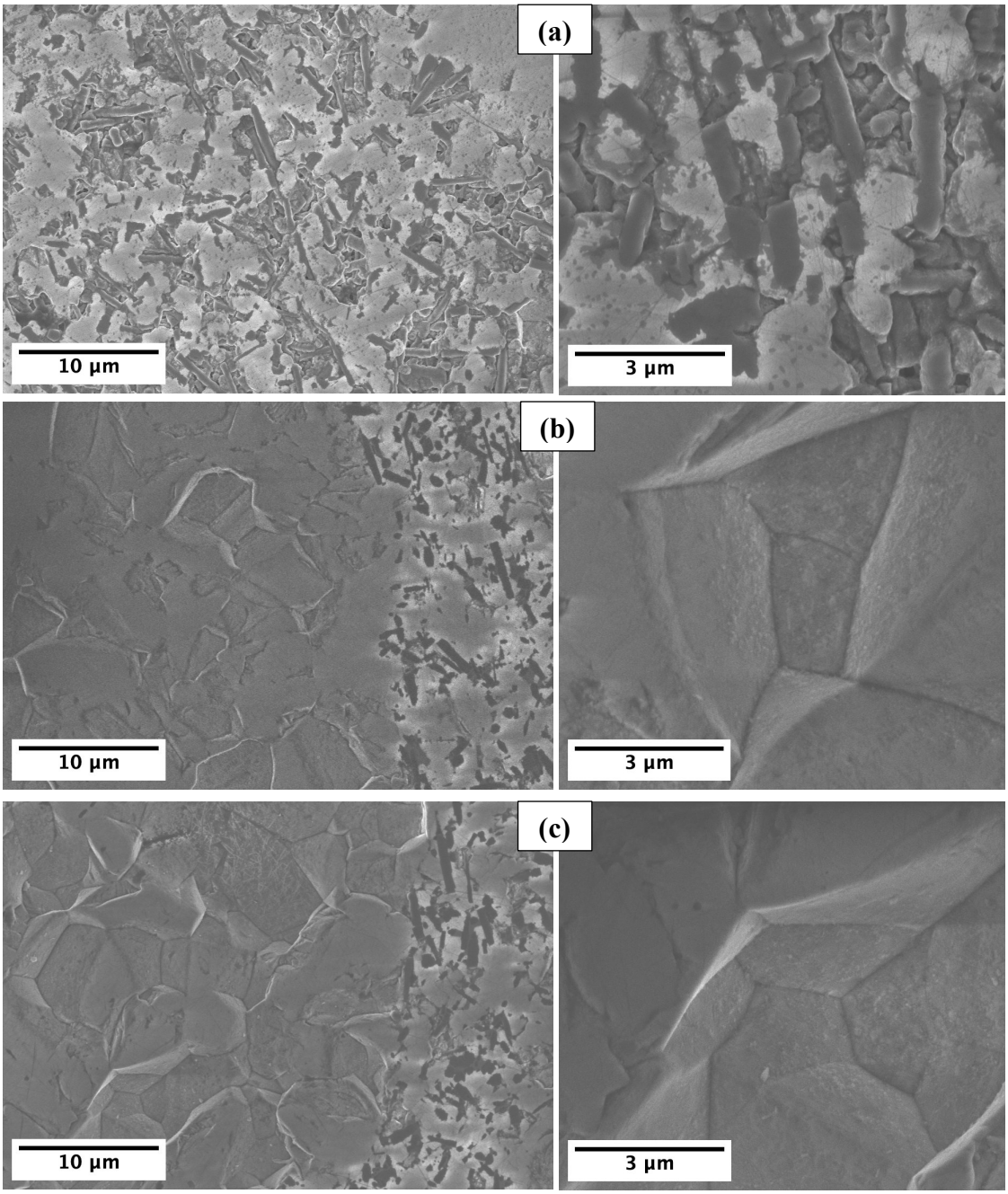

Figure 5.2.7 SEM images of samples (a) 15% SiC_w-Al_2O_3 S1, (b) 3YSZ-SiC_w-Al_2O_3 annealed in air S5, and (c) 3YSZ- SiC_w-Al_2O_3 annealed in O_2 S8.

As with the optical images, it is clear in the SEM images that the 15% SiC_w-Al_2O_3 composite in Figure 5.2.7(a) is more porous than the 15% Type E SiC_w-Al_2O_3 composite in Figure 5.2.4(a). Additionally, it appears that in the 15% SiC_w-Al_2O_3 sample, although the SiC_w are relatively well dispersed, they do "bunch up" more so than in the Advanced Composite Materials alumina samples, likely partly due to the differences in the mixing procedure. The annealed 3YSZ- SiC_w-Al_2O_3 samples again have distinct regions similar to the 3YSZ-SiC_w-Al_2O_3 not annealed sample, in which there are alumina matrix regions, dispersed SiC whiskers in the alumina regions, and 3YSZ agglomerates. There are however, no SiC_w agglomerates due to the extended mortar and pestle time for these mixes. For the alumina regions in these samples however, the Al_2O_3 grains and grain boundaries were well-defined as compared to other samples as seen in Figure 5.2.7(b)-(c).

As mentioned previously, the AdValue alumina samples were spray dried, which resulted in ~200μm agglomerates. This was confirmed to be alumina agglomerates by using EDS mapping on an agglomerate imaged in sample 3YSZ-SiC_w-Al_2O_3 annealed in O_2 S8 in Figure 5.2.8. As shown, the gray agglomerate is devoid of any significant yttrium, zirconium, silicon, and carbon but contains high amounts of aluminum and oxygen. This indicates that these gray regions are AdValue alumina agglomerates that were not dispersed during the mixing process, partly due to insufficient mixing but also because the alumina was spray dried in the manufacturing process.

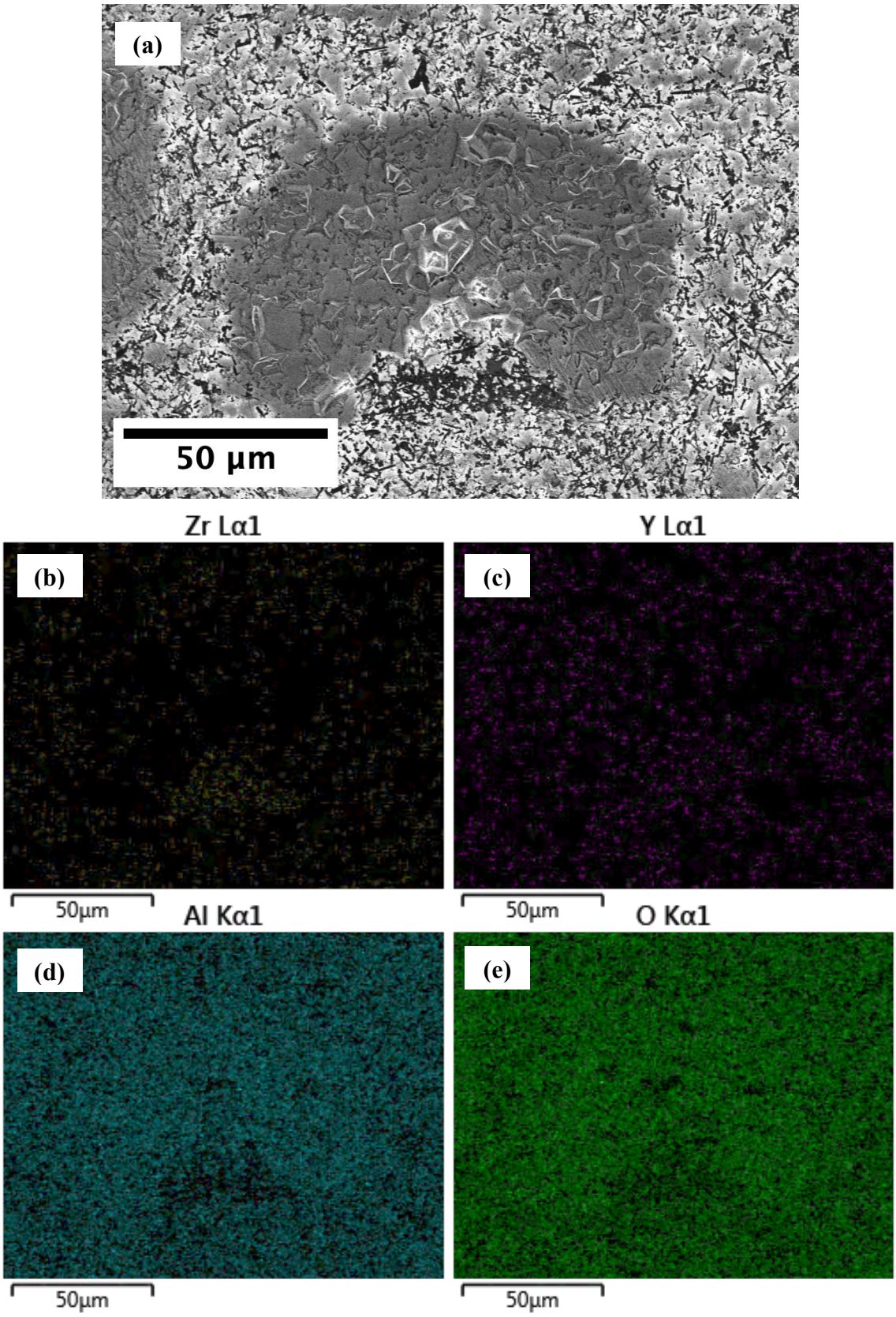
(a)
50 µm
Zr Lα1
(b)
50µm
Y Lα1
(c)
50µm
Al Kα1
(d)
50µm
O Kα1
(e)
50µm

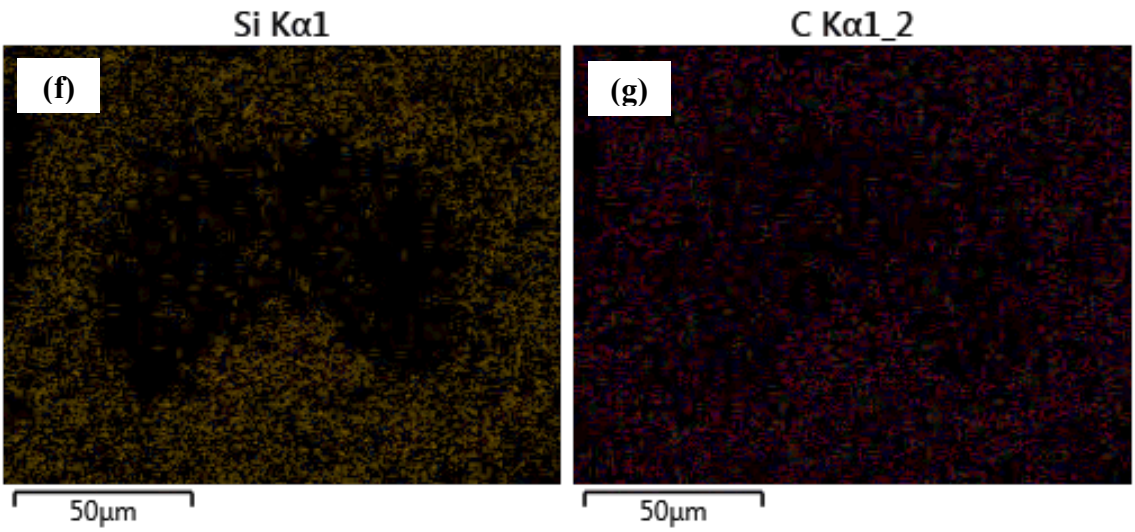

Figure 5.2.8 (a) SEM image of 3YSZ-SiC_w-Al_2O_3 annealed in O_2 S8 and EDS elemental mapping of (b) yttrium, (c) zirconium, (d) aluminum, (e) oxygen, (e) silicon, and (f) carbon.

5.3 Error Analysis

The error analysis calculations outlined in Chapter 1 were also carried out on the samples described in this chapter. For the sake of conciseness, the samples plotted in Figures 5.1.4 – 5.1.6 are used to represent the repeatability errors between electrical measurements done of the same sample, which are presented in Table 5.3.1.

Table 5.3.1 Total repeatability errors across the measured frequency range in all resistivity measurements of a representative sample of all 2% 3YSZ- SiC_w-Al_2O_3 and 15% SiC_w-Al_2O_3 composites.

Sample	Repeatability Error – Real Resistivity (%)	Repeatability Error – Imaginary Resistivity (%)	Repeatability Error – Resistivity Magnitude (%)	Repeatability Error – Resistivity Phase Angle (%)
15% SiC_w-Al_2O_3 S1	0.033	0.076	0.031	0.078
3YSZ-SiC_w-Al_2O_3 Not Annealed S1	0.080	0.038	0.080	0.039
3YSZ-SiC_w-Al_2O_3 Annealed in Air S4	0.034	0.077	0.043	0.036
3YSZ-SiC_w-Al_2O_3 Annealed in O_2 S9	0.095	0.106	0.124	0.104
15% Type E SiC_w-Al_2O_3 S1	0.032	0.044	0.036	0.040
3YSZ-Type E SiC_w-Al_2O_3 Not Annealed S1	0.029	0.017	0.027	0.025
3YSZ-Type E SiC_w-Al_2O_3 Annealed in Air S4	0.034	0.039	0.030	0.043

Overall, the repeatability errors are very low regardless of the type of alumina used or the annealing treatment done on the samples, at <0.1% overall in all parts of the resistivity response. Despite only a single sample being presented of each group, the

respective samples from each group not shown have similar errors and can be found in Appendix Chapter A.2. The sample with the highest repeatability error is the 3YSZ-SiC_w-Al_2O_3 sample annealed in O_2, with the imaginary resistivity, resistivity magnitude, and resistivity phase angle all having a repeatability error just over 0.1%. Most samples have resistivity errors far below the 0.1% error margin, particularly in the resistivity magnitude. The 3YSZ-Type E SiC_w-Al_2O_3 sample that is not annealed, shows the lowest repeatability errors overall with a particularly low imaginary resistivity error at 0.017%. The error analysis carried out for the repeatability measurements again confirm that electrical measurements done consecutively on the same sample under identical conditions produce highly repeatable results.

Table 5.3.2 shows the reproducibility measurements, calculated using the three samples made from each sample group shown in Figures 5.1.4 – 5.1.6. Similar to the samples presented in Chapter 4, the reproducibility errors between samples made of the same mix and annealing treatment fall <5%, generally. The obvious exception to this generalization are the 3YSZ-SiC_w-Al_2O_3 samples annealed in air and the 3YSZ-SiC_w-Al_2O_3 samples annealed in O_2. The high repeatability errors are to be expected looking at Figure 5.1.2 (b) and (c), which shows that the respective samples show high variance in electrical response of the real resistivity between each other. This is especially true for the 3YSZ-SiC_w-Al_2O_3 samples annealed in air, which have an extremely high real resistivity reproducibility error of 45.6% due to the varying levels of oxidation leading to varying electrical responses.

Table 5.3.2 Total reproducibility errors across the measured frequency range in all resistivity measurements of all 2% 3YSZ- SiC_w-Al_2O_3 and 15% SiC_w-Al_2O_3 composites.

Sample	Reproducibility Error – Real Resistivity (%)	Reproducibility Error – Imaginary Resistivity (%)	Reproducibility Error – Resistivity Magnitude (%)	Reproducibility Error – Resistivity Phase Angle (%)
15% SiC_w-Al_2O_3	4.01	3.51	3.87	4.33
3YSZ-SiC_w-Al_2O_3 Not Annealed	6.90	4.83	6.16	5.12
3YSZ-SiC_w-Al_2O_3 Annealed in Air	45.6	36.2	38.9	27.1
3YSZ-SiC_w-Al_2O_3 Annealed in O_2	37.2	28.8	31.4	28.2
15% Type E SiC_w-Al_2O_3	5.23	6.05	5.88	4.68
3YSZ-Type E SiC_w-Al_2O_3 Not Annealed	3.56	2.99	3.12	4.65
3YSZ-Type E SiC_w-Al_2O_3 Annealed in O_2	4.35	4.08	4.77	3.29

Although the 3YSZ-SiC_w-Al_2O_3 samples annealed in O_2 also have high reproducibility errors around 30% across all parts of the resistivity, they are less than the reproducibility errors of the 3YSZ-SiC_w-Al_2O_3 samples annealed in air because the samples oxidized to more similar levels when annealed in an O_2 atmosphere. However, all the AdValue alumina samples had large alumina agglomerates in the microstructure which could have dominated the electrical response depending on the level of oxidation reached during the annealing treatment between samples of the same composition and annealing treatment. This is another potential reason for why the reproducibility errors were particularly high for the 3YSZ-SiC_w-Al_2O_3 samples annealed air and in O_2.

Not including the 3YSZ-SiC_w-Al_2O_3 samples annealed in air and in O_2 however, the reproducibility errors are generally low at <5% indicating that composite samples, although heterogenous in nature, display reproducibility in their electrical responses when they are made carefully and methodically.

5.4 Summary

In this Chapter, 3YSZ- SiC_w-Al_2O_3 composites were made using aluminas from two different manufacturers: Advanced Composite Materials and AdValue. The samples then underwent different annealing treatments to oxidize the 3YSZ which became reduced during SPS sintering in vacuum. Despite samples having the same compositions and annealing treatments, the electrical responses and microstructures imaged using SEM were extremely different due to the different aluminas used. However, in all samples with the

3YSZ 2% volume, the 3YSZ formed agglomerates, and likely needs a more thorough mixing procedure to be dispersed evenly in the samples.

Overall, the electrical resistivity of the samples increases regardless of the alumina used when the samples are annealed. This is to be expected as oxidation results in more insulating behavior. The 3YSZ-SiC_w-Al_2O_3 samples that were annealed in air and O_2 resulted in the highest electrical resistivity and conversely, the 15% Type E SiC_w-Al_2O_3 sample resulted in the lowest electrical resistivity. In terms of error analysis, all samples show very high repeatability in the electrical measurements, but the 3YSZ-SiC_w-Al_2O_3 samples annealed in air and O_2 had extremely high reproducibility errors. This was likely due to different levels of oxidation occurring during the annealing between respective samples of the same composition and annealing treatment.

6 SIMULATED MICROWAVE HEATING

This chapter presents the COMSOL software simulation results of microwave radiation heating of the composite samples fabricated experimentally from the percolation study in Chapter 4 and the 3YSZ composite samples in Chapter 5. This chapter outlines the microwave oven set-up created and the specific physics conditions used to enable electromagnetic heating in the model. It also provides the specific parameters used for materials that make up the microwave oven itself as well as the materials for the simulations of microwave heating. The results of this chapter focus on the transient heat transfer to the samples using a stationary, frequency-domain electromagnetic analysis.

6.1 Model Set-Up

The microwave oven made in COMSOL was of 270 mm width, 270 mm depth, and 190 mm height and was connected to a microwave radiation source using a rectangular waveguide of 50 mm width, 80 mm depth, and 18 mm height. Although all the samples made experimentally and presented in Chapter 3 have a diameter of ~ 10 mm and a thickness of ~ 1.5 mm, a larger sample placed in the center of the microwave oven cavity was used to simulate the microwave heating with a diameter of 60 mm and a thickness of 55 mm. This was done because the small samples, representative of the fabricated samples presented in this work in Chapter 3, lacked the thermal mass needed to sufficiently heat the sample in a relatively moderate amount of time. Using a larger sample in the model allowed for the heating to occur relatively quickly thereby decreasing model size and computing

cost. Additionally, a diameter of 60 mm and a thickness of 55 mm was chosen to maintain an area to thickness ratio of ~5 cm to keep the area to thickness ratio similar to the physically fabricated samples. A mesh was made of the model using a maximum element size of 0.0174 and minimum element size of 0.00127 to provide for a relative fine resolution in the model. The model and its created mesh are shown in Figure 6.1.1.

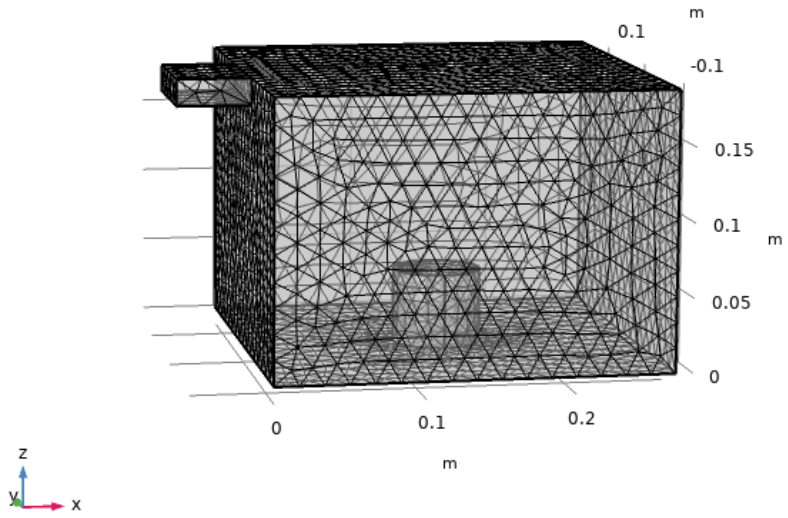

Figure 6.1.1 Modeled microwave oven and waveguide with the sample inside the microwave oven cavity. The created mesh is also shown.

The microwave oven and waveguide walls were modeled using the default copper material properties and the cavity was modeled using the default air material properties included in the COMSOL software [60]. These material properties are included in Table 6.1.1.

Table 6.1.1 Microwave oven and waveguide walls and cavity material properties used in the model [60].

	Copper	Air
$\boldsymbol{\rho}$ **(kg/m^3)**	8960	1.225
$\boldsymbol{\mu_r}$ **(unitless)**	1	1
$\boldsymbol{\varepsilon_r}$ **(unitless)**	1	1
$\boldsymbol{\sigma}$ **(S/m)**	5.998e7	0
$\boldsymbol{C_p}$ **(J/kgK)**	385	1
$\boldsymbol{\kappa}$ **(W/mK)**	400	0.025

The resistive metals losses, although small, are accounted for using the impedance boundary condition placed on these walls, expressed in Equation 6.1.1 [61]. In this equation, μ_0 is the vacuum permeability of 1.257 H/m, μ_r is the relative permeability of the material, ε_r is the relative permittivity of the material, $\boldsymbol{H}$ is the magnetic field in A/m, $\boldsymbol{E}$ is the electric field in V/m, $\boldsymbol{n}$ is the normal vector, and $\boldsymbol{E_s}$ is the source electric field in V/m.

$$\sqrt{\frac{\mu_0\mu_r}{\varepsilon_r}}\,\boldsymbol{n}\times\boldsymbol{H}+\boldsymbol{E}-(\boldsymbol{n}\cdot\boldsymbol{E})\boldsymbol{n}=(\boldsymbol{n}\cdot\boldsymbol{E_s})\boldsymbol{n}-\boldsymbol{E_s} \tag{6.1.1}$$

The model was also assumed to be a perfect magnetic conductor by adding the boundary condition expressed in Equation 6.1.2 [61].

$$\boldsymbol{n} \times \boldsymbol{H} = \boldsymbol{0} \tag{6.1.2}$$

The waveguide port was used as the source of the microwave radiation in the model, and was excited using a transverse electric wave of mode TE_{10} at an excitation frequency of 2.45 GHz and a power input of 1000 W. The propagation constant β for the port was given by the excitation frequency f and cut-off frequency f_c, both expressed in Hz, and the speed of light c and expressed in Equation 6.1.3 [61].

$$\beta = \frac{2\pi}{c}\sqrt{f - f_c} \tag{6.1.3}$$

To simulate the microwave heating in the model, Maxwell's electromagnetic equation, expressed in Equation 6.1.4 was used to solve for the electric field vector E inside of the microwave oven and waveguide cavity [61], [62]. In this equation, k_0 is the wave number in free space, σ is the electrical conductivity in S/m, and ω is the angular frequency in rad/s.

$$\nabla \times (\mu_r^{-1} \nabla \times \boldsymbol{E}) - k_0^2 \left(\varepsilon_r - \frac{j\sigma}{\omega \varepsilon_0}\right) \boldsymbol{E} = 0 \tag{6.1.4}$$

In solving the simulation, the following assumptions were made. First, that the study was frequency-transient meaning that the material properties are constant during a period of microwave frequency oscillation. The heat equation was then solved with time. Second, that the microwave frequency is constant at 2.45 GHz with an input power of 1000W. Lastly, that the initial temperature of both the air and the sample starts at 20°C.

6.2 Microwave Heating of SiC_w-Al_2O_3 Samples from the Percolation Study

In modeling the composite samples, the material properties of different SiC whisker composition samples were calculated using the rule of mixtures shown in Equation 6.2.1. In this Equation P_c is the property being calculated of the composite, P_1 is the property of material 1, P_2 is the property of material 2, V_1 is the volume fraction of material 1, and $V_2$is the volume fraction of material 2, and so on and so forth.

$$P_c = P_1V_1 + P_2V_2 + \cdots \tag{6.2.1}$$

This was done for all properties shown in Table 6.2.1 except for the electrical conductivity σ which was taken directly from experimental data in attempt to make the simulations more representative of the experimentally fabricated samples, which is presented separately in Table 6.2.2. All the material properties except electrical conductivity presented in Table 6.2.2 for SiC and Al_2O_3 however, were used in Equation 6.2.1 to calculate the bulk material properties of the composite samples from Chapter 4.

Table 6.2.1 Material properties of SiC and Al_2O_3 used to calculate the bulk material properties of SiC_w- Al_2O_3 composites of varying SiC whisker content.

	Temperature Range (K)	SiC [63], [64]	Al_2O_3 [65]
ρ (kg/m^3)	273-2200	3210	3950
μ_r (unitless)	273-2200	1	1
ε_r (unitless)	273-2200	$6.4 - (1.67\times10^{-3})T + (1.88\times10^{-6})T^2$	$8.3 + (1.34\times10^{-3})T$
σ (S/m)	273-2200	5×10^{-2}	1×10^{-14}
C_p (J/kgK)	273-673	$-8.35 + 3.08T - 0.00293T^2 + (1.0268\times10^{-6})T^3$	850
	673-2200	$772 + 0.431T - (2.1\times10^{-5})T^2$	
κ (W/mK)	273-2200	$192 - 0.326T + (2.74\times10^{-4})T^2 - (7.71\times10^{-8})T^3$	$39500T^{-1.26}$

Table 6.2.2 Electrical conductivity of SiC_w-Al_2O_3 composite samples taken directly from experimental data collected in Chapter 4 used for COMSOL simulations.

SiC Content (%)	σ (S/m)
1.09	7.21×10^{-11}
3.52	9.77×10^{-11}
5.81	1.16×10^{-10}
7.68	2.45×10^{-7}
9.96	1.48×10^{-6}
12.2	8.93×10^{-4}
14.5	1.54×10^{-3}
17.0	5.59×10^{-3}
19.1	9.05×10^{-3}
24.0	2.23×10^{-2}
28.2	3.28×10^{-2}

The relative permittivity, specific heat capacity at constant pressure, and thermal conductivity of SiC, and the relative permittivity and thermal conductivity of Al_2O_3 are all

functions of temperature expressed in K. Ideally, the electrical conductivity should also be expressed as a function of temperature but was assumed to be constant for the samples in the model. For each SiC_w- Al_2O_3 composition, the simulation was ran for a total of 500s with a time step of 2s.

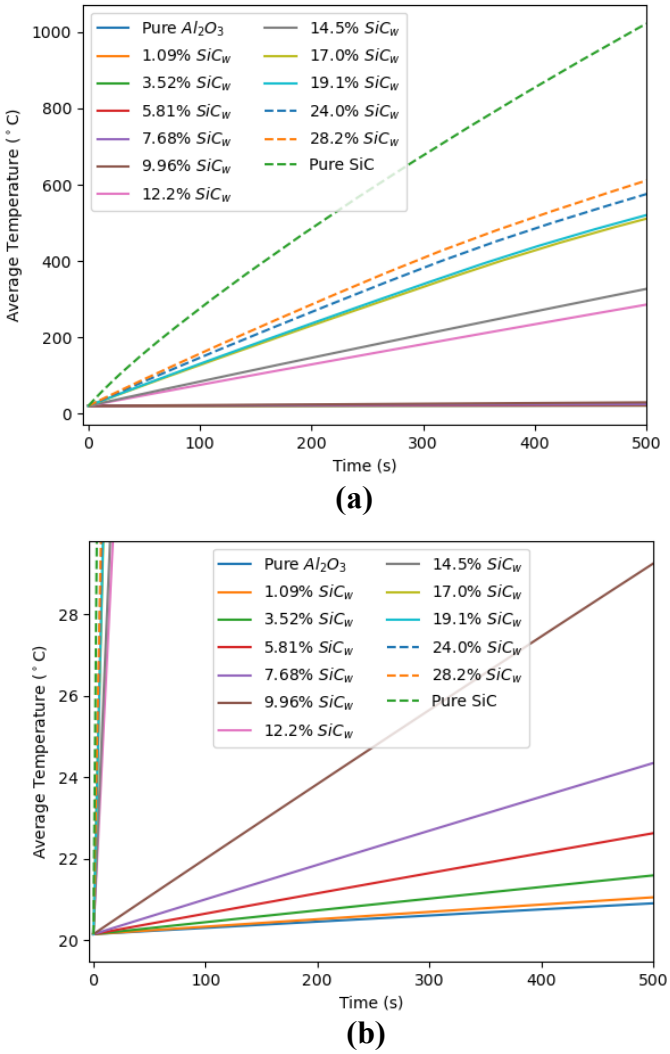

Figure 6.2.1 Average temperature of (a) SiC_w- Al_2O_3 samples of varying composition, pure SiC, and pure Al_2O_3 samples over the simulating time and (b) a zoomed in view.

The average temperature of each SiC_w- Al_2O_3 composition is plotted as well as pure SiC and Al_2O_3 over time in Figure 6.2.1. The heating rate of each sample is calculated as the slope of the average temperature increase over time and the maximum average temperature reached at 500s is presented in Table 6.2.3. As seen in both Figure 6.2.1 and Table 6.2.3, the heating rate and maximum average temperature increases with increasing SiC content, with the maximum heating rate being achieved with the pure SiC sample. This is to be expected as SiC has a resonant frequency at 2.45 GHz and more readily converts electromagnetic energy to thermal energy when subjected to this frequency than does Al_2O_3.

Table 6.2.3 Maximum average temperature and calculated heating rate of simulated microwave heated SiC_w- Al_2O_3 samples.

Sample	Heating Rate (°C/s)	Maximum Average Temperature (°C)
Pure Al_2O_3	0.0016	20.93
1.09% SiC Content	0.0019	21.08
3.52% SiC Content	0.0030	21.63
5.81% SiC Content	0.0051	22.69
7.68% SiC Content	0.0086	24.46
9.96% SiC Content	0.0187	29.49
12.2% SiC Content	0.5451	292.69
14.5% SiC Content	0.6344	337.35
17.0% SiC Content	1.0067	523.52
19.1% SiC Content	1.0155	527.89
24.0% SiC Content	1.1383	589.32
28.2% SiC Content	1.2112	625.78
Pure SiC	2.0044	1022.37

There are also significant increases in the heating rates between compositions as the SiC phase begins to dominate the overall composite behavior. The first of which is the sharp increase from the 9.96% SiC whisker content sample to the 12.2% SiC whisker content sample. The percolation threshold was previously established in Chapter 4 at a SiC whisker content of 7.68%, but in the microwave heating simulations this 7.68% whisker content composition has a relatively low heating rate and maximum average temperature comparable to the pure Al_2O_3 sample at 0.0086°C/s and 24.46°C, respectively. This indicates that although the percolation threshold occurs at 7.68% SiC whisker content, the SiC whisker behavior only begins to dominate the bulk response of the composite in being able to more rapidly heat up when exposed to a microwave frequency at higher SiC whisker contents where more conducting paths are present.

The next significant increase in both the heating rate and maximum average temperature reached occurs between the 14.5% SiC whisker content and the 17.0% SiC whisker content samples. The heating rate nearly doubles from 0.6344 °C/s to 1.0067°C/s and the maximum temperature reached increases from 337.35°C to 523.52°C between these two samples. This again demonstrates that although the SiC begins to dominate the electrical response at the percolation threshold of 7.68% whisker content, it does not begin to dominate the microwave heating response until a much higher whisker content of 17.0%.

The temperatures plotted in Figure 6.2.1 however, are average temperatures of the respective sample. To better understand the overall heating of the samples, Figure 6.2.2 presents the electric field, resistive heating, and the temperature through the center of sample viewed in the X-Z plane after the 500 simulated seconds. The pure Al_2O_3 sample,

the 7.68% SiC content sample, 17.0% SiC content sample, and pure SiC sample are shown for the sake of conciseness. Note the large differences in the scales of the legends between each respective sample. This was done to preserve higher resolution of both the electric field and temperature local maxima and minima in the microwave oven cavity as well as in the sample.

In all samples, there is variation in the electric field in the microwave cavity which is due to the interference of the reflected electric field from the microwave cavity and waveguide walls, which was enforced using the impedance boundary condition mentioned earlier in Equation 6.1.1. In the 7.68% and 17.0% SiC content samples, there is a maximum in the electric field in the sample itself. For the 17.0% SiC sample in particular, this electric field maximum of 1.13×10^5 V/m corresponds to the same location in the sample where a thermal hotspot is observed of 588.98°C. It is also in the 17.0% SiC sample that the temperature profile through the center of the sample in the X-Z plane is most symmetrical. With all other samples plotted in Figure 6.2.2, the temperature profile through the center of the sample in the X-Z is not symmetric. The pure Al_2O_3 sample and the 7.68% SiC content sample have respective thermal hotspots further along the X-axis while the pure SiC sample has a thermal hotspot closer towards the origin on the X-axis.

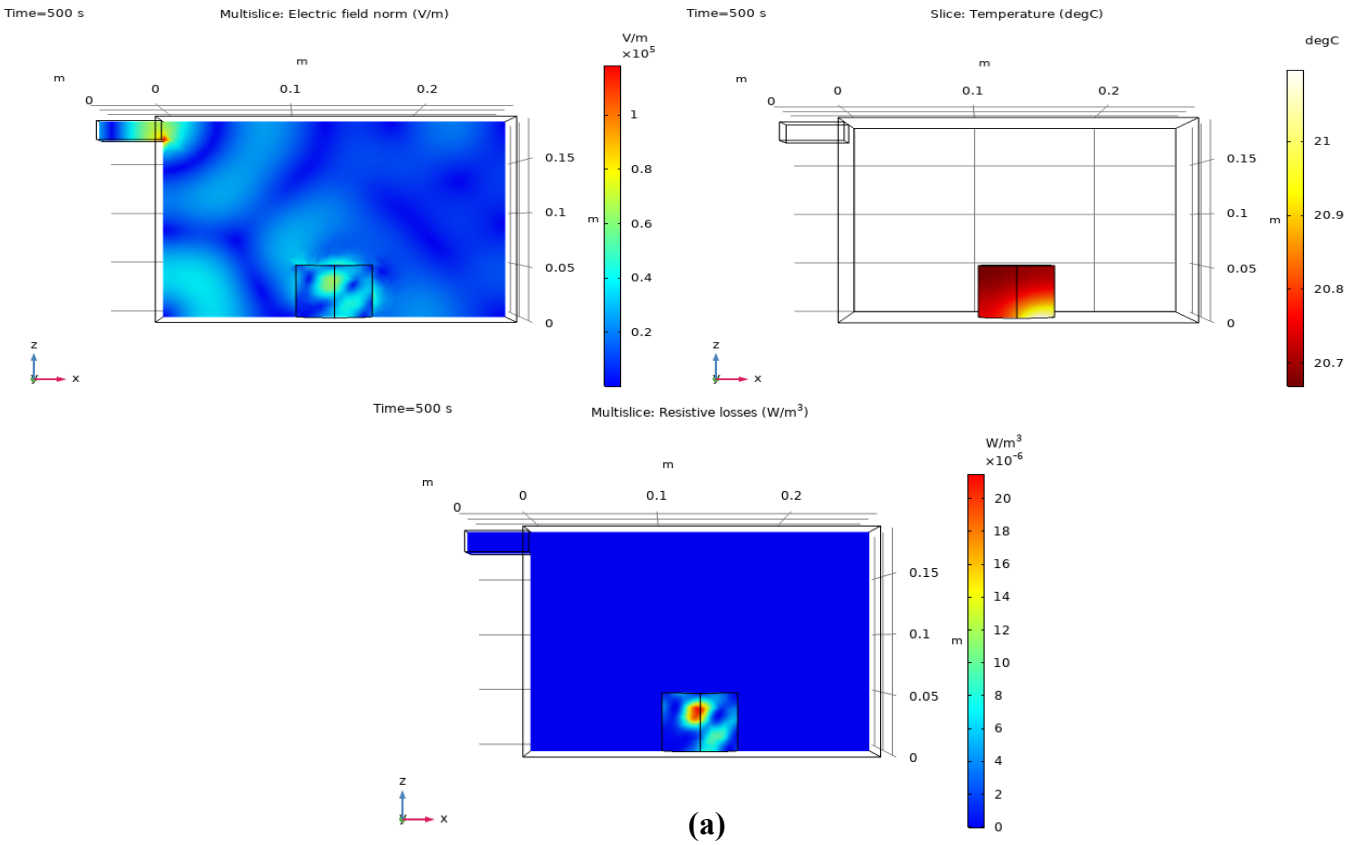
Time=500 s
Multislice: Electric field norm (V/m)
V/m
×10^5
Time=500 s
Slice: Temperature (degC)
degC
Time=500 s
Multislice: Resistive losses (W/m^3)
W/m^3
×10^-6

(a)

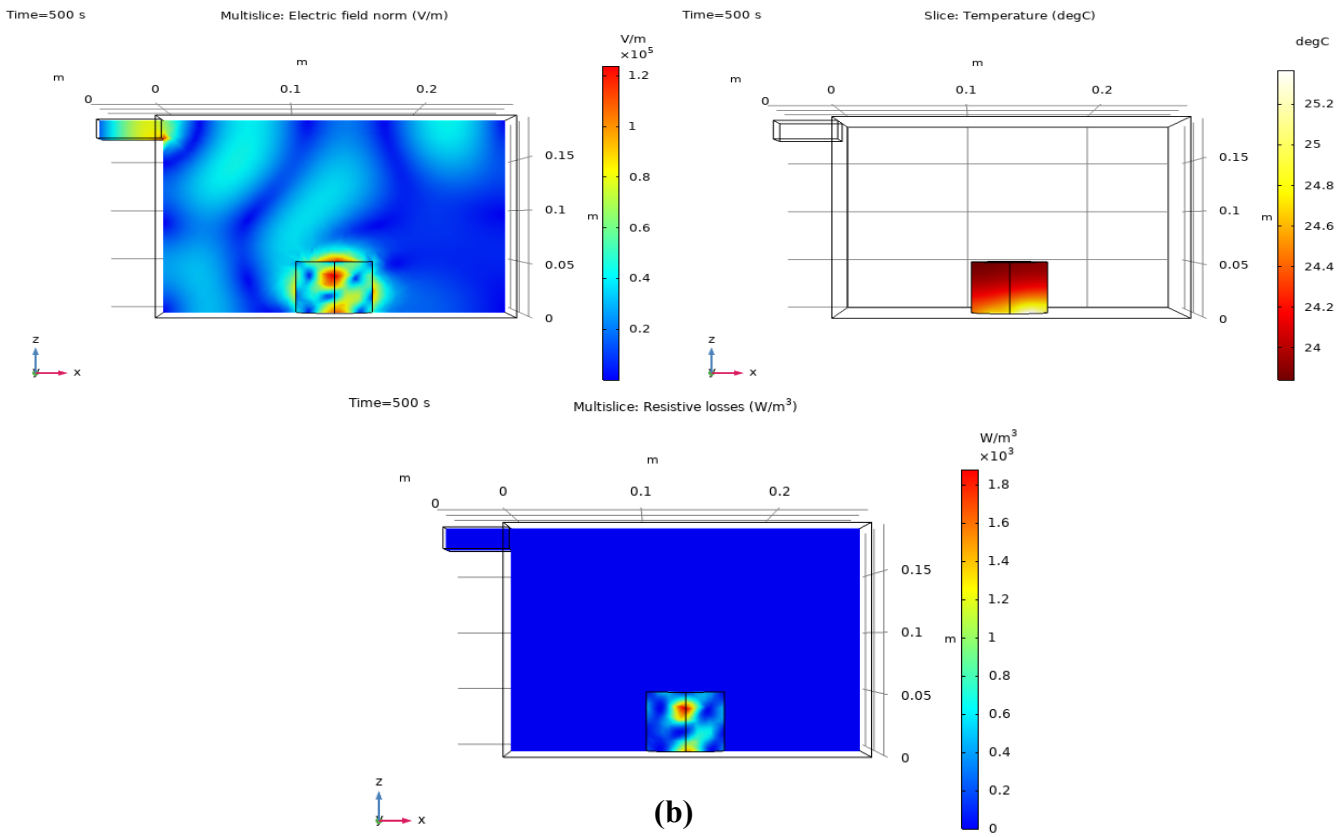
Time=500 s
Multislice: Electric field norm (V/m)
V/m
×10^5
Time=500 s
Slice: Temperature (degC)
degC
Time=500 s
Multislice: Resistive losses (W/m^3)
W/m^3
×10^3

(b)

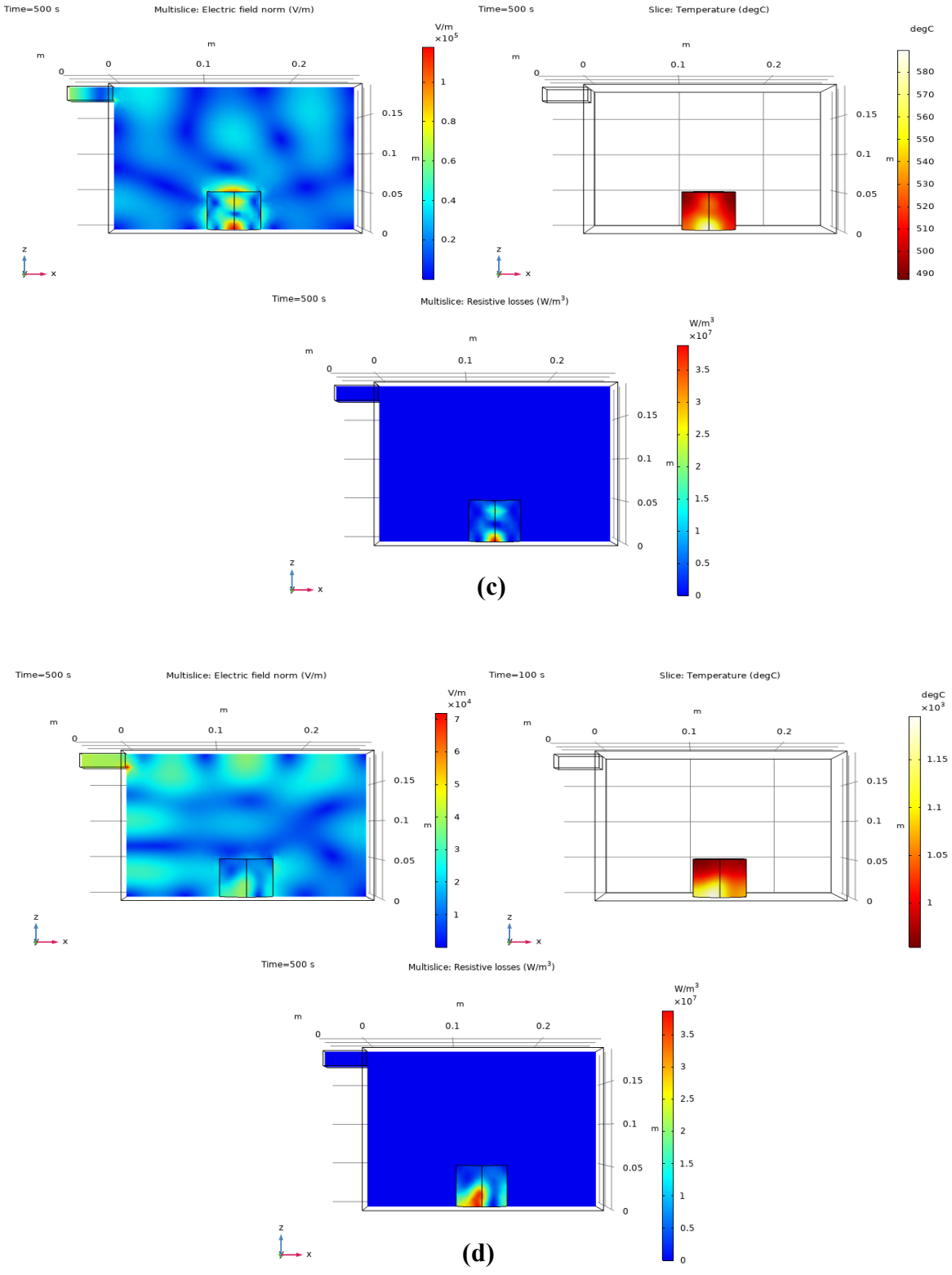

Figure 6.2.2 Electric field, sample temperature, and resistive losses through the center in the X-Z plane after 500s of (a) the pure Al_2O_3 sample, (b) the 7.76% SiC content sample, (c) the 17.0% SiC content sample, and (d) the pure SiC sample.

Additionally, the resistive losses in all samples shown in Figure 6.2.2. are negligible in air but are highest in each respective sample. In the pure alumina and 7.68% SiC sample, the respective maximum resistive losses do not occur in the same location as the thermal hotspot. In the pure alumina sample, although it appears that there is a high resistive loss in the sample, the maximum resistive loss of only 21.7×10^{-6} W/m^3 is very low and thus negligible compared to the other samples. In the 7.68% SiC sample, there is a higher maximum resistive loss of 1.84×10^{3} W/m^3 that occurs towards the top center of sample in the same location as the maximum electric field, when viewing in the X-Z plane. For the 17.0% SiC sample, there is a significant rise again in the resistive loss to 3.72×10^{7} W/m^3 which is comparable to the pure SiC sample which has a maximum resistive loss of 3.73×10^{7} W/m^3. This indicates that for these two samples, the resistive losses that occur due to the induced microwave frequency is dominated by the SiC. Furthermore, both the 17.0% SiC and pure SiC samples have their respective high resistive losses in the same locations of which the thermal hotspot occurs in the samples. This could indicate that in these locations, the SiC particles are surrounded by more SiC particles and that heat is retained more efficiently as opposed to heat being lost towards the sample edges which interface with air.

This is supported by Figure 6.2.2 where the SiC whisker behavior begins to dominate the microwave heating response not at the percolation threshold of 7.68% SiC content, but rather a higher SiC content of 17.0%. In the pure Al_2O_3 and 7.68% SiC content sample, the electric field increases in strength in a location near the top-center of the sample. The electric field variation in the entire simulation appears very similar between

the two respective samples, with the 7.68% SiC content sample having a slightly stronger electric field than the pure Al_2O_3 sample.

In the 7.68% SiC content sample however, there does begin to appear an electric field hotspot on the bottom-center of the sample along the interface of the bottom of the sample and the bottom microwave oven wall. A similar area of increased electric field is also seen in the same location in the 17.0% SiC content, which corresponds to the location of the thermal hotspot in the 17.0% SiC content sample. As the SiC behavior begins to dominate the microwave heating response of the overall composite sample, it appears that areas in the sample that experience higher electric fields correspond to the same areas in which a thermal hotspot is observed. This is to be expected as the SiC microwave frequency resonance is the primary heating mechanism in the composite samples, and thus areas subjected to higher electric fields more rapidly convert electromagnetic energy to thermal energy.

To better illustrate the relation between the maximum temperature and the maximum resistive loss, Figure 6.2.3, plots the maximum temperature and resistive loss on 2 separate axes as a function of SiC whisker content. There is a clear correlation between the maximum temperature reached and the maximum resistive loss experienced after the simulated time of 500s. As the maximum temperature rises sharply from 9.96% to 17.0% SiC whisker content, so does the resistive loss in the sample. Resistive losses thus are the primary heating mechanism in these samples regardless of composition and generate heat inside the materials by reducing the amplitude of the microwave field [66].

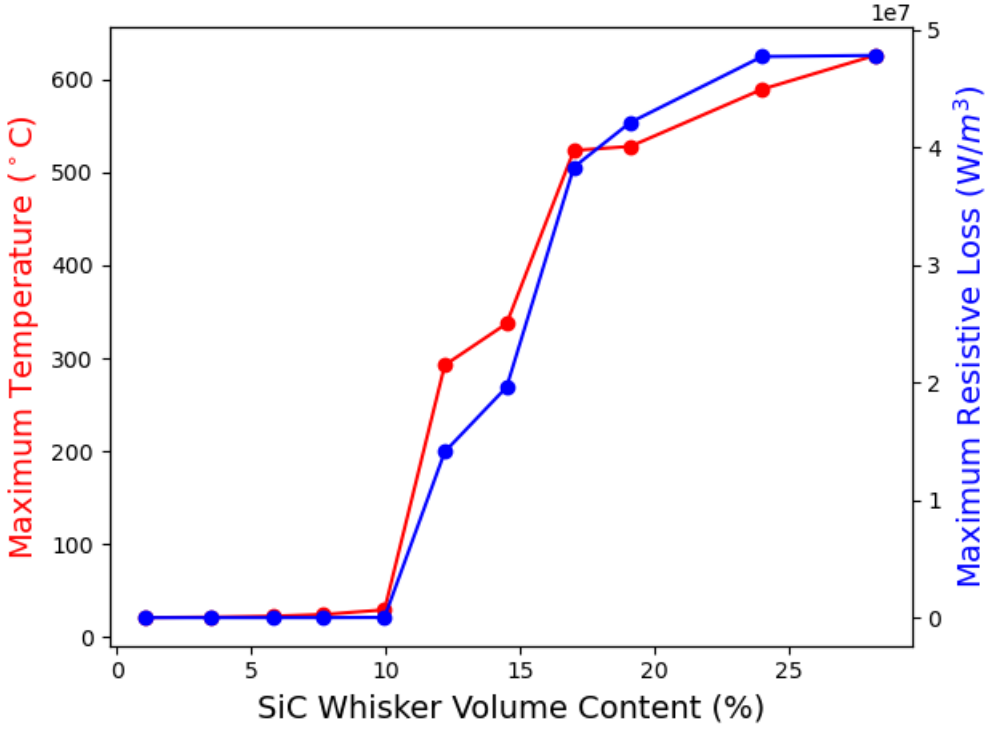

Figure 6.2.3 Maximum temperature and resistive loss in all simulated SiC_w-Al_2O_3 compositions after 500s.

6.3 Microwave Heating of 3YSZ-SiC_w-Al_2O_3 Samples

The 3YSZ-SiC_w-Al_2O_3 samples simulated in this chapter are based off the composite samples presented in Chapter 5. The material properties used for the SiC and Al_2O_3 are the same ones presented in Table 6.2.1 in Section 6.2. The material properties used for the 3YSZ [37], [67], presented below in Table 6.3.1, were used with the material properties in Table 6.2.1 using the rule of mixtures to calculate the relative permittivity, specific heat capacity at constant pressure, and thermal conductivity of the composite sample as functions of temperature in K.

Table 6.3.1 Material properties of 3YSZ used to calculate the bulk material properties of 3YSZ-SiC_w-Al_2O_3 composites.

Temperature Range (K)	ρ (kg/m^3)	μ_r (unitless)	ε_r (unitless) [67]	σ (S/m) [37]	C_p (J/kgK) [37]	κ (W/mK) [37]
273	6050	1	$5.38 - (4.34\times10^{-3})T + (2.22\times10^{1}) + (1.37\times10^{-2})T$	0.0258	217	0.198
342				0.0045	324	0.290
373				0.0033	363	0.320
412				0.0029	398	0.344
454				0.0036	426	0.362
501				0.0043	450	0.373
549				0.0050	470	0.381
597				0.0058	487	0.385
644				0.0078	501	0.381
693				0.0121	514	0.391
744				0.0185	526	0.399
796				0.0288	537	0.407
847				0.0442	547	0.414
909				0.0664	558	0.405
971				0.0975	568	0.412
1025				0.1416	575	0.417
1082				0.2003	583	0.421
1138				0.2786	590	0.426
1194				0.4083	597	0.430
1246				0.5942	603	0.433
1292				0.8220	607	0.436
1338				1.2190	612	0.439
2200				1.6661	615	0.441

As with the previous chapter, the sample conductivity of the samples presented in this sub-chapter were taken from the electrical data taken in Chapter 5 in an effort to have the samples more closely resemble the experimental samples fabricated. The 15% SiC_w-Al_2O_3, 3YSZ-SiC_w-Al_2O_3 not annealed, and 15% Type E SiC_w-Al_2O_3 samples have a noticeably higher electrical conductivity than the 14.5% SiC_w-Al_2O_3 samples previously made with compositions made by Brian Bertram as demonstrated in Table 6.3.2. These

samples have an electrical conductivity on the order of magnitude of 10^{-1}, while the 14.5% SiC_w-Al_2O_3 sample has a conductivity on the order of magnitude of 10^{-3}. This is likely due to the mixes made by Bertram becoming oxidized over time and forming SiO_2, which is a well-known electrical insulator. For the Type E samples, once the 3YSZ is added to the composite composition, the electrical conductivity more closely resembles the electrical conductivity measurement taken of the 15% SiC_w-Al_2O_3 sample. More specifically, the 3YSZ-Type E SiC_w-Al_2O_3 not annealed sample was measured to have an electrical conductivity of 5.2836×10^{-3} S/m, the 3YSZ-Type E SiC_w-Al_2O_3 sample annealed in O_2 1.3636×10^{-3} S/m, while the 14.5% SiC_w-Al_2O_3 sample from the percolation study has an electrical conductivity value of 1.54×10^{-3} S/m. This is not the case with the 3YSZ-SiC_w-Al_2O_3 samples annealed in air and O_2, which have noticeably lower electrical conductivities of 2.1843×10^{-5} and 2.2741×10^{-5} S/m, respectively.

Table 6.3.2 Electrical conductivity of 3YSZ-SiC_w-Al_2O_3 composite samples taken directly from experimental data collected in Chapter 5 used for COMSOL simulations.

Sample	σ (S/m)
15% SiC_w-Al_2O_3	6.3203×10^{-1}
3YSZ-SiC_w-Al_2O_3 Not Annealed	4.8134×10^{-1}
3YSZ-SiC_w-Al_2O_3 Annealed in Air	2.1843×10^{-5}
3YSZ-SiC_w-Al_2O_3 Annealed in O_2	2.2741×10^{-5}
15% Type E SiC_w-Al_2O_3	1.3532×10^{-1}
3YSZ-Type E SiC_w-Al_2O_3 Not Annealed	5.2836×10^{-3}
3YSZ-Type E SiC_w-Al_2O_3 Annealed in O_2	1.3636×10^{-3}

Along with the samples listed above, a pure 3YSZ heating simulation was performed to measure the baseline heating properties of 3YSZ under a 2.45 GHz microwave frequency, specifically to characterize the thermal runaway effect that occurs causing the 3YSZ to rapidly heat up. For the pure 3YSZ sample, a simulation of 740s with a 2s time step was used as this was sufficient time to demonstrate the thermal runaway without being so long that the model was unable to converge as the thermal runaway effect began to take over. The heating behavior of 3YSZ is plotted below in Figure 6.3.1 over time, plotting the maximum temperature, minimum temperature, and average temperature in the sample.

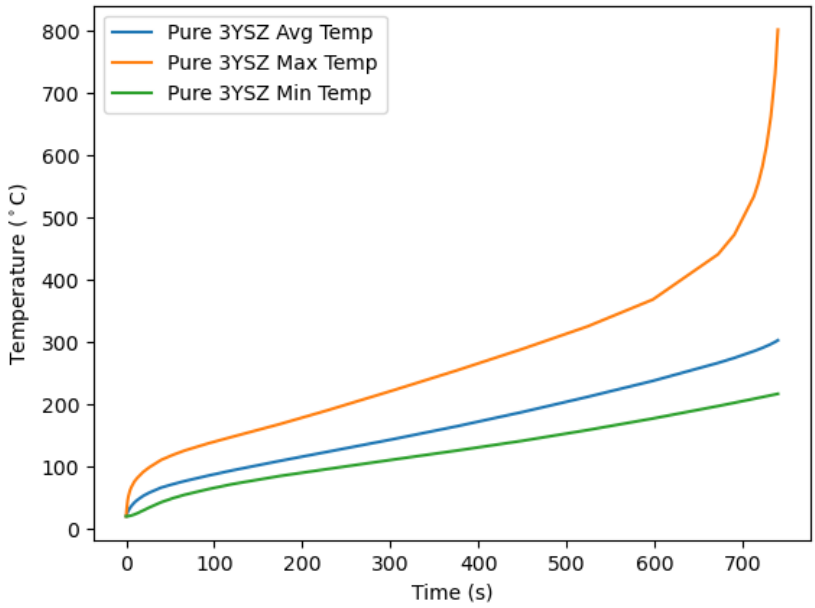

Figure 6.3.1 Average, maximum, and minimum temperature of pure 3YSZ sample during 2.45 GHz microwave heating.

As seen in the plot, there is a clear thermal runaway effect that occurs in the maximum temperature where the sample begins to rapidly heat up to temperatures approaching 1000°C starting at a temperature of ~350°C. This thermal runaway effect is only seen in the maximum temperature as that is the only temperature measured during the simulation that surpassed 350°C. In theory, this thermal runaway effect should occur in any region of the sample that reaches 350°C, but this is not confirmed in this work due to the model not being able to converge in the time-dependent solver past a simulated time of 740s.

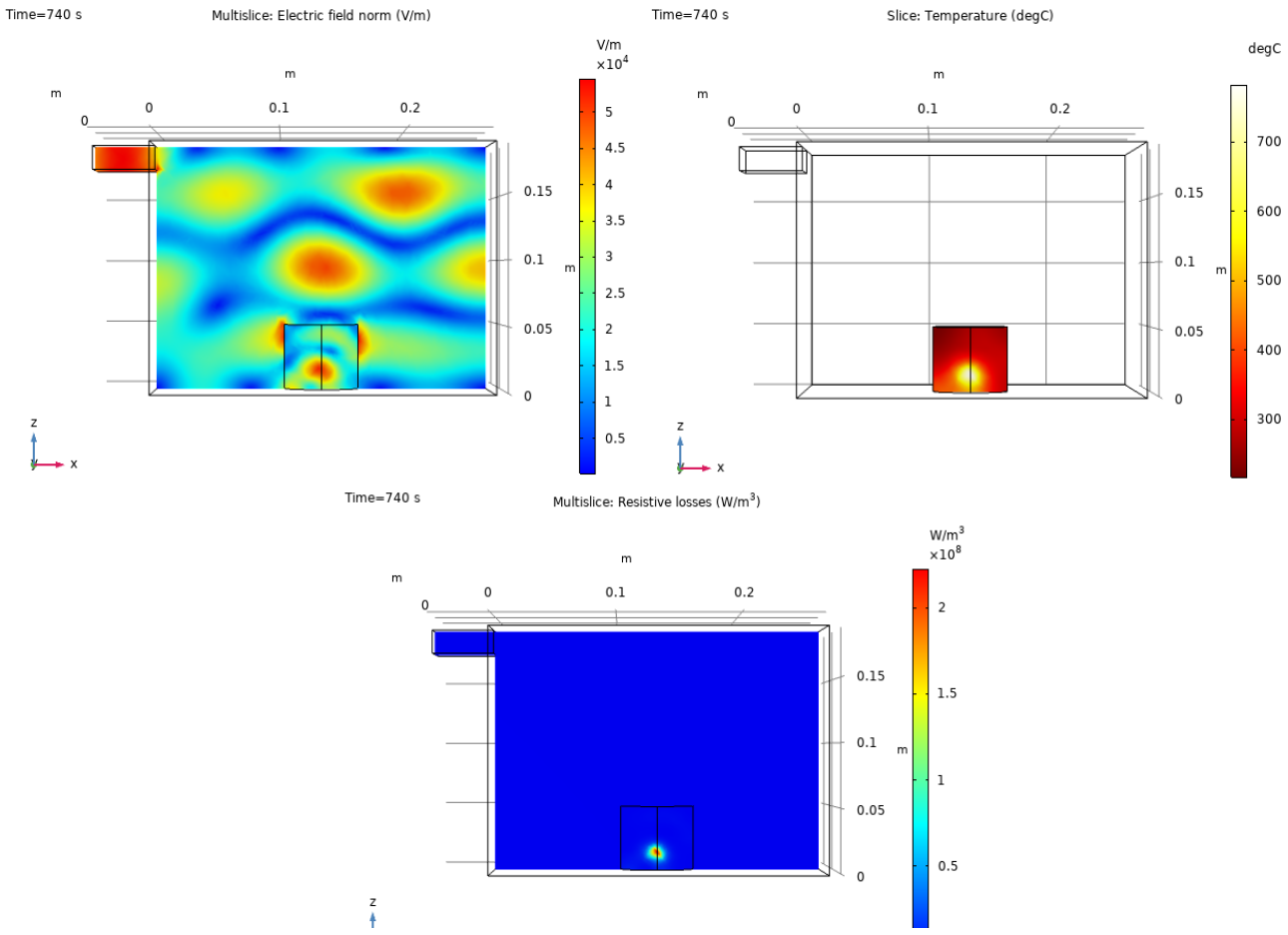

Figure 6.3.2 Electric field, temperature, and resistive losses though the center of the pure 3YSZ sample viewing in the X-Z plane.

To better visualize the heating behavior of the pure 3YSZ sample, Figure 6.3.2 plots the electric field, temperature, and resistive losses though the center of the sample in the X-Z plane at the end of the simulation. In electric field, there are local fluctuations in the microwave oven cavity due to the interaction of the electric field with the microwave and waveguide walls. However, the highest electric field is 5.37×10^4 V/m and is observed at the center of the sample where the thermal hotspot and thermal runaway effect occurs. The electric field is also highest on the sides of the sample likely due to high electric field reflection between the 3YSZ sample and the microwave and waveguide walls.

The location of the thermal hotspot in the 3YSZ sample which reaches a maximum of 801°C also coincides with the location of which the resistive losses are the highest at a maximum of 2.77×10^7 W/m^3. This again is an indication that the resonance of the 3YSZ particles in the sample is highest at this location and heats quickly due to being surrounded by many 3YSZ particles, as compared to the outer edges of the sample.

The samples fabricated in Chapter 5 were also simulated under a 2.45GHz microwave frequency to study the influence 3YSZ has on the overall microwave heating behavior of the composite samples. Initially, all samples were ran for a simulated time of 740s for better comparison against the pure 3YSZ sample. However, the 3YSZ-SiC_w-Al_2O_3 samples annealed in air and O_2, as well as the 3YSZ-Type E SiC_w-Al_2O_3 sample annealed in O_2 were ran for a total simulation time of 1500s to allow for sufficient time for the sample to heat up. Figure 6.3.3 plots the maximum temperature of each respective composite sample made in Chapter 5 as well as the pure 3YSZ sample for comparison. The

maximum is plotted as the thermal runaway effect would be most easily captured in the maximum temperature of the sample.

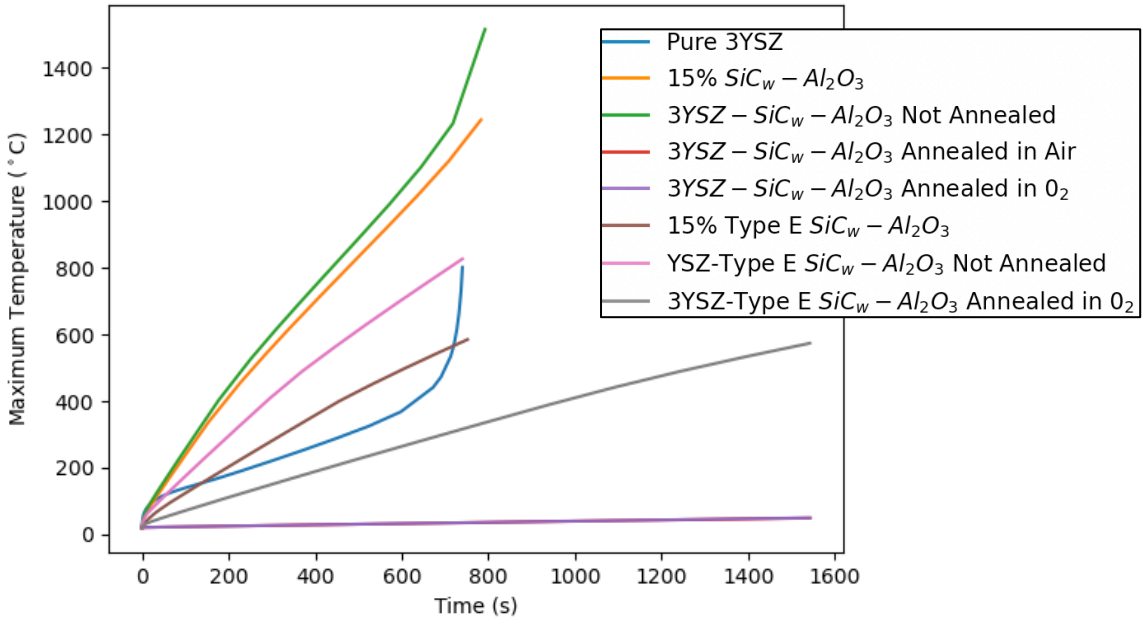

Figure 6.3.3 Maximum temperature of all samples presented in Table 6.3.2 and pure 3YSZ over the simulated time.

In the plot, it is clear that there is no thermal runaway effect observed in any of the samples, although the 3YSZ-SiC_w-Al_2O_3 not annealed sample shows the start of a thermal runaway effect at ~1200°C. However, in comparison to the pure 3YSZ sample, the thermal runaway seen in the 3YSZ-SiC_w-Al_2O_3 not annealed sample occurs at a significantly higher temperature and the heating is not as rapid. This sample is the exception however, with all the other samples containing 3YSZ shown in Figure 6.3.3 not displaying any thermal runaway effect. This is true despite the 3YSZ-Type E SiC_w-Al_2O_3 samples, both not annealed and annealed in O_2, reaching temperatures above 350°C, which was the

temperature at which the pure 3YSZ began to display thermal runaway. It is also worth noting that all samples that underwent an annealing treatment did not reach a high maximum temperature relative to the other samples, despite having ample time to do so with a microwave heating simulation time of 1500s.

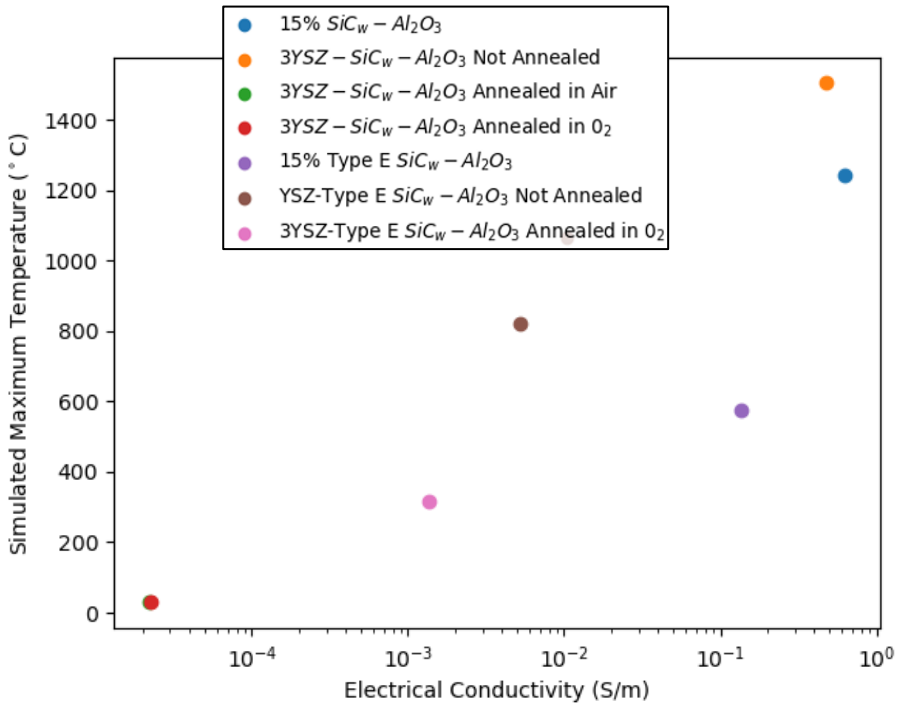

Figure 6.3.4 Electrical conductivity of 3YSZ-SiC_w-Al_2O_3 composite samples taken directly from experimental data collected in Chapter 5 and the maximum simulated temperature after 740s.

This is likely due to the electrical conductivity of the annealed samples being significantly lower than the electrical conductivity of samples with no annealing treatment as seen in Table 6.3.2. The experimentally measured electrical conductivity of the samples presented in Chapter 5 are plotted against the simulated maximum temperature after 740s of simulating heating time in Figure 6.3.4. As seen in the plot, as electrical conductivity

increases, the maximum temperature reached generally increases which is to be expected since the electrical conductivity of a sample accounts for all resistive losses in the material [66], [67].

For both the 15% SiC_w-Al_2O_3 and 15% Type E SiC_w-Al_2O_3 samples however, made with the AdValue and Advanced Composite Materials aluminas, respectively, the maximum temperature increases with the addition of 3YSZ with no annealing treatment done. This is true despite the electrical conductivities decreasing from 6.3203×10^{-1} to 4.8134×10^{-1} S/m between the 15% SiC_w-Al_2O_3 and 3YSZ-SiC_w-Al_2O_3 samples, and 1.3532×10^{-1} to 5.2836×10^{-3} S/m between the 15% Type E SiC_w-Al_2O_3 and 3YSZ-Type E SiC_w-Al_2O_3 samples. However, once the 3YSZ-SiC_w-Al_2O_3 samples are annealed, the electrical conductivity decreases sharply as does the maximum temperature reached in the composite after 740s.

To better study the heating behavior of all the 15% SiC_w-Al_2O_3 and 3YSZ-SiC_w-Al_2O_3 composite samples presented in Chapter 5, Figure 6.3.5 shows the electric field, temperature, and resistive losses through the center of the sample in the X-Z plane after the total simulated heating time. For the 3YSZ-SiC_w-Al_2O_3 samples annealed in air and O_2 and 3YSZ-Type E SiC_w-Al_2O_3 sample annealed in O_2, this time was 1500s, and for the 15% SiC_w-Al_2O_3, 15% Type E SiC_w-Al_2O_3, 3YSZ-SiC_w-Al_2O_3 not annealed, and 3YSZ-SiC_w-Al_2O_3 not annealed samples, this time was 740s.

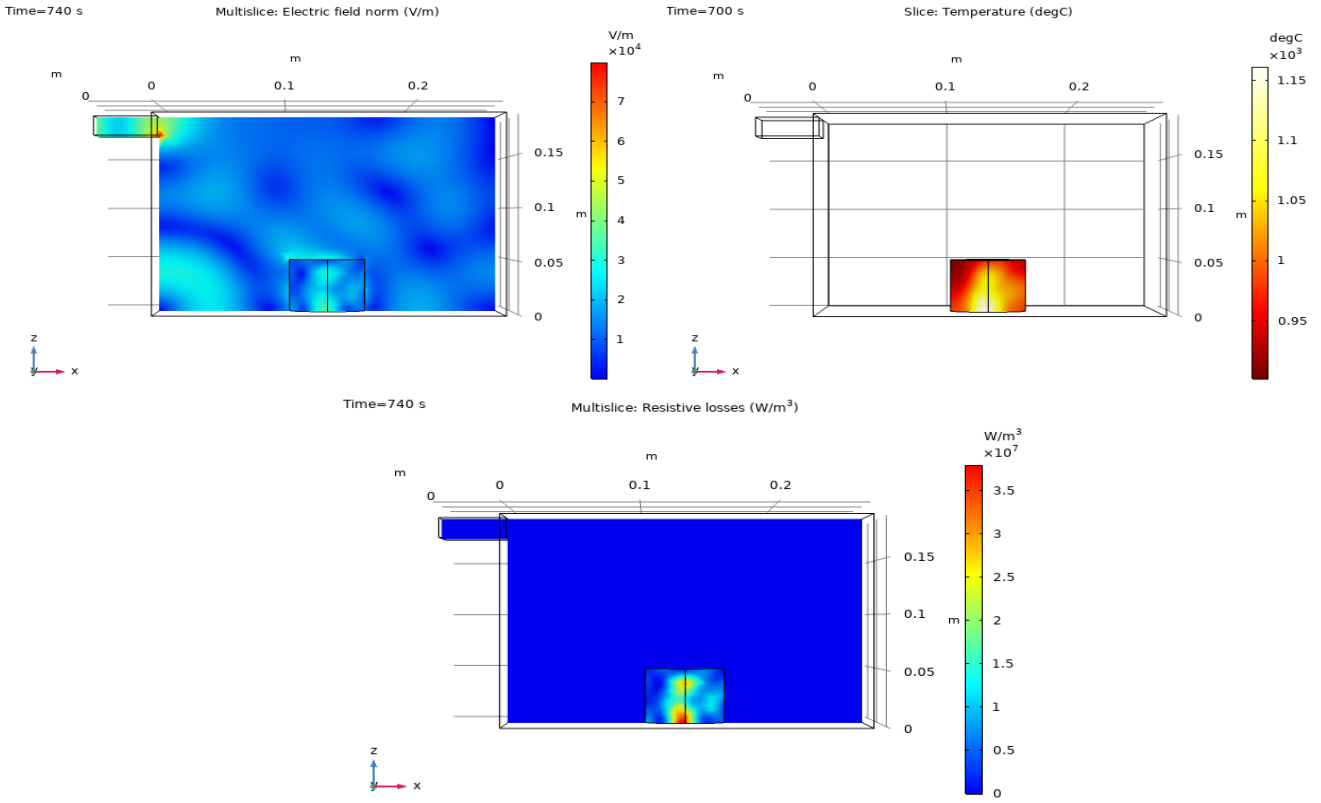
Time=740 s
Multislice: Electric field norm (V/m)
V/m
×10^4
Time=700 s
Slice: Temperature (degC)
degC
×10^3
Time=740 s
Multislice: Resistive losses (W/m^3)
W/m^3
×10^7

(a)

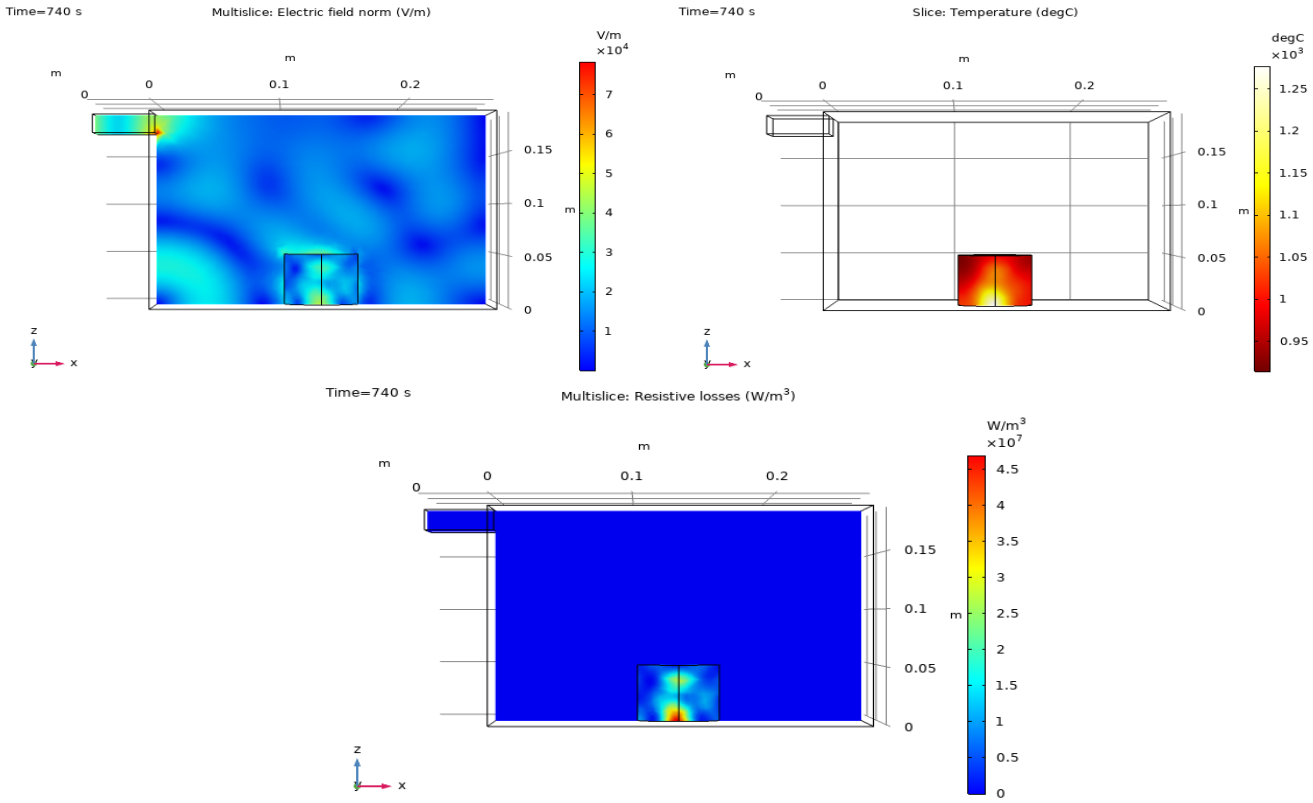
Time=740 s
Multislice: Electric field norm (V/m)
V/m
×10^4
Time=740 s
Slice: Temperature (degC)
degC
×10^3
Time=740 s
Multislice: Resistive losses (W/m^3)
W/m^3
×10^7

(b)

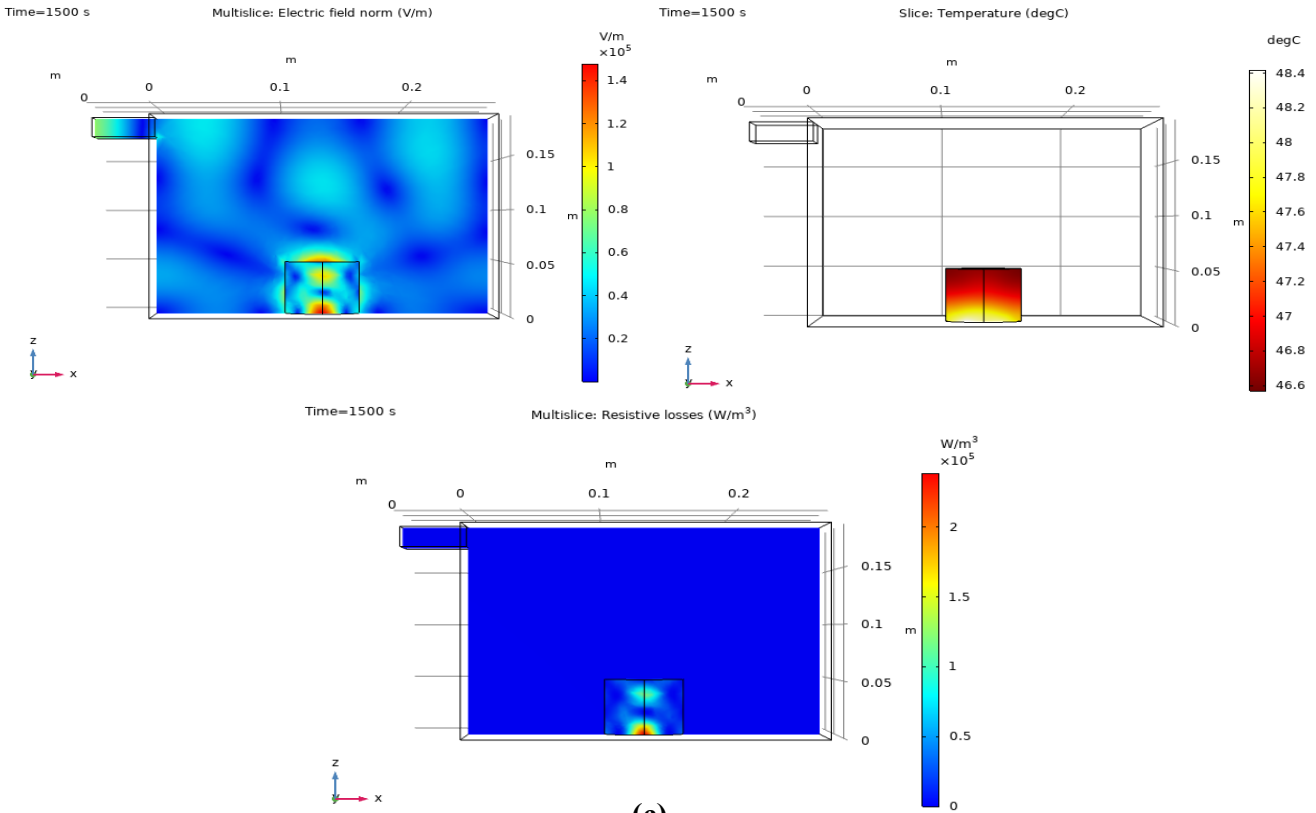
Time=1500 s
Multislice: Electric field norm (V/m)
V/m
×10^5
Time=1500 s
Slice: Temperature (degC)
degC
Time=1500 s
Multislice: Resistive losses (W/m^3)
W/m^3
×10^5

(c)

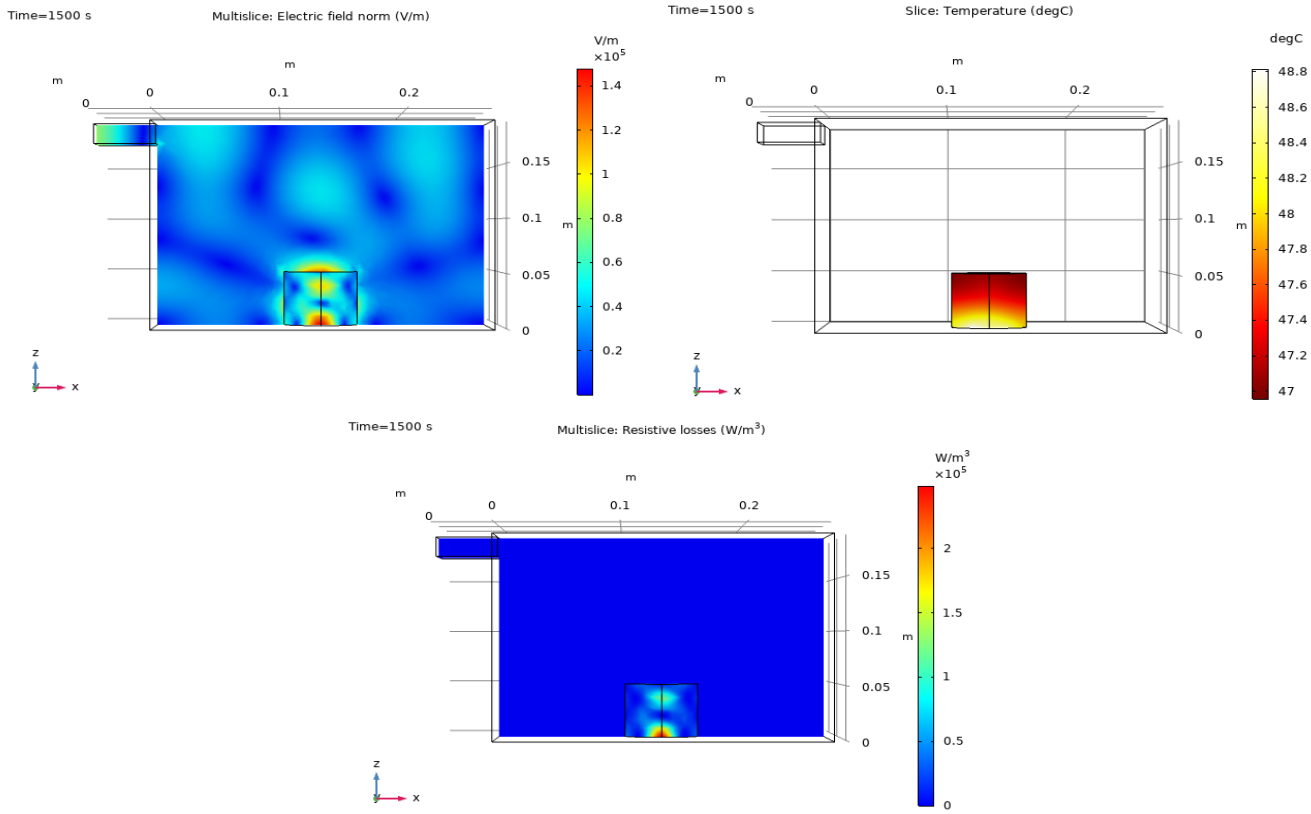
Time=1500 s
Multislice: Electric field norm (V/m)
V/m
×10^5
Time=1500 s
Slice: Temperature (degC)
degC
Time=1500 s
Multislice: Resistive losses (W/m^3)
W/m^3
×10^5

(d)

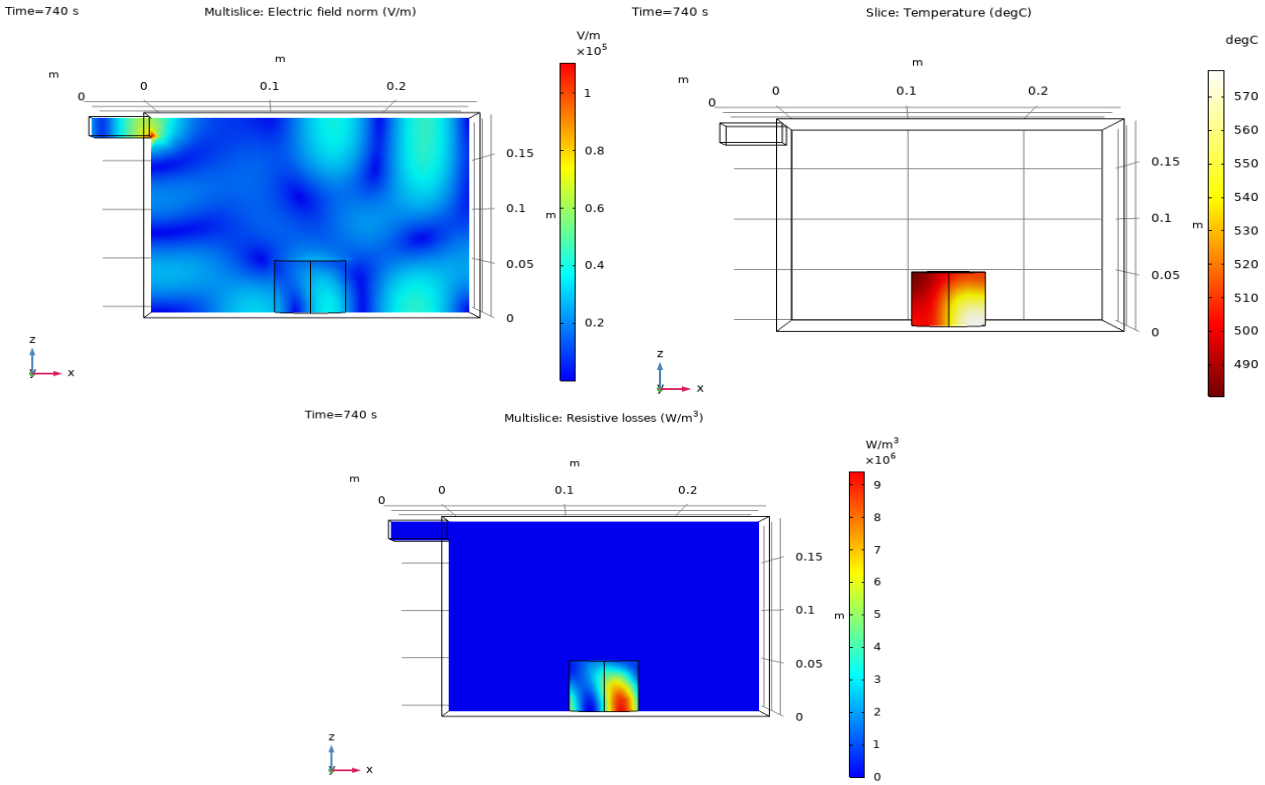
Time=740 s
Multislice: Electric field norm (V/m)
V/m
×10^5
Time=740 s
Slice: Temperature (degC)
degC
Time=740 s
Multislice: Resistive losses (W/m^3)
W/m^3
×10^6

(e)

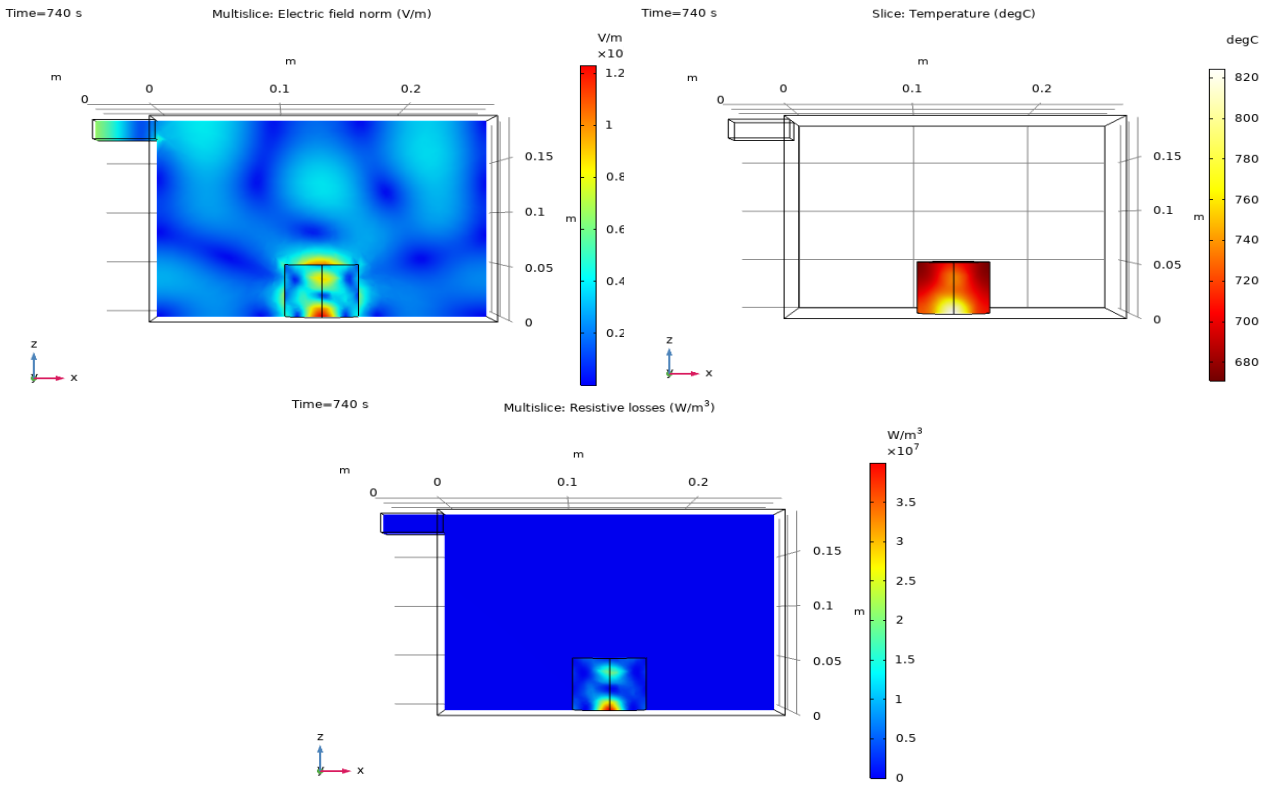
Time=740 s
Multislice: Electric field norm (V/m)
V/m
×10
Time=740 s
Slice: Temperature (degC)
degC
Time=740 s
Multislice: Resistive losses (W/m^3)
W/m^3
×10^7

(f)

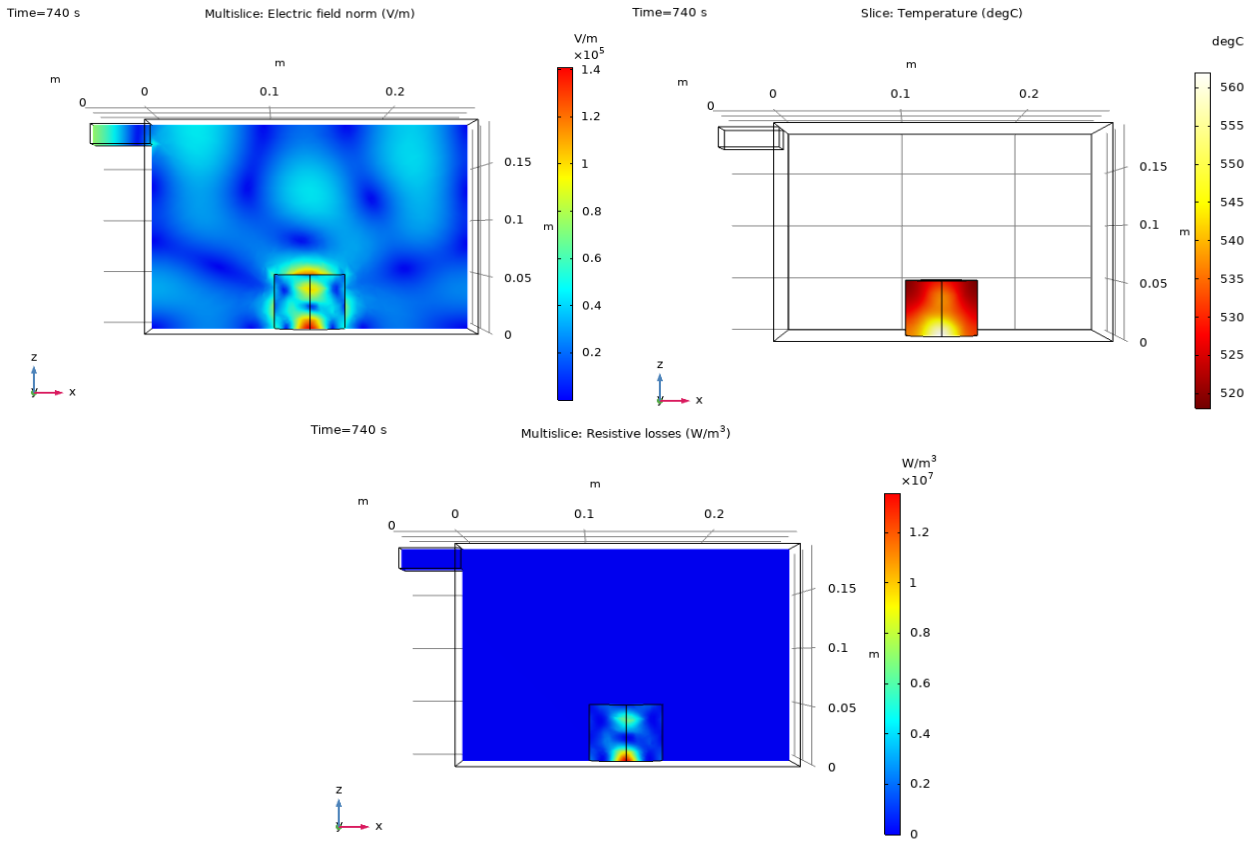

(g)

Figure 6.3.5 Electric field, temperature, and resistive losses through the center of the sample in the X-Z plane of (a) 15% SiC_w-Al_2O_3, (b) 3YSZ-SiC_w-Al_2O_3 Not Annealed, (c) 3YSZ-SiC_w-Al_2O_3 Annealed in Air, (d) 3YSZ-SiC_w-Al_2O_3 Annealed in O_2, (e) 15% Type E SiC_w-Al_2O_3, (f) 3YSZ-Type E SiC_w-Al_2O_3 Not Annealed, (g) 3YSZ-Type E SiC_w-Al_2O_3 Annealed in O_2 samples.

For all samples in Figure 6.3.5, there is slight variation in the electric field in the microwave cavity as well as no or negligible resistive loss in the air of the microwave cavity. Additionally, for every sample the highest electric field and resistive loss generally occurs in the same location as the thermal hotspot in the X-Z plane. The exceptions to this are possibly the 15% SiC_w-Al_2O_3, 3YSZ-SiC_w-Al_2O_3 not annealed, and 15% Type E SiC_w-

Al_2O_3 samples which have their respective electric field maxima in the corner between the waveguide and the microwave.

At a volume of 15% of SiC_w, the samples are past the percolation threshold and thus conductive in their bulk electrical response. Additionally, this is the SiC_w content at which the SiC dominates the microwave heating response as shown in Chapter 6.2, which agrees with the electric field coinciding with the thermal hotspot in the samples presented in Figure 6.3.5. Additionally, the 15% SiC_w-Al_2O_3, 3YSZ-SiC_w-Al_2O_3 not annealed, and 15% Type E SiC_w-Al_2O_3 samples where the electric field maximum is on the waveguide/microwave corner and rather than in the sample, also happen to have the highest electrical conductivities of 6.3203×10^{-1}, 4.8134×10^{-1}, and 1.3532×10^{-1} S/m, respectively.

Lastly, the 3YSZ does not appear to have a large influence on the microwave heating of the composite samples in Figure 6.3.5(b)-(d), and Figure 6.3.5(f)-(g). The pure 3YSZ sample in Figure 6.3.2 simulated microwave heating response was characterized by large variations in the electric field in the microwave cavity as well as a very localized, concentrated, and small thermal hotspot and high resistive hotspot. This is likely due to there not being enough 3YSZ content by volume to sufficiently dominate the microwave heating response.

6.4 Summary

For the SiC_w-Al_2O_3 composites, as the SiC content was increased in the samples, both the maximum temperature reached after 500s, and the heating rate achieved increased. This

was to be expected however, as SiC displays far stronger microwave absorption properties as compared to Al_2O_3. Resistive losses were observed to be the primary heating mechanism in all samples regardless of composition, reducing the amplitude of the microwave frequency and converting the electromagnetic energy to thermal energy. Additionally, it was previously established in Chapter 4 that the percolation threshold, where the bulk electrical behavior transitions from insulating to conducting, for the SPS SiC_w-Al_2O_3 composites was at 7.68% SiC whisker content. However, in simulating the microwave heating behaviors, the SiC begins to dominate the bulk behavior at a much higher whisker content of 17.0%.

This was identified by not only comparing the heating rate and maximum temperature reached to the pure SiC, but also by analyzing the thermal profile, electric field, and resistive losses through the center of the simulated samples in the X-Z plane. As the SiC whisker content increases, there is a large increase in the heating rate and maximum temperature comparable to the pure SiC sample at a whisker content of 17.0%. Additionally, there is stronger electric field interaction in the microwave cavity and a more localized thermal hotspot towards the bottom of the sample for the 17.0% SiC_w sample, which again correlates to the pure SiC sample behavior.

For the 3YSZ-SiC_w-Al_2O_3 composites, it was ultimately found that regardless of the type of alumina used or the annealing treatment done, there was not sufficient 3YSZ volume content to induce thermal runaway in the simulated samples. The only samples that displayed any significant heating were the samples which were not annealed at all and thus had higher electrical conductivities on the order of 10^{-3} and above. The 3YSZ did not have a large influence on the microwave heating behavior of any the composites as whole.

Rather the samples which were more conducting were instead dominated by the SiC microwave heating behavior.

Overall, the resistive losses of the 3YSZ-SiC_w-Al_2O_3 composites are the primary heating mechanisms of the samples as with the SiC_w-Al_2O_3 composite previously. It was noted that all thermal hotspots in the simulated samples corresponded to areas of the highest resistive losses in the samples. Additionally, there was a linear relationship between the electrical conductivities of the samples and the maximum temperature reached after a simulated 740s of microwave heating. Higher electrical conductivities corresponded to higher maximum temperatures reached in the composite samples, generally, which was to be expected since resistive losses in the material are accounted for by electrical conductivity.

7 CONCLUSIONS AND FUTURE WORK

7.1 Conclusions

In this thesis, SiC_w-Al_2O_3 composites were fabricated using spark plasma sintering to characterize the bulk electrical behavior transition from insulating to conducting as SiC_w content is increased from 1.09% to 28.2%. Ultimately, the goal of this study was to establish the percolation threshold and to compare SPS SiC_w-Al_2O_3 composite samples to previously made hot-pressed SiC_w-Al_2O_3 samples as the two techniques are very similar in their use of a uniaxial pressing direction, elevated temperatures, and elevated pressures to densify the material. The SPS SiC_w-Al_2O_3 composites behaved very similarly to the previously made hot-pressed samples with comparable electrical conductivities, with similar percolation thresholds at 7.68% SiC_w content. However, the SPS SiC_w-Al_2O_3 composites were slightly lower in conductivity past the percolation threshold than the hot-pressed samples which can be attributed to the SPS SiC_w-Al_2O_3 samples having a lower density at the higher SiC whisker content compositions.

The repeatability errors on the resistivity measurements of the SPS SiC_w-Al_2O_3 samples were all very low at <0.1%, indicating that consecutive electrical measurements done on the same sample yield highly repeatable results. For samples far below or above the percolation threshold, the repeatability error was especially low at <0.05% generally. At the percolation threshold however, the repeatability errors were slightly higher but still <0.1% generally. Similarly, the reproducibility errors between SPS SiC_w-Al_2O_3 composites of the same composition were calculated to be highest at the percolation threshold. However, overall, the reproducibility errors were <5% which, despite the inherent

heterogenous nature of composites, is relatively low. This reproducibility error is especially high at the percolation threshold because at this composition, the SiC whiskers have just begun to form the conducting percolating path and thus are most sensitive to slight changes in whisker contact. This was further supported by SEM imaging.

Furthermore, 3YSZ-SiC_w-Al_2O_3 composites were fabricated at a fixed SiC_w volume content at 15% as this was a composition where the samples were relatively conducting, and the behavior was not sensitive to whisker contact heterogeneity. The composite samples were made with 2 different aluminas from Advanced Composite Materials and AdValue with 2% 3YSZ volume content. The samples were then annealed under different conditions to oxidize the 3YSZ which was reduced during sintering under vacuum. All annealed samples had higher electrical resistivities than the samples with no annealing treatment, which was to be expected, regardless of the alumina used. The samples made with the Advanced Composite Materials alumina resulted in more conducting samples as opposed to samples made with the AdValue alumina.

Completing the error analysis on the resistivity measurements of the 3YSZ-SiC_w-Al_2O_3 composite samples, the repeatability errors were again low at <0.1% generally. The reproducibility errors for the 3YSZ-SiC_w-Al_2O_3 composites samples that were annealed in air and O_2 however, were noticeably high with some errors being above 40% in the electrical resistivity. This was because different samples likely oxidized to different extents during the annealing process and thus resulted in large variations in the electrical response between samples of the same composition and annealing treatment.

In the SEM images of the samples, it is also apparent that the samples made with the Advanced Composite Materials were also more homogenous and less porous. This is because the SiC_w-Al_2O_3 mix used with alumina from Advanced Composite Materials was previously ball milled for 2 hours prior to any 3YSZ being added. In comparison, the samples made with the AdValue alumina were speed-mixed and mortar and pestled for ~35 minutes. This resulted in agglomerations of Al_2O_3, SiC_w, and 3YSZ in the samples which was identified in the SEM images. Additionally, the AdValue alumina was spray dried during the manufacturing process resulting in large alumina agglomerates.

Simulations were also completed in COMSOL to simulate the microwave heating behavior of the experimentally fabricated and sintered SiC_w-Al_2O_3 and 3YSZ-SiC_w-Al_2O_3 composites. Due to the size of the samples however, experimental data could not be captured on them because they lacked the thermal mass to induce significant heating, and thus COMSOL simulations were done using bulk electrical data captured experimentally. The simulation included a microwave oven and a waveguide which provided a 2.45GHz frequency at 1000W power.

For the SiC_w-Al_2O_3 samples it was found that despite the percolation threshold being established at 7.68% SiC_w content, the SiC began to dominate the electromagnetic microwave heating behavior at a much higher content at 17.0%. This was characterized by measuring the maximum temperature reached as well as the heating rate of SiC_w-Al_2O_3 samples made with various compositions after a simulated heating time of 500s. Thus, despite a percolating electrically conducting path being formed and the SiC behavior beginning to dominate the electrical response at 7.68% SiC whisker content, this is not enough to influence the microwave heating behavior.

For the 3YSZ-SiC_w-Al_2O_3 composites, it was ultimately found that 2% volume content was not sufficient in the composites to induce the thermal runaway effect observed in a simulated pure 3YSZ samples. This was true despite certain samples reaching the ~350°C needed to induce the thermal runaway effect in the pure 3YSZ sample. However, some samples, namely the 3YSZ-SiC_w-Al_2O_3 composites annealed in air and O_2, were unable to reach temperatures above 100°C. A general linear relationship was found between electrical conductivity and maximum temperature reached, and thus the 3YSZ-SiC_w-Al_2O_3 composites annealed in air and O_2 were likely too electrically insulating to sufficiently heat up under a microwave frequency.

7.2 Suggested Future Work

Although progress has been made in completing this thesis, there is still room for future study and experiments. A full percolation curve was made for SPS SiC_w-Al_2O_3 composites samples but some samples at higher SiC_w contents yielded relatively low densities. Future work can be done in varying the hold temperature or pressure to yield fully dense SPS SiC_w-Al_2O_3 samples as there is still a significant amount of powder mixes left of each SiC_w composition.

Additionally, the SiC_w-Al_2O_3 mixes used in this study did not include any sintering aids, and thus an additional study can be done in exploring the effect of sintering aids on the percolation threshold of SPS SiC_w-Al_2O_3 composites. Both the volume content of sintering aids, as well as what sintering aids are used can be varied to study the effects on overall electrical behavior as they are commonly used in commercial practice. Although

some work has been done in this area by Justin Brandt [45], a full percolation study has not been completed exploring sintering aids specifically.

Sample geometry can also be explored regarding the SPS SiC_w-Al_2O_3 composites using the same composition mixes. Due to the limitations of the SPS machine at Georgia Tech, the samples made were limited to a diameter of ~10mm. Thus, a diameter to thickness ratio of 10 as described by the ASTM D-150 standard needed to measure the true bulk behavior of the sample [68] was difficult to achieve. It is possible that edge effects are slightly skewing the electrical measurements completed in this thesis. If possible, it would be beneficial to repeat the percolation study with a SPS machine capable of fabricating samples with a diameter to thickness ratio of 10 or higher, as some studies have found a diameter to thickness ratio of 30 is more representative of the bulk behavior [69].

Regarding the 3YSZ-SiC_w-Al_2O_3 samples, there was not enough 3YSZ to induce a thermal runaway effect in the 3YSZ-SiC_w-Al_2O_3 composite samples, despite the samples reaching the necessary temperatures needed to induce thermal runaway in the pure 3YSZ sample. Thus, a more detailed study is required where additional 3YSZ is added to the 3YSZ-SiC_w-Al_2O_3 composites to find the critical 3YSZ volume composition required to induce thermal runaway in the composites. This will also aid in better and more fully understanding the effect 3YSZ has on the electrical and microwave heating behavior of SiC_w-Al_2O_3 composites, as in this thesis only 2% by volume 3YSZ was added to form 3YSZ-SiC_w-Al_2O_3 composites.

Furthermore, it was established in Chapter 6 that the SiC begins to dominate the microwave heating behavior of the SiC_w-Al_2O_3 composite samples, increasing the

microwave absorption properties of the bulk composite at a whisker content of 17.0%. In this work, the 3YSZ-SiC_w-Al_2O_3 composites were studied using a fixed SiC whisker content of 14.5%. It would be beneficial to explore including 3YSZ as an additional filler phase at a fixed SiC whisker content of 17.0%, to see if this would achieve thermal runaway at a lower 3YSZ content.

It would also be beneficial to supplement the simulation work with experimental work where a more intensive mixing process is used to better disperse the 3YSZ. As mentioned previously, the samples made with the SPS machine at Georgia Tech lacked the thermal mass needed to experimentally induce microwave heating due to their small size. Although expensive, it would be useful to fabricate samples with the geometry used in the simulation work to experimentally subject to microwave frequency. This would allow for verification that the simulation model used was accurate and yielded results reflective of real samples.

Lastly, the electrical conductivities used in the COMSOL model for the SiC_w-Al_2O_3 and 3YSZ-SiC_w-Al_2O_3 samples were all taken from experimental data taken at room temperature and assumed to be constant. In reality, the electrical conductivity of materials, particularly SiC and 3YSZ, are temperature dependent. A more in-depth study exploring the effects of temperature of the electrical behavior of SiC, 3YSZ, and Al_2O_3 is needed to further understand the microwave heating behavior of 3YSZ-SiC_w-Al_2O_3 composites.

APPENDIX A. ERROR ANALYSIS

In this chapter, additional error analysis is detailed of the SiC_w-Al_2O_3 and 3YSZ-SiC_w-Al_2O_3 composite samples from Chapters 4 and 5, respectively. The repeatability errors are provided for all samples made in this thesis to provide additional support to the analyses of the electrical measurement repeatability made in Sections 4.1.1 and 5.3.

A.1 SiC_w-Al_2O_3 Composites

The repeatability errors of all SiC_w-Al_2O_3 composites, made with varying compositions, are presented below in Table A.1.1. Note that generally, all repeatability errors for the SiC_w-Al_2O_3 samples are <0.05%. This supports the conclusion that consecutive electrical measurements done on the sample are extremely repeatable. Additionally, near the percolation threshold of 7.68% SiC whisker content, the samples made from compositions containing 5.81% and 9.96% SiC whiskers also have relatively high repeatability errors around 0.1%. This again supports the conclusion that near the percolation threshold, the errors are higher due to SiC whisker contact heterogeneity and their influence on electrical behavior.

Table A.1.1 Total repeatability errors across the measured frequency range in all resistivity measurements of all SiC_w-Al_2O_3 composite samples fabricated from Chapter 4.

SiC_w Content (%)		Repeatability Error – Real Resistivity (%)	Repeatability Error – Imaginary Resistivity (%)	Repeatability Error – Resistivity Magnitude (%)	Repeatability Error – Resistivity Phase Angle (%)
1.09	S1	0.088	0.018	0.017	0.026
	S2	0.059	0.014	0.024	0.023
	S3	0.032	0.014	0.044	0.067
3.52	S1	0.038	0.080	0.080	0.013
	S2	0.057	0.031	0.031	0.008
	S3	0.040	0.032	0.031	0.006
5.81	S1	0.057	0.074	0.044	0.045
	S2	0.112	0.034	0.068	0.089
	S3	0.078	0.046	0.033	0.026
7.68	S1	0.045	0.103	0.034	0.010
	S2	0.066	0.170	0.058	0.015
	S3	0.374	0.480	0.178	0.410
9.96	S1	0.087	0.045	0.067	0.088
	S2	0.051	0.092	0.036	0.037
	S3	0.045	0.105	0.066	0.035
12.2	S1	0.032	0.047	0.030	0.055
	S2	0.036	0.052	0.053	0.031
	S3	0.049	0.044	0.042	0.040
14.5	S1	0.074	0.024	0.039	0.028
	S2	0.034	0.025	0.048	0.023
	S3	0.032	0.065	0.037	0.047
17.0	S1	0.047	0.019	0.048	0.038
	S2	0.038	0.021	0.32	0.030

	S3	0.040	0.056	0.049	0.032
19.1	S1	0.054	0.039	0.032	0.049
	S2	0.040	0.033	0.038	0.022
	S3	0.036	0.047	0.028	0.031
24.0	S1	0.047	0.034	0.043	0.029
	S2	0.056	0.051	0.040	0.024
	S3	0.051	0.033	0.064	0.048
28.2	S1	0.039	0.045	0.039	0.067
	S2	0.011	0.043	0.011	0.053
	S3	0.038	0.089	0.038	0.013

A.2 3YSZ-SiC_w-Al_2O_3 Composites

The repeatability errors of all 3YSZ-SiC_w-Al_2O_3 composite samples from Chapter 5 are presented below. Table A.2.1 contains the repeatability errors for the samples made from the AdValue alumina and Table A.2.2 contains the repeatability errors for the samples made from the Advanced Composites Materials alumina. Apart from Type E SiC_w-Al_2O_3 S4, the repeatability errors in the resistivity measurements also fall at roughly <0.1% for all 3YSZ- SiC_w-Al_2O_3. However, samples made from the AdValue alumina in Table A.2.1 have slightly higher errors than the samples made from the Advanced Composite Materials alumina in Table A.2.2. This is likely due to the Advanced Composite Materials alumina samples being ball milled [45], thus resulting in better homogeneity in the respective powder mixes than the samples made with the AdValue alumina, which were only speed-mixed and mortar and pestled.

Table A.2.1 Total repeatability errors across the measured frequency range in all resistivity measurements of all 3YSZ-SiC_w-Al_2O_3 composite samples fabricated from Chapter 5.

Sample		Repeatability Error – Real Resistivity (%)	Repeatability Error – Imaginary Resistivity (%)	Repeatability Error – Resistivity Magnitude (%)	Repeatability Error – Resistivity Phase Angle (%)
15% SiC_w-Al_2O_3	S1	0.031	0.084	0.031	0.078
	S2	0.047	0.080	0.047	0.074
	S3	0.128	0.014	0.127	0.015
3YSZ-SiC_w-Al_2O_3 Not Annealed	S1	0.081	0.039	0.080	0.039
	S2	0.032	0.052	0.031	0.055
	S3	0.031	0.036	0.031	0.036
3YSZ-SiC_w-Al_2O_3 Annealed in Air	S4	0.036	0.052	0.043	0.036
	S5	0.051	0.071	0.056	0.054
	S6	0.033	0.050	0.063	0.067
3YSZ-SiC_w-Al_2O_3 Annealed in O_2	S7	0.097	0.048	0.078	0.066
	S8	0.063	0.063	0.062	0.061
	S9	0.083	0.099	0.124	0.104

Table A.2.2 Total repeatability errors across the measured frequency range in all resistivity measurements of all 3YSZ-Type E SiC_w-Al_2O_3 composite samples fabricated from Chapter 5.

Sample		Repeatability Error – Real Resistivity (%)	Repeatability Error – Imaginary Resistivity (%)	Repeatability Error – Resistivity Magnitude (%)	Repeatability Error – Resistivity Phase Angle (%)
15% Type E SiC_w-Al_2O_3	S1	0.022	0.061	0.024	0.052
	S2	0.034	0.039	0.048	0.028
	S3	0.049	0.044	0.029	0.023
3YSZ-Type E SiC_w-Al_2O_3 Not Annealed	S1	0.026	0.035	0.027	0.025
	S2	0.049	0.056	0.053	0.035
	S3	0.024	0.029	0.024	0.022
3YSZ-Type E SiC_w-Al_2O_3 Annealed in O_2	S4	0.138	0.102	0.145	0.114
	S5	0.030	0.055	0.030	0.044
	S6	0.037	0.089	0.035	0.078

REFERENCES

[1] J. W. Essam, "Percolation theory," *Reports on progress in physics*, vol. 43, no. 7, p. 833, 1980.

[2] H. Derakhshankhah, R. Mohammad-Rezaei, B. Massoumi, M. Abbasian, A. Rezaei, H. Samadian, and M. Jaymand, "Conducting polymer-based electrically conductive adhesive materials: Design, fabrication, properties, and applications," *Journal of Materials Science: Materials in Electronics*, vol. 31, no. 14, pp. 10947–10961, 2020.

[3] X. Wang, W. Zhang, Y. Zhao, H. Bei, and Y. Gao, "Micromechanical investigation of the role of percolation on ductility enhancement in metallic glass composites," *Materials Science and Engineering: A*, vol. 769, p. 138531, 2020.

[4] Z. Q. Liu, G. Liu, R. T. Qu, Z. F. Zhang, S. J. Wu, and T. Zhang, "Microstructural percolation assisted breakthrough of trade-off between strength and ductility in CuZr-based metallic glass composites," *Sci Rep*, vol. 4, no. 1, pp. 1–6, 2014.

[5] J. Cho, A. R. Boccaccini, and M. S. P. Shaffer, "Ceramic matrix composites containing carbon nanotubes," *Journal of Materials Science*, vol. 44, no. 8, pp. 1934–1951, 2009.

[6] S. Rul, F. Lefèvre-Schlick, E. Capria, C. Laurent, and A. Peigney, "Percolation of single-walled carbon nanotubes in ceramic matrix nanocomposites," *Acta Materialia*, vol. 52, no. 4, pp. 1061–1067, 2004.

[7] C.-W. Nan, Y. Shen, and J. Ma, "Physical properties of composites near percolation," *Annual Review of Materials Research*, vol. 40, no. 1, pp. 131–151, 2010.

[8] Z. Rimska, V. Křuesálek, and J. Špaček, "AC conductivity of carbon fiber–polymer matrix composites at the percolation threshold," *Polym Compos*, vol. 23, no. 1, pp. 95–103, 2002.

[9] Y. Chen, S. Wang, F. Pan, and J. Zhang, "A numerical study on electrical percolation of polymer-matrix composites with hybrid fillers of carbon nanotubes and carbon black," *Journal of Nanomaterials*, vol. 2014, 2014.

[10] B. D. Bertram, "Effects of interfaces and preferred orientation on the electrical response of composites of alumina and silicon carbide whiskers," Doctorate of Philosophy, Georgia Institute of Technology, 2011.

[11] M. Watt, "Effect of Conductive Network Formation and Particle Morphology on the Electrical Properties of Composites," Doctorate of Philosophy, Georgia Institute of Technology, Atlanta, GA, 2020.

[12] A. C. and Metaxas and R. J. Meredith, *Industrial microwave heating*, no. 4. IET, 1983.

[13] D. E. Clark, D. C. Folz, and J. K. West, “Processing materials with microwave energy,” *Materials Science and Engineering: A*, vol. 287, no. 2, pp. 153–158, 2000.

[14] E. T. Thostenson and T.-W. Chou, “Microwave processing: fundamentals and applications,” *Composites Part A: Applied Science and Manufacturing*, vol. 30, no. 9, pp. 1055–1071, 1999.

[15] T. E. Quantrille, “Ceramic Composites for Microwave Grilling and Speed Cooking,” 2008.

[16] B. D. Bertram and R. A. Gerhardt, “Room temperature properties of electrical contacts to alumina composites containing silicon carbide whiskers,” *Journal of Applied Physics*, vol. 105, no. 7, p. 074902, 2009.

[17] D. S. Mebane and R. A. Gerhardt, “Interpreting impedance response of silicon carbide whisker/alumina composites through microstructural simulation,” *Journal of the American Ceramic Society*, vol. 89, no. 2, pp. 538–543, 2006.

[18] D. S. Mebane, A. M. Gokhale, and R. A. Gerhardt, “Trivariate, Stereological Length–Radius–Orientation Unfolding Derived and Applied to Alumina–Silicon Carbide Whisker Composites,” *Journal of the American Ceramic Society*, vol. 89, no. 2, pp. 620–626, 2006.

[19] D. S. Mebane, A. M. Gokhale, and R. A. Gerhardt, “The Effect of Microstructural Interconnectivity on the Resistivity of Anisotropic Al_2O_3-

SiC_w Composites," in *AIP Conference Proceedings*, 2004, vol. 712, no. 1, pp. 350–354.

[20] D. S. Mebane, S. I. Lieberman, A. M. Gokhale, and R. A. Gerhardt, "Bivariate stereological unfolding procedure for randomly oriented chopped fibers or whiskers," *Acta Mater*, vol. 53, no. 18, pp. 4943–4953, 2005.

[21] B. D. Bertram, R. A. Gerhardt, and J. W. Schultz, "Impedance response and modeling of composites containing aligned semiconductor whiskers: Effects of dc-bias partitioning and percolated-cluster length, topology, and filler interfaces," *Journal of Applied Physics*, vol. 111, no. 12, p. 124913, 2012.

[22] B. D. Bertram and R. A. Gerhardt, "Effects of Frequency, Percolation, and Axisymmetric Microstructure on the Electrical Response of Hot-Pressed Alumina–Silicon Carbide Whisker Composites," *Journal of the American Ceramic Society*, vol. 94, no. 4, pp. 1125–1132, 2011.

[23] B. D. Bertram, R. A. Gerhardt, and J. W. Schultz, "Extruded and Pressureless-Sintered Al_2O_3–SiC_w Composite Rods: Fabrication, Structure, Electrical Behavior, and Elastic Modulus," *Journal of the American Ceramic Society*, vol. 94, no. 12, pp. 4391–4398, 2011.

[24] R. A. Gerhardt and R. Ruh, "Volume Fraction and Whisker Orientation Dependence of the Electrical Properties of SiC-Whisker-Reinforced Mullite Composites," *Journal of the American Ceramic Society*, vol. 84, no. 10, pp. 2328–2334, 2001.

[25] H.-J. Yang, J. Yuan, Y. Li, Z.-H. Hou, H.-B. Jin, X.-Y. Fang, and M.-S. Cao "Silicon carbide powders: temperature-dependent dielectric properties and enhanced microwave absorption at gigahertz range," *Solid State Commun*, vol. 163, pp. 1–6, 2013.

[26] X. Liu, Z. Zhang, and Y. Wu, "Absorption properties of carbon black/silicon carbide microwave absorbers," *Composites Part B: Engineering*, vol. 42, no. 2, pp. 326–329, 2011.

[27] H. Sugawara, K. Kashimura, M. Hayashi, S. Ishihara, T. Mitani, and N. Shinohara, "Behavior of microwave-heated silicon carbide particles at frequencies of 2.0–13.5 GHz," *Applied Physics Letters*, vol. 105, no. 3, p. 034103, 2014.

[28] M. Wei, H. Wang, L. Jiang, L. Zhao, L. Yang, and X. Chen, "Dependence of composition of SiC–Al_2O_3 composite absorbers on microwave heating characteristics," *Ceramics International*, vol. 48, no. 14, pp. 19576–19582, 2022.

[29] R. Behrend, C. Dorn, V. Uhlig, and H. Krause, "Investigations on container materials in high temperature microwave applications," *Energy Procedia*, vol. 120, pp. 417–423, 2017.

[30] Y. Liu, F. Luo, J. Su, W. Zhou, and D. Zhu, "Mechanical, dielectric, and microwave-absorption properties of alumina ceramic containing dispersed Ti3SiC2," *Journal of Electronic Materials*, vol. 44, no. 3, pp. 867–873, 2015.

[31] Y. Wu and Y. Chiang, “The m–t Transformation and Twinning Analysis of Hot-Pressed Sintered 3YSZ Ceramics,” *Journal of the American Ceramic Society*, vol. 94, no. 7, pp. 2200–2212, 2011.

[32] M. Ghatee, M. H. Shariat, and J. T. S. Irvine, “Investigation of electrical and mechanical properties of 3YSZ/8YSZ composite electrolytes,” *Solid State Ionics*, vol. 180, no. 1, pp. 57–62, 2009.

[33] E. Drożdż, “The influence of the method of addition of Al_2O_3 to 3YSZ material on its thermal and electrical properties,” *Journal of Thermal Analysis and Calorimetry*, vol. 118, no. 2, pp. 1345–1353, 2014.

[34] Y. Mo, T. Liu, X. Wang, J. Li, and M. Yi, “Microstructure, phase structure, and electrical properties of nitrided 3 mol% Y_2O_3 stabilized ZrO_2 (3YSZ),” *Ceramics International*, vol. 45, no. 3, pp. 3680–3686, 2019.

[35] R. I. Todd, E. Zapata-Solvas, R. S. Bonilla, T. Sneddon, and P. R. Wilshaw, “Electrical characteristics of flash sintering: thermal runaway of Joule heating,” *J Eur Ceram Soc*, vol. 35, no. 6, pp. 1865–1877, 2015.

[36] J. Wang, J. Binner, B. Vaidhyanathan, N. Joomun, J. Kilner, G. Dimitrakis, and T.E. Cross, “Evidence for the microwave effect during hybrid sintering,” *Journal of the American Ceramic Society*, vol. 89, no. 6, pp. 1977–1984, 2006.

[37] V. V. Yakovlev, S. M. Allan, M. L. Fall, and H. S. Shulman, “Computational study of microwave processing of zirconia: Effects of frequency and

temperature-dependent material parameters," in *Proceedings of the 13th Seminar Computer Modeling in Microwave Engineering & Applications—Advances in Determining Material Parameters, Thun, Switzerland*, 2011, pp. 7–8.

[38] A. Goldstein, N. Travitzky, A. Singurindy, and M. Kravchik, "Direct microwave sintering of yttria-stabilized zirconia at 2· 45 GHz," *J Eur Ceram Soc*, vol. 19, no. 12, pp. 2067–2072, 1999.

[39] R. A. Gerhardt, "Impedance spectroscopy and mobility spectra," Chapter in Encyclopedia of Condensed Matter Physics, *Elsevier Press*, 350-363 (2005).

[40] R. Gerhardt, "Impedance and dielectric spectroscopy revisited: distinguishing localized relaxation from long-range conductivity," *Journal of Physics and Chemistry of Solids*, vol. 55, no. 12, pp. 1491–1506, 1994.

[41] R. A. Gerhardt, "Impedance and Dielectric Spectroscopy," *Atlanta, GA*. Georgia Institute of Technology, Lecture, 2021.

[42] R. A. Gerhardt, "Relaxation time constants for different functions," *Atlanta, GA*. Georgia Institute of Technology, Lecture, 2021.

[43] R. A. Gerhardt, "What is Impedance and Dielectric Spectroscopy?," *IEEE Instrumentation & Measurement Magazine*, vol. 25, no. 4, pp. 14–20, 2022.

[44] M. Rath and R. Gerhardt, "Repeatability and Reproducibility of Electrical Measurements of Spark-Plasma-Sintered Alumina-SiC_w Composites," in

2022 IEEE International Instrumentation and Measurement Technology Conference (I2MTC), 2022, pp. 1–6.

[45] J. Brandt, "Effect of Sample Processing on Percolated Al_2O_3-SiC_w Composites," Master of Science, Georgia Institute of Technology, Atlanta, GA, 2014.

[46] M. Mohankumar, A.N. Shankar, T.S. Karthik, R. Saravanakumar, H. Oruganti, S. Prabhu, and N. Rakesh, "A Comparative Study on Crack-Healing Ability of Al_2O_3/SiC Structural Ceramic Composites Synthesized by Microwave Sintering and Conventional Electrical Sintering," *Advances in Materials Science and Engineering*, vol. 2021, 2021.

[47] M. Madhan and G. Prabhakaran, "Microwave versus conventional sintering: Microstructure and mechanical properties of Al_2O_3–SiC ceramic composites," *Boletín de la Sociedad Española de Cerámica y Vidrio*, vol. 58, no. 1, pp. 14–22, 2019.

[48] T. P. Deksnys, R. R. Menezes, E. Fagury-Neto, and R. Kiminami, "Synthesizing Al_2O_3/SiC in a microwave oven: A study of process parameters," *Ceram Int*, vol. 33, no. 1, pp. 67–71, 2007.

[49] M. A. Ibrahim, Y. Sahin, A. Y. Gidado, and M. T. Said, "Mechanical properties of aluminium matrix composite including SiC/Al_2O_3 by powder metallurgy-a review," *GSJ*, vol. 7, no. 3, pp. 23–38, 2019.

[50] T. T. Meek, R. D. Blake, and J. J. Petrovic, “Microwave Sintering of Al_2O_3 and Al_2O_3-SiC Whisker Composites,” in *11th Annual Conference on Composites and Advanced Ceramic Materials: Ceramic Engineering and Science Proceedings*, 1987, vol. 8, pp. 861–871.

[51] Y. V. Bykov, S.V. Egorov, A.G. Eremeev, I.V. Plotnikov, K.I. Rybakov, A.A. Sorokin, and V.V. Kholoptsev, “Effect of specific absorbed power on microwave sintering of 3YSZ ceramics,” in *IOP Conference Series: Materials Science and Engineering*, 2017, vol. 218, no. 1, p. 012001.

[52] C. Zhang, G. Zhang, S. Leparoux, H. Liao, C.-X. Li, C.-J. Li, and C. Coddet, “Microwave sintering of plasma-sprayed yttria stabilized zirconia electrolyte coating,” *J Eur Ceram Soc*, vol. 28, no. 13, pp. 2529–2538, 2008.

[53] A. Eqbal, K. S. Arya, and T. Chakrabarti, “In-depth study of the evolving thermal runaway and thermal gradient in the dog bone sample during flash sintering using finite element analysis,” *Ceramics International*, vol. 46, no. 8, pp. 10370–10378, 2020.

[54] J. G. P. da Silva, H. A. Al-Qureshi, F. Keil, and R. Janssen, “A dynamic bifurcation criterion for thermal runaway during the flash sintering of ceramics,” *J Eur Ceram Soc*, vol. 36, no. 5, pp. 1261–1267, 2016.

[55] M. Rath and R. Gerhardt, “Assessment of Homogeneity in Percolated SPS $Al2O_3$-SiC_w Composite Samples,” Presentation at MS&T 21 Conference, *Columbus, OH,* 2021.

[56] Georgia Institute of Technology, “Zeiss Ultra 60 SEM,” *https://mcf.gatech.edu/tools/zeiss-ultra-60-sem/*.

[57] T. J. Rudzik and R. A. Gerhardt, “Effect of spark plasma sintering current and voltage on the microstructure and electrical properties of borosilicate glass–indium tin oxide composites,” *Advanced Engineering Materials*, vol. 22, no. 5, p. 1901431, 2020.

[58] R. A. Gerhardt, J. Runyan, C. Sana, D. S. McLachlan, and R. Ruh, “Electrical properties of boron nitride matrix composites: III, observations near the percolation threshold in BN–B_4C composites,” *Journal of the American Ceramic Society*, vol. 84, no. 10, pp. 2335–2342, 2001.

[59] COMSOL AB, “COMSOL v. 5.6.” Stockholm, Sweden.

[60] COMSOL, “RF Module User’s Guide Version 4.3,” *COMSOL*. COMSOL, 2012.

[61] P. K. Loharkar and A. Ingle, “Numerical analysis of microwave heating: Fundamentals and applications,” in *IOP Conference Series: Materials Science and Engineering*, 2020, vol. 810, no. 1, p. 012061.

[62] I. Ghorbel, P. Ganster, N. Moulin, C. Meunier, and J. Bruchon, “Experimental and numerical thermal analysis for direct microwave heating of silicon carbide,” *Journal of the American Ceramic Society*, vol. 104, no. 1, pp. 302–312, 2021.

[63] D. K. Patel, N. K. Bhoi, and H. Singh, “Microwave Heating Capabilities of Different Susceptor Material: Experimental and Simulation Study,” *Silicon*, pp. 1–15, 2021.

[64] S. Marinel, C. Manière, A. Bilot, C. Bilot, C. Harnois, G. Riquet, F. Valdivieso, C. Meunier, C. Coureau, and F. Barthélemy, “Microwave sintering of alumina at 915 MHz: modeling, process control, and microstructure distribution,” *Materials*, vol. 12, no. 16, p. 2544, 2019.

[65] S. Tamang and S. Aravindan, “3D numerical modelling of microwave heating of SiC susceptor,” *Applied Thermal Engineering*, vol. 162, p. 114250, 2019.

[66] C. Manière, T. Zahrah, and E. A. Olevsky, “Fully coupled electromagnetic-thermal-mechanical comparative simulation of direct vs hybrid microwave sintering of 3Y-ZrO_2,” *Journal of the American Ceramic Society*, vol. 100, no. 6, pp. 2439–2450, 2017.

[67] ASTM, “ASTM D-150: Standard Test Methods for AC Loss Characteristics and Permittivity (Dielectric Constant) of Solid Electrical Insulation,” *ASTM*, vol. 10.01.

[68] S. Kumar and R. A. Gerhardt, “Role of geometric parameters in electrical measurements of insulating thin films deposited on a conductive substrate,” *Measurement Science and Technology*, vol. 23, no. 3, p. 035602, 2012.